Accepted Manuscript

Detrital and volcanic zircon U-Pb ages from southern Mendoza (Argentina): an insight on the source regions in the northern part of the Neuquén Basin

Maximiliano Naipauer, Felipe Tapia, José Mescua, Marcelo Farías, Marcio M. Pimentel, Victor A. Ramos

PII: S0895-9811(15)30066-3

DOI: 10.1016/j.jsames.2015.09.013

Reference: SAMES 1465

To appear in: *Journal of South American Earth Sciences*

Received Date: 29 May 2015

Revised Date: 18 September 2015

Accepted Date: 21 September 2015

Please cite this article as: Naipauer, M., Tapia, F., Mescua, J., Farías, M., Pimentel, M.M., Ramos, V.A., Detrital and volcanic zircon U-Pb ages from southern Mendoza (Argentina): an insight on the source regions in the northern part of the Neuquén Basin, *Journal of South American Earth Sciences* (2015), doi: 10.1016/j.jsames.2015.09.013.

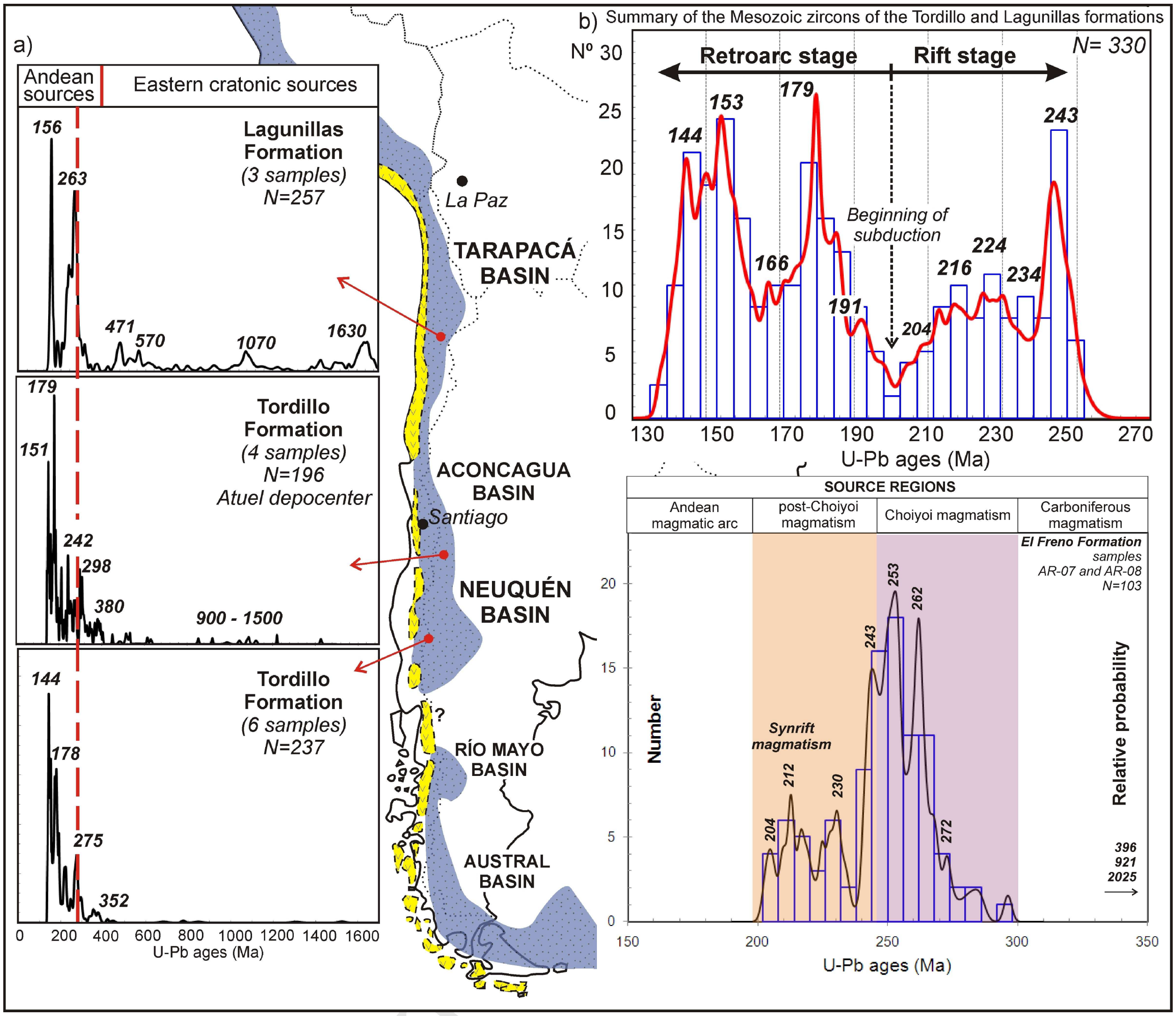
a)
Andean sources
Eastern cratonic sources
Lagunillas Formation
(3 samples)
N=257
156
263
471
570
1070
1630
Tordillo Formation
(4 samples)
N=196
Atuel depocenter
179
151
242
298
380
900 - 1500
Tordillo Formation
(6 samples)
N=237
144
178
275
352
0 200 400 600 800 1000 1200 1400 1600
U-Pb ages (Ma)
La Paz
TARAPACÁ BASIN
ACONCAGUA BASIN
Santiago
NEUQUÉN BASIN
RÍO MAYO BASIN
AUSTRAL BASIN
b) Summary of the Mesozoic zircons of the Tordillo and Lagunillas formations
Nº
Retroarc stage
Rift stage
N= 330
144
153
179
166
191
204
216
224
234
243
Beginning of subduction
130 150 170 190 210 230 250 270
U-Pb ages (Ma)
SOURCE REGIONS
Andean magmatic arc
post-Choiyoi magmatism
Choiyoi magmatism
Carboniferous magmatism
El Freno Formation
samples
AR-07 and AR-08
N=103
Number
Relative probability
Synrift magmatism
204
212
230
243
253
262
272
396
921
2025
150 200 250 300 350
U-Pb ages (Ma)

Detrital and volcanic zircon U-Pb ages from southern Mendoza (Argentina): an insight on the source regions in the northern part of the Neuquén Basin

Maximiliano Naipauer[1], Felipe Tapia[2], José Mescua[3], Marcelo Farías[2], Marcio M. Pimentel[4] and Victor A. Ramos[1]

[1] Instituto de Estudios Andinos "Don Pablo Groeber" (Departamento de Ciencias Geológicas, FCEN - Universidad de Buenos Aires) and CONICET, maxinaipauer@gl.fcen.uba.ar

[2] Departamento de Geología, Facultad de Ciencias Físicas y Matemáticas, Universidad de Chile.

[3] Instituto Argentino de Nivología, Glaciología y Ciencias Ambientales (IANIGLA), CCT Mendoza, CONICET. jmescua@mendoza-conicet.gob.ar

[4] Instituto de Geociências, Universidade de Brasília, Brasília, Distrito Federal, Brazil.

Abstract. The infill of the Neuquén Basin recorded the Meso-Cenozoic geological and tectonic evolution of the southern Central Andes being an excellent site to investigate how the pattern of detrital zircon ages varies trough time. In this work we analyze the U-Pb (LA-MC-ICP-MS) zircon ages from sedimentary and volcanic rocks related to synrift and retroarc stages of the northern part of the Neuquén Basin. These data define the crystallization age of the synrift volcanism at 223 ± 2 Ma (Cerro Negro Andesite) and the maximum depositional age of the original synrift sediments at ca. 204 Ma (El Freno Formation). Two different pulses of rifting could be recognized according to the absolute ages, the oldest developed during the Norian and the younger during the Rhaetian-Sinemurian. The source regions of the El Freno Formation show that the Choiyoi magmatic province was the main source rock of sediment supply. An important amount of detrital zircons with Triassic ages was identified and interpreted as a source area related to the synrift magmatism. The maximum depositional age calculated for the Tordillo Formation in the Atuel-La Valenciana depocenter is at ca. 149 Ma; as well as in other places of the Neuquén Basin, the U-Pb ages calculated in the Late Jurassic Tordillo Formation do not agree with the absolute age of the Kimmeridgian-Tithonian boundary (ca. 152 Ma). The main source region of sediment in the Tordillo Formation was the Andean magmatic arc. Basement regions were also present with age peaks at the Carboniferous, Neoproterozoic, and Mesoproterozoic; these regions were probably located to the east in the San Rafael Block. The pattern of zircon ages summarized for the Late Jurassic Tordillo and Lagunillas formations were interpreted as a record of the magmatic activity during the Triassic and Jurassic in the southern Central Andes. A waning of the magmatism is inferred to have happened during the Triassic. The evident lack of ages observed around ca. 200 Ma suggests cessation of the synrift magmatism. The later increase in magmatic activity during the Early Jurassic is attributed to the onset of Andean subduction, with maximum peaks at ca. 191 and 179 Ma. The trough at ca. 165 Ma and the later increase in the Late Jurassic could be explained by changes in the relative convergence rate in the Andean subduction regime, or by the shift to a more mafic composition of the magmatism with minor zircon fertility.

Keywords: southern Central Andes, Jurassic, provenance, Andean basin

1. Introduction

The infill of the Neuquén Basin composed of thick marine and continental sedimentary sequences with minor volcanic rocks interbedded, recorded the Meso-Cenozoic geological evolution of the southern Central Andes (Ramos 1999; 2010). The tectonic regime along the

Andean margin is also reflected in the tectonic history of the basin that began with isolated rift depocenters during the Triassic, continued with a thermal retroarc stage (*sensu* Jordan, 1995) between the Jurassic and Early Cretaceous (Figure 1), and finished as a foreland basin during the Late Cretaceous and Paleocene (Vergani et al., 1995; Franzese and Spalletti, 2001; Ramos and Folguera, 2005; Ramos 2010). This succession of tectonic settings makes the Neuquén Basin an excellent site to investigate how the pattern of detrital zircon ages varies trough the time in different tectonic regimes. Recent geochronological data provided valuable information about the changes in sedimentary provenance that occurred in the retroarc stage and the passage to the foreland stage (Tunik et al., 2010; Di Giulio et al., 2012; Naipauer et al., 2012, 2015; Balgord and Carrapa, 2015). However, there is a lack of U-Pb data from the rift stage, which prevents determining either the age of the sedimentary and volcanic infill, or the temporal correlations between depocenters or the potential sedimentary source areas.

The end of the rift stage and the beginning of the thermal retroarc stage are not clearly defined yet in the Neuquén Basin (Leanza et al., 2013; Veiga et al., 2013). This tectonic change coincides with the installation of the Andean magmatic arc in the present position of the Coastal Cordillera in Chile (Mpodozis and Ramos, 1989; 2008; Charrier et al, 2007). Accordingly, since the Jurassic the basin was located in the retroarc with a western boundary defined by the contemporaneous volcanic arc and an eastern boundary composed by an ancient cratonic basement (Digregorio et al., 1984; Vergani et al., 1995; Mpodozis and Ramos, 1989). Direct evidence of the activity in the arc are the several tuff layers interbedded in the sedimentary fill (Kamo and Riccardi 2009; Aguirre-Urreta et al, 2008, 2015; Leanza et al., 2013; Vennari et al., 2014). However, the extension and activity of the Jurassic volcanic arc along the Central Andes, and therefore its role as a source of the volcanic contribution, is not well known.

The purpose of this work is to constrain the timing of the volcanism and continental sedimentation of two different extensional periods developed in the northern of the Neuquén Basin. U-Pb (LA-MC-ICP-MS; laser ablation multi-collector inductively coupled plasma mass spectrometer) analyses of detrital and volcanic zircons were carried out to accomplish the study aims. Key continental and volcanic sequences of the synrift and retroarc stages were selected. In the synrift stage, continental deposits of the El Freno Formation and volcanic rocks from the Cerro Negro Andesite were chosen because they are the oldest units, without robust biostratigraphic markers, in the Atuel and Río Grande depocenters, respectively. The dataset presented constrains the age of the synrift in each depocenter and shows the possible correlations with other synrift depocenters south of the basin. In the retroarc stage, the Tordillo Formation was analyzed to know its sediment sources given its particular setting. In the study region these deposits recorded important thickness variations related to local synsedimentary normal faults, which show local extensional reactivation during the retroarc stage (Mescua et al., 2008; 2014).

The age patterns of detrital zircons obtained were compared with data published for the Tordillo Formation from the southern part of the basin and with the coeval Lagunillas Formation of the northern Tarapacá basin. The results show variations in the provenance patterns along the Andean retroarc basins during the Late Jurassic (Figure 1b). The record of the magmatic activity along the margin is also evident in the pattern of detrital zircon ages of the analyzed units. Late Jurassic sediments from the Andean retroarc basin show important peaks and troughs of zircon ages which are here related to the episodic magmatism developed between the Triassic and Jurassic along the southern areas of the Central Andes.

Figure 1 around here

2. Geological background of the Neuquén Basin

The Neuquén Basin is a retroarc basin located between 32º and 41º SL along the eastern side of the Andean volcanic arc (Digregorio et al., 1984; Legarreta and Uliana, 1999). The subduction regime was installed in the Early Jurassic and generated a volcanic arc located near the present Coastal Cordillera of Chile (Mpodozis and Ramos, 1989; 2008, Charrier, 2007, 2015) (Figure 2). The basin infill corresponds to sedimentary rocks of marine and continental origin with interbedded volcanogenic rocks deposited between the Late Triassic and Paleogene. These rocks cover more than 120,000 km^2 and reach a thickness of 7,000 m (Legarreta and Uliana, 1999). The Neuquén Basin petroleum system, which contains the largest hydrocarbon reserves in Argentina, is the major economic basin in the region. The stratigraphic, structural, paleontological, and tectonic knowledge of the basin was established by pioneering studies during the last century (Groeber, 1948; Ramos, 1978; Uliana and Biddle, 1988; Legarreta and Uliana 1991; Vergani et al., 1995; among others). Its knowledge is constantly advancing motivated by the discovery of unconventional oil and gas reservoirs during the last years.

The sedimentary infill was deposited in three different tectonic settings that include a Late Triassic-Early Jurassic rift stage, followed by a Middle Jurassic to Early Cretaceous period of thermal sag and finally a Late Cretaceous-Cenozoic foreland stage (Vergani et al., 1995, Franzese and Spalletti, 2001; Mpodozis and Ramos, 2008; Tunik et al., 2010). The deposits of these stages have been recognized throughout the Principal Cordillera between 32° and 40° SL (Figure 2).

Late Triassic to Early Jurassic synrift deposits fill several isolated depocenters with different orientation (Uliana and Biddle, 1988): a NNW-trending fault system which is predominant in the north (Atuel-La Valenciana, Río del Cobre-Río Grande, Malargüe, and Cordillera del Viento depocenters); as well as NW and WNW-trending faults control the southern Neuquén Embayment (Entre Lomas, Estancia Vieja, and Loma La Lata depocenters, among others). This was probably influenced by the Huincul deformation zone in the southern part of the basin (Mosquera and Ramos, 2006; Franzese et al., 2007; Silvestro and Zubiri, 2008; Cristallini et al., 2009; Pángaro et al., 2009). The synrift deposits (Precuyano Cycle) are composed of continental and pyroclastic sediments with interbedded volcanic rocks (Gulisano, 1981; Carbone et al., 2011). Typical wedge geometries produce significant variations in thickness, between 1,000 and 5,000 m. Giambiagi et al. (2012) identified a passive rift in the northern depocenters and active rifts in the southern depocenters based on the presence or absence of volcanic rocks in the successions.

Tectonic subsidence ceased in the Early Jurassic and was followed by a thermal subsidence retroarc stage. This phase continued until the Early Cretaceous and was characterized by the development of three main transgression-regression cycles (Legarreta and Gulisano 1989). Marine transgressions from the paleo-Pacific Ocean overstepped the Andean volcanic arc flooding the retroarc region. Based on these cycles, the sedimentary and volcanic deposits were separated into four different lithostratigraphic groups: Cuyo, Lotena, Mendoza, and Rayoso (Dellape et al., 1978; Leanza, 1992; Stipanicic et al., 1968).

The sag phase ended by the Early Cretaceous and the tectonic regime changed to compressive in the southern Central Andes (Ramos 2010). Consequently, the Neuquén Basin became a foreland basin, where the eastward migration and uplift of the fold and thrust belt and the orogenic front produced the first synorogenic deposits (Zamora Valcarce et al. 2006; Tunik et al. 2010). This occurs at approximately 100 Ma with the deposition of the Neuquén Group and subsequently the Malargüe Group (Stipanicic et al., 1968; Legarreta et al., 1989).

Figure 2 around here

3. Geology and stratigraphy of the study area

The study region is located between 34º30´ and 35º SL north of the Cortaderas Lineament, where the Neuquén Basin has about 200 km of width between the present volcanic arc and the cratonic region (Figure 2). In northern Mendoza and southern San Juan provinces this is known as the Aconcagua Basin (Figure 1) (Mpodozis and Ramos, 1989). It is important to note that south of the Cortaderas Lineament is the Neuquén embayment that expands the basin about 500 km to the east (Bracaccini, 1970; Ramos, 1978) (Figure 2).

The structural framework of the studied region is characterized by the presence of the Atuel-La Valenciana and Río del Cobre-Río Grande depocenters (Figure 3). The Atuel-La Valenciana depocenter extends from the Río Atuel to the Río Malargüe (Figure 3) and is approximately 95 km long and 31 km wide (Manceda and Figueroa, 1995; Giambiagi et al., 2008). The Río del Cobre-Río Grande depocenter is located along the westernmost part of the Neuquén Basin exposed for 85 km from the Río del Cobre to the Río Grande, with a width of 35 km (Figure 3). The two depocenters are separated by a basement high known as the Tordillo

High (Gerth, 1931; Davidson and Vicente, 1973; Legarreta and Kozlowski, 1984, Legarreta and Uliana, 1999).

The basement of the study area crops out in southern part of the Frontal Cordillera, in the San Rafael Block, and in the Principal Cordillera (Tordillo High) (Figures 2 and 3). To the north (~ 33º 30´ SL) in the Cordón del Portillo, Mesoproterozoic to Neoproterozoic metamorphic rocks conform the basement of the Frontal Cordillera of Mendoza (Ramos and Basei 1997; Willner et al., 2008; López de Azarevich et al., 2009). An Ordovician sedimentary succession (Lagunitas Formation) and Devonian igneous rocks (e.g.: Cerro Carrizalito Granodiorite ca. 389 Ma) crop out in the Cordón del Carrizalito in the southern part of the Frontal Cordillera (Tickyj et al., 2009), close to the Atuel-La Valenciana depocenter. Mesoproterozoic metamorphic rocks and Paleozoic sedimentary and igneous rocks are exposed in the San Rafael Block (González Díaz 1972; Kleiman and Japas, 2009; Varela et al., 2011). However, the most conspicuous basement outcrops are igneous rocks of the Permian-Triassic Choiyoi magmatic province (Kay et al., 1989; Llambías and Sato, 2011). Plutonic and volcanic rocks of this magmatic province are present in the Principal Cordillera (e.g.: El Fortín sedimentary and volcanic complex), Frontal Cordillera and San Rafael Blok and are considered the structural basement of the Neuquén Basin at this latitude (Giambiagi et al., 2008).

Recent contributions have provided detailed information on the sedimentological and structural features of both the Atuel-La Valenciana (Manceda and Figueroa, 1995; Lanés 2005; Spalletti et al., 2007; Giambiagi et al., 2008; Lanés et al., 2008; Mescua et al., 2008; Bechis et al., 2009; and references therein) and the Río del Cobre-Río Grande (Tapia et al., 2013; Mescua et al., 2014) depocenters.

Figure 3 around here

The oldest sediments in the Atuel-La Valenciana depocenter are the Late Triassic marine shales with invertebrates (bivalves, brachiopods, gastropods, nautiloids and corals) described and grouped in the Arroyo Malo Formation (Figure 4) (Riccardi et al., 1997). This unit comprises the only record of Triassic fossiliferous marine rocks in the Neuquén Basin. This succession can be correlated to Late Triassic marine rocks of the Coastal Cordillera in central Chile, northern Chile, and central Perú. During the Late Triassic to Early Jurassic, deposition of continental sandstones and minor conglomerates of the El Freno Formation (Figure 4) (Stipanicic and Bonetti, 1970) took place in braided fluvial systems (Spalletti et al., 2007). Fan delta deposits are described in the lower part of the Puesto Araya Formation (Figure 4); these are correlated to the fluvial facies of the El Freno Formation (Lanés, 2005; Lanés et al., 2008). These units, exposed predominantly in the western side of the depocenter, are included within the Precuyano cycle and are interpreted as the initial synrift fill of the Neuquén Basin at these latitudes (Lanés, 2005; Lanés et al., 2008; Giambiagi et al., 2008) (Figure 4). A different stratigraphic scheme was proposed by Spalletti et al. (2005) based on the succession and relationship of these three units. These authors indicated that the marine strata of the Arroyo Malo are covered by the continental sediments of the El Freno Formation in the Arroyo Pedrero and Arroyo Malo localities; and the El Freno Formation is covered with marine sediments of the Puesto Araya Formation. These authors suggest that the sedimentation of the El Freno Formation corresponds to a period of relative calm in the tectonic subsidence and the post-rift sedimentation began with the Puesto Araya Formation. However, Lanes et al. (2008) have not recognized the El Freno Formation in the Arroyo Pedrero and Arroyo Malo sections. Nevertheless, recent studies showed that normal faulting controlled the deposition of the El Freno Formation and the base of the Puesto Araya Formation in the Atuel depocenter (Bechis et al., 2009).

On the other hand, the Precuyano cycle along the Río del Cobre-Río Grande depocenter is composed mainly of volcanic rocks with few sedimentary intercalations, grouped in the Cerro Negro Andesite and the Remoredo Formation (Lanés and Salani, 1998) (Figure 4). These Late Triassic-Early Jurassic rocks represent the synrift deposits (Legarreta and Gulisano, 1989; Legarreta et al., 1993). The Cerro Negro Andesite is a green-porphyritic andesitic intrusive which crops out in isolated bodies along the Río Grande. It underlies the Remoredo Formation and intrudes rocks of the Choiyoi Group (Figure 5a). The Remoredo Formation is a pyroclastic succession with intercalations of lacustrine sandstones and limestones deposited close to volcanic centers (Lanés and Palma, 1998; Lanés and Salani, 1998). Lanés and Salani (1998) recognized that the lithic fragments of the tuff layers of the Remoredo Formation show the same petrographic features of the Cerro Negro Andesite which is, therefore, interpreted as the volcanic neck remnants of the emission center of the pyroclastic flows, as well as the source of the lithic fragments of the volcaniclastic rocks of the Remoredo Formation.

Above the synrift deposits, in the latest Early Jurassic, a marine transgression took place in the two depocenters, and marine shelf deposits forms the Upper Puesto Araya (fine sandstones and mudstones) and Tres Esquinas (shales) formations (Lanés et al., 2008; Mescua et al., 2014) (Figure 4). These deposits were considered to represent the beginning of the sag stage (Giambiagi et al., 2008; Lanés et al., 2008). During the Middle Jurassic, deposition of evaporites of the Tábanos Formation and shales and carbonates of the Lotena Group took place (Figure 4). During this interval the facies variations were controlled principally by thermal subsidence and by the eustatic global sea-level changes (Gulisano and Gutiérrez Pleimling, 1994).

Figure 4 around here

A significant episode of desiccation and continentalization of the basin occurred during the Late Jurassic and evaporites of the Auquilco Formation (Oxfordian) and the red beds of the Tordillo Formation (Kimmeridgian) were deposited. In the Atuel-La Valenciana depocenter the Tordillo Formation is composed of fluvial deposits associated with aeolian and playa lake deposits (Figure 5b and c). The Tordillo Formation in the Río del Cobre-Río Grande depocenter has volcanic layers at the top of the sequence (Mescua et al., 2014) in agreement with the expansion of the Jurassic volcanic arc. These deposits present significant variations in thickness between both depocenters which are related to the presence of local synsedimentary normal faults (Mescua et al., 2008; 2014). Typical black shale facies of the Vaca Muerta Formation (Tithonian-Early Valanginian) deposited above the Tordillo Formation during a sea level high stand. In concordance, reef limestones from the Chachao Formation followed, and coquina limestones and green shales from the Agrio Formation (Hauterivian-Barremian) deposited at the end of this marine cycle (Gulisano and Gutiérrez Pleimling, 1994; Nullo et al., 2005). The Tordillo, Vaca Muerta, Chachao and Agrio formations define a transgressive cycle included in the Mendoza Group by Gulisano and Gutiérrez Pleimling (1994). A thick evaporite and limestone sequence of the Rayoso Group (Albian-Aptian) marks the final desiccation of the basin.

The basement and the sedimentary cover (Triassic to Jurassic and Lower Cretaceous) were exhumed in the Late Cretaceous and Neogene during the growth of the Malargüe fold and thrust belt (Kozlowski et al., 1993; Manceda and Figueroa, 1995; Ramos et al., 1996; Giambiagi et al., 2009; Mescua et al., 2014). As a result of the first episode of Andean contraction and exhumation, thick sequences of continental sediments of the Neuquén and Malargüe groups produced the filling of the first Andean foreland basin at this latitude (Tunik et al., 2010; Mescua et al., 2014).

4. Method and studied samples

The U-Pb samples were taken from the classical profiles of the Atuel-La Valenciana and Río del Cobre-Río Grande depocenters. In the Río Grande section, a volcanic rock (sample AR-15) from the Cerro Negro Andesite was taken to constrain the crystallization age of volcanic rocks of the Precuyano cycle (Figure 3). Two samples of sandstones (AR-07 and AR-08) of the El Freno Formation were taken in the northern margin of the Río Atuel. Four samples of fine red sandstones were taken from the Tordillo Formation: AR-09 was sampled from the northern margin of the Río Atuel and JTCC-420 of the southern margin of Río Atuel; AR-11 and JTRS-407 sample are from the southern margin of the Río Salado (Figure 3).

Figure 5 around here

Zircon grains were separated using standard preparation methods at the Department of Geology of the University of Chile, using a vibrating Gemini table, Frantz magnetic separator and heavy liquid procedures. Final grain selection was undertaken by hand-picking, using a binocular microscope. The sedimentary samples of the El Freno and Tordillo formations were analyzed by U-Pb (LA-MC-ICP-MS) in the Laboratório de Geocronologia, Instituto de Geociências da Universidade de Brasília, Brasil; the volcanic sample of the Cerro Negro Andesite was analyzed in the Laboratorio de Estudios Isotópicos, Geoscience Center, Universidad Nacional Autónoma de México. Sample coordinates, analytical methods, and U-Pb (LA-MC-ICP-MS) age measurements of zircons grains are available in the Supplementary Material.

5. U-Pb geochronological results

5.1. Cerro Negro Andesite

Zircon grains from the Cerro Negro Andesite (sample AR-15) were separated and analyzed by U-Pb to constrain the age of the Precuyano cycle in the studied region. LA-MC-ICP-MS U-Pb ages were obtained from 27 volcanic zircons, 5 analyses were rejected by their discordance of more than 15% (Figure 6a). The 22 concordant analyses form one simple population, except for one youngest age which was rejected. The $^{206}Pb/^{238}U$ weighted mean age of 223.3 ± 1.9 Ma (95% confidence) (Figure 6b) is interpreted as the best age estimate for the timing of eruption of the original volcanic rock.

Figure 6 around here

5.2. El Freno Formation

Zircon grains from two samples of the El Freno Formation (AR-07 and AR-08) were separated and analyzed. Most of the grains are 100µm to 300µm long subidiomorphic to idiomorphic crystals with prismatic habit, with only a few grains presenting rounded edges. The SEM (Secondary Electron Microscopy) images show faint internal structures; oscillatory zoning is recognized indicating the igneous origin of the zircons (Figure 7a and b). Concordia plots are shown in Figure 8 where only the concordant analyses used in the frequency histogram and relative probability plots are plotted.

Eighty two U-Pb analyses for sample AR-07 were carried out, but 29 analyses were rejected due to excessive discordance or large uncertainties. The concordant ages are between 204 and 269 Ma with one isolated age at ca. 2025 Ma (Figure 7a). The pattern of detrital zircon ages is characterized by two main groups of ages between the Triassic and Permian: the youngest group is between 204 Ma and 249 Ma (64%) with maximum peaks at ca. 212 Ma, 224

Ma, and 243 Ma; and the oldest group is between 250 and 269 Ma (34%); the maximum peak is at ca. 260 Ma (Figure 7a) (Table 1).

Sixty two ages for detrital grains from sample AR-08 were obtained and twelve were rejected due to high discordance. The 50 concordant ages are between 203 and 296 Ma with two single zircons at ca. 396 and 921 Ma. The detrital zircon ages pattern have the maximum peaks distributed similarly to those in sample AR-07 in the Triassic and Permian, but a main population with ages between 250 and 296 Ma (65%) has a maximum peak at 262 Ma. A minor group can be distinguished between 203 and 249 Ma (28%) with maximum peaks at ca. 230 Ma and 242 Ma (Figure 7b) (Table 1).

Table 1 around here

Figure 7 around here

5.3. Tordillo Formation

Four samples (AR-09, AR-11, JTRS-407 and JTCC-420) from the Tordillo Formation were analyzed; the zircon grains studied are characterized by subidiomorphic to subrounded form and prismatic habit. Minor crystals presented long prismatic habit and idiomorphic form indicating a volcanic origin. The size of the grains varies in length between 100 μ and 400 μ. In the SEM images oscillatory zoning can be distinguished indicating a magmatic origin of the zircons (Figure 9a, b, c, and d). Concordia plots are shown in Figure 8 in which only the concordant analyses used in the frequency histogram and relative probability are plotted.

Figure 8 around here

Forty seven zircon grains in sample AR-09 were analyzed but five were rejected due to high discordance. The 42 concordance ages produced a pattern with a multimodal distribution, with the zircon ages varying between ca. 152 and 1221 Ma. The most representative population present Jurassic ages (152 Ma to 195 Ma) comprising 55 % of the zircons dated; the maximum peaks are at ca. 152 and 174 Ma. Other less representative groups showed maximum peaks at ca. 225 Ma (Triassic) and 308 Ma (Carboniferous); there are also single results showing Ordovician, Cambrian, Neoproterozoic and Mesoproterozoic ages (Figure 9a) (Table 1).

A total of sixty eight zircon grains from sample JTRS-407 were analyzed and seven of them were rejected due to high discordance. The age pattern is characterized by a main group of Jurassic ages (51%) with two peaks at ca. 149 and 179 Ma. Minor age groups are in the Triassic (peak at ca. 243 Ma; 10%), Early Permian (peak at ca. 297 Ma; 13%), and Late Devonian (peak at ca. 379 Ma; 11%). There are also isolated ages in the Cambrian and Neoproterozoic (Figure 9d) (Table 1).

Figure 9 around here

Fifty three zircon grains from sample JTCC-420 were analyzed and one discordant analysis was rejected. The concordant ages cover the range between 145 and 1123 Ma and display a multimodal distribution. The pattern of detrital ages is complex with peaks at ca. 149 Ma, 172 Ma, 213 Ma, 255 Ma, 299 Ma and 368 Ma; two Mesoproterozoic ages were also observed (Figure 9b) (Table 1).

Fifty two zircons from sample AR-11 were dated and eleven discordant analyses were rejected. The best ages are between 145 and 1426 Ma and several groups in the pattern of detrital zircons can be distinguished at ca. 145-190 Ma (39%), 244-278 Ma (20%), 300-321 Ma (12%), and 379-451 Ma (12%); and 853-1426 Ma (12%). The peaks are at ca. 151 Ma, 163 Ma, 188 Ma, 272 Ma, and 383 Ma (Figure 9c) (Table 1).

6. Discussion

6.1. Crystallization age of the Cerro Negro Andesite and maximum depositional age of the El Freno Formation

The crystallization age of the Andesite Cerro Negro at 223.3 ± 1.9 (Norian age) Ma is the oldest absolute age obtained for the Precuyano Cycle in the Río Grande depocenter and also in the Neuquén Basin (Rapela et al., 1983; Pángaro et al., 2002; Franzese et a., 2006, Pángaro et al., 2009). This value is 25 My older than synrift volcanic rocks dated in the southern of Neuquén Basin in subsurface of the Huincul high (204 ± 0.2 and 199 ± 1.5 Ma; Schiuma and Llambías, 2008) and 30 My older than the Piedra del Águila Formation (192 ± 3 Ma; Spalletti et al, 2010). Thus, the correlation between the synrift volcanic sequences of the Río Grande depocenter (Cerro Negro Andesite) with other synrift deposits to the south of the basin is not reasonable based on their age differences.

On the other hand, the age of the El Freno Formation is assigned roughly between the Late Triassic and Early Jurassic but the precise age is still under discussion. Stratigraphic relationships are difficult to establish because it is highly deformed by the Late Cretaceous and Neogene folding and thrusting (Spalletti et al., 2005; Bechis et al., 2009). The minimum age in the Sinemurian is constrained by the overlying Puesto Araya Formation, which is assigned to the Sinemurian-Toarcian (Damborenea and Maceñido, 1993). However, the top of the El Freno Formation is diachronic and transitional with the marine sediments of the Puesto Araya Formation (Riccardi et al., 1988) and this relation introduces local uncertainties concerning the relative ages of both units. An additional difficulty comes from the fact that the base of the El Freno Formation in the Río Atuel section is not exposed (Damborenea, 1993; Gulisano and Gutiérrez Pleimling, 1994): it is in fault contact with marine sedimentary rocks of the Arroyo Malo Formation which was assigned to the Rhaetian-Hettangian (Riccardi et al., 1997; Riccardi and Iglesias Llanos, 1999). Moreover, according to some authors the Arroyo Malo Formation may be a lateral equivalent of the lower part of the El Freno Formation (Giambiagi et al., 2008; Tunik et al., 2008). On the other hand, studies by Spalletti et al. (2005; 2007) considered that the age of the El Freno Formation is Early Jurassic (Sinemurian) based on sedimentological, stratigraphic and paleobotanical data. Therefore it is important to define a maximum depositional age of the El Freno Formation based on their U-Pb detrital zircon ages.

The data presented here show that the statistically most significant youngest peak in the El Freno Formation is ca. 204 Ma according to the frequency histogram and relative probability plots of the AR-07 sample (Figure 7). This youngest age peak is formed by two single ages at 204 ± 2 and 206 ± 1 Ma which are overlapping in age at 1 sigma. In the sample AR-08 there is not a statistically significant young peak, but the youngest zircon at 203 ± 2 Ma (AR-08) is compatible with the peak at 204 Ma considering the error. Therefore, the most reliable maximum depositional age for us is at ca. 204 Ma into the Rhaetian at the end of the Triassic (numerical age and name follow the International Commission on Stratigraphy; Cohen et al., 2013). This value indicates that the El Freno Formation was deposited during the end of the Triassic and the earliest Early Jurassic (Rhaetian-Hettangian age). A potential correlation between the El Freno Formation and the Remoredo Formation from the Río Grande depocenter cannot be ruled out; new U-Pb analyses in course can provide reliable information about the absolute age of the Remoredo Formation.

The maximum depositional age obtained here for the El Freno Formation (ca. 204 Ma) resulted at least 20 My younger than the crystallization age of the Andesite Cerro Negro (223.3 ± 1.9 Ma). Thus, it is possible to suggest two different pulse of rifting according to the available absolute ages, the oldest represented by the Andesite Cerro Negro with a Norian age and developed in the northwestern of the basin and another younger pulse in Rhaetian to Sinemurian, represented by clastic and volcanic deposits in several depocenters from the north and south of the basin (e.g.: El Freno, Remoredo, Piedra del Águila formations).

6.2. Maximum depositional age of the Tordillo Formation

In contrast to the El Freno Formation, the red beds of the Tordillo Formation have a good stratigraphic control and are well represented through the entire Neuquén Basin. The age of the Tordillo Formation is classically assigned to the Kimmeridgian to earliest Tithonian age. This unit is unconformably deposited over the Lotena Group (Callovian-Oxfordian) and is conformably covered by the overlying Vaca Muerta Formation. The age of the base of Vaca Muerta Formation is late early Tithonian while the top is early Valanginian, based on its abundant ammonoid fauna and other biostratigraphic markers (Vennari et al., 2014; and references therein). U-Pb (LA-MC-ICP-MS) detrital zircon ages for several samples of the Tordillo Formation distributed through the central and southern part of the Neuquén Basin were recently obtained, and the ages indicating a statistically robust measure of the maximum depositional age at ca. 144 Ma (see for discussion Naipauer et al., 2012; 2015). This peak is in agreement with other ages obtained in the Río Damas-Tordillo Formation, close to the Chile and Argentina border, at ca. 146 Ma (Rossel et al., 2014). Also, U-Pb detrital zircon ages separated from Lagunillas Formation in the Tarapacá Basin, north of Chile, yielded a group of younger ages between 148.5 ± 5.1 and 144.6 ± 3.5 Ma (Oliveros et al., 2012) which support the temporal correlation between Lagunillas and Tordillo formations. It is important to note that the U-Pb results showed a discrepancy of at least 7 Ma with the absolute ages accepted for the Kimmeridgian (ca. 157 – 152 Ma) and Tithonian (ca. 152 – 145 Ma) boundaries in the chronostratigraphic timescale of Cohen et al. (2013).

Figure 10 around here

In the samples of the Tordillo Formation from the Atuel-La Valenciana depocenter the youngest graphical peaks are at ca. 152 Ma (AR-09), 149 Ma (JTCC-420), 151 Ma (AR-11), and 149 Ma (JTRS-407). These values between 149 and 152 Ma are considered here as the maximum depositional ages of the Tordillo Formation in the northern part of the basin. The maximum age at ca 152 Ma indicates a post-Kimmeridgian deposition during the Tithonian, according to the numerical age proposed by the International Commission on Stratigraphy (Cohen et al., 2013). As well as in other places of the Neuquén Basin, the U-Pb ages calculated for the Tordillo Formation do not agree with sedimentation during the Kimmeridgian, if the absolute age of the Kimmeridgian-Tithonian boundary is accepted at 152.1 ± 0.9 Ma following Cohen et al. (2013). In the Atuel-La Valenciana depocenter it should be noted that the values between 152 and 149 Ma are older than the peak at ca. 144 Ma obtained in the Tordillo Formation from the central and southern part of the basin (Naipauer et al., 2015). There may be two ways to explain the discrepancy in the maximum ages. The most probable is that the red-beds here analyzed correspond to the base of the Tordillo Formation; but it is difficult to define the precise correlations with other parts of the basin because the Tordillo sections are condensed in the study area (Mescua et al., 2014). Another possibility is that the source rocks supplying the youngest zircons of ca. 144 Ma in the central part of the basin, is absent in the north.

6.3. Source regions

Rift stage (El Freno Formation)

Sedimentary provenance analyses in the synrift deposits have been carried out for rocks of the Atuel-La Valenciana depocenter. Sandstone petrographic data in the Arroyo Malo, El Freno, and Puesto Araya formations show a clear provenance from volcanic sources (Lanés et al. 2008; Tunik et al. 2008). Paleocurrent analyses of the El Freno Formation indicate potential eastern and southeastern source regions and point out to the San Rafael Block as the main source (Lanés 2005; Spalletti et al., 2007; Tunik et al. 2008). The petrographic analyses of this unit indicate provenance from a volcanic arc or a dissected arc according to the Dickinson et al. (1983) diagram (Tunik et al., 2008). Moreover, these studies suggest that the main volcanic and plutonic source rocks were the Choiyoi magmatic province with minor participation of the Precuyano magmatism.

The U-Pb detrital zircon ages are consistent with the previous analyses. However, the summary of the detrital zircon ages of the El Freno Formation produced a more detailed picture of the source rocks (Figure 10). The data show that the main source rock of sediment is Late Permian to Early Triassic with maximum peaks at ca. 253 Ma, 262 Ma, and 272 Ma. These peaks are consistent with the age of the Choiyoi magmatic province. This source probably was close to the Atuel depocenter since the zircon grains analyzed have subidiomorphic to idiomorphic forms (Figure 7). There are many outcrops of Choiyoi rocks in the surrounding area of the region, indicating that they possibly acted as source regions for the El Freno Formation sediments. Towards the south, the El Fortín sedimentary and volcanic complex has the U-Pb age of ca. 250 Ma (Llambías et al., 2005) and to the east, in the San Rafael Block, the Choiyoi magmatism has U-Pb ages of ca. 252 Ma, 265 Ma, and 281 Ma (Rocha-Campos et al., 2011). All of these ages are consistent with the age peaks and the paleocurrents observed in the El Freno Formation.

The peaks in the Middle Triassic at ca. 243 Ma and 230 Ma are compatible with magmatic sources of the post-Choiyoi magmatism associated with extensional tectonics (Uliana et al., 1989; Ramos and Kay, 1991; Sato et al., 2015). Many U-Pb ages between 246 and 230 Ma are described in tuffs and volcanic rocks to the east and northeast of the studied region (Ávila et al., 2006; Spalletti et al., 2008; Mancuso et al., 2010; Barredo et al., 2011). In the San Rafael Block, acidic volcanic rocks from the Puesto Viejo Group (Cuyo Basin) were recently dated at ca. 236 Ma (U-Pb SHRIMP; Ottone et al., 2014).

An additional major source of Late Triassic detrital contribution is defined by peaks at ca. 204 Ma, 212 Ma, and 224 Ma (Figure 10). The older peak is consistent with the age of the Cerro Negro Andesite suggesting that it was exhumed during the deposition of the El Freno Formation. The youngest peak at ca. 204 Ma is similar to the values published by Schiuma and Llambías (2008) for volcanic rocks from two hydrocarbon boreholes located along the Huincul High. According to the idiomorphic shape of the zircons observed in the El Freno Formation (see Figure 7a), this could be interpreted as a volcanism coeval or slightly older than the sedimentation of the El Freno Formation.

Retroarc stage (Tordillo Formation)

Previous provenance analyses of the Tordillo Formation from the Atuel-La Valenciana depocenter were performed by Mescua et al. (2008). These authors presented a provenance study based on sandstone petrography showing that the sediment came from two main source regions: a basic volcanic source associated with the contemporaneous retroarc volcanism (Río Damas Formation), and a basement source composed of acidic volcanic and plutonic rocks (Choiyoi magmatic province) and metamorphic rocks. These interpretations are supported by the pattern of detrital zircon ages presented in this work (Figure 11). It may be also emphasized, however, that the composition of the source area is much more complex according to the multimodal distribution of the age peaks.

The summary of the U-Pb zircon ages of the Tordillo Formation shows that the main source areas of sediment supply were: a) the Jurassic magmatic arc developed to the west of the Atuel-La Valenciana depocenter, and b) the igneous-metamorphic basement located to the east. The major peak at ca. 152 Ma indicates that the volcanic rocks from the Río Damas Formation were one of the main volcanic sources; this magmatism was coeval with the deposition of the clastic sediments of the Tordillo Formation. Early to Middle Jurassic peaks suggest that older volcanic rocks of the Andean arc were also part of the source area. These zircon grains may also be derived from the reworking of previous sedimentary units which were probably exhumed during the tectonic extension observed in the Tordillo Formation (Mescua et al., 2008; 2014). Late Triassic grains might be derived from reworking of previous volcanic and sedimentary units located to the west of the Atuel-La Valenciana depocenter in a structural basement high (e.g.: Tordillo High).

Middle Triassic sources are well represented in the pattern of detrital ages. These ages possibly indicate source areas related to the post-Choiyoi magmatism (Sato et al., 2015). Moreover, there are age peaks consistent with the Choiyoi magmatism indicating that these rocks were also source of the original sediments. These source rocks are located to the east in the San Rafael Block and surrounding areas.

Figure 11 around here

The provenance of the Carboniferous zircons remains difficult to explain due to the absence of igneous rocks with this age in the surrounding areas. During the Late Carboniferous in the south of Mendoza province a marine and continental retroarc basin developed, locally known as the San Rafael basin in the San Rafael Block, where a thick sedimentary sequence of the El Imperial Formation was the main infill (Azcuy et al., 1999). To the west of the Atuel-La Valenciana depocenter, in the Tordillo High, a small outcrop of metasedimentary rocks (Arroyo Mendino Formation), which could be equivalent to the El Imperial Formation, was identified (Aparicio, 1950). Therefore the Late Carboniferous detrital zircons could be derived from reworking of the El Imperial-Arroyo Mendino formations but a complete U-Pb data set for these rocks is not available (Rocha-Campos et al., 2011). An alternative is a western provenance, from the Coastal Cordillera of Chile (Figure 2), where an extended Late Carboniferous batholith is exposed. U-Pb ages of these igneous rocks range between 300 and 320 Ma (Hervé et al., 2013). The problem with this alternative is that the detritus would need to cross over the coeval Late Jurassic volcanic arc, even though these zircons may be recycled from Triassic-Jurassic deposits. Thus, the provenance of the Carboniferous detrital zircons remains poorly understood.

It is much simpler to identify the source regions of the Neoproterozoic and Mesoproterozoic zircons since basement exposures with these ages are recognized to the east, in the San Rafael Block (Abre et al., 2012; Thomas et al., 2012). Precambrian ages are interpreted as a signal of the cratonic region, recorded in the Atuel-La Valenciana depocenter because of its proximity to the San Rafael Block.

The pattern of detrital zircon ages described in the Tordillo Formation of the Atuel-La Valenciana depocenter is similar to those found in samples from the south of the Neuquén Basin (Naipauer et al., 2012; 2015). However, peaks in the Carboniferous (ca. 308 Ma and 328 Ma) and several single ages in the Neoproterozoic and Mesoproterozoic in the Atuel-La Valenciana depocenter (Figure 11) are absent in samples south of the basin. This is possibly due to the shape of the basin, its proximity to the San Rafael Block, and the extensional control on deposition of the Tordillo Formation at the latitude of this depocenter.

6.4. Comparison of the pattern of zircon ages between the Neuquén and Tarapacá basins

The Tarapacá Basin is a retroarc basin located between 20º and 28º SL in the northern Chilean Andes (Figure 1b), and just as the Neuquén Basin was filled by marine and continental deposits interbedded with volcanic rocks related to the Andean arc (Oliveros et al., 2012 and references therein). Two transgressive-regressive cycles deposited between the Jurassic and Early Cretaceous was recognized in the infill of the basin. A sequence composed by red sandstones, coarse conglomerates and lava flows reaching over 400 m of thickness, deposited during the Late Jurassic, marks the end of the first transgressive-regressive cycle. In the south of the Tarapacá Basin, these red sediments and volcanic deposits are grouped in the Lagunillas Formation which is correlated to the Tordillo Formation of the Neuquén Basin based on their stratigraphic position, depositional environment, and maximum depositional age (Kimmeridgian-Tithonian) (Oliveros et al., 2012; Naipauer et al., 2015). This correlation indicates that the marine regression of the first cycle was synchronous over extensive regions of the Andean margin between 20º and 40º SL (Vicente, 2006; Oliveros et al., 2012). The depositional facies in the regressive cycle were controlled by several factors as eustatic sea-level changes, tectonics and magmatic activity rates in the arc, but the relative importance of each factor is not clear (Hallam, 1991; Vicente, 2006; Oliveros et al., 2012).

The provenance patterns of these deposits could provide key elements to understand the paleogeography and the relative importance of the tectonic and magmatic activities in the Andean margin during the end of the first marine regressive cycle. The detrital zircon ages of the Andean retroarc basin (Neuquén and Tarapacá) during the Late Jurassic are characterized by the dominance of Jurassic zircons, derived mainly from the coeval magmatic arc (Figure 12a). The participation of the Andean arc as the main source rock in the analyzed basins confirmed the importance of the volcanic arc activity during this regressive cycle (Eppinger and Rosenfeld, 1996).

The abundance of Early Paleozoic and Precambrian zircons represents the major difference between the units in the Neuquén and Tarapacá basins. It is interpreted that these zircons came from the cratonic blocks in the eastern margin of the basin. The exhumation of the cratonic region can be explained in several ways in the analyzed zone. In the southern depocenters of the Neuquén Basin, Precambrian detrital ages are absent from the age populations of the Tordillo Formation. The shape of the basin with a large embayment where basement regions were probably covered by previous sediments could explain the absence of older zircons. Devonian and Permian zircons are the only present ages; this fact is interpreted as derivation from an ancient positive element within the southern Neuquén Basin, known as the Huincul deformation zone (Naipauer et al., 2012). Several studies have recently proposed a contractional intraplate deformation to explain the complex structure, uplift and exhumation of the Huincul deformation zone during the Jurassic (Naipauer et al. 2012 and references therein). To the north in the Atuel-La Valenciana depocenter, the pattern of detrital zircon ages of the Tordillo Formation showed a signal of Paleozoic and Precambrian ages (Figure 12a). The presence of these zircons is interpreted as a result of its proximity to the San Rafael Block. In this area, the basin occupies a narrow zone between the volcanic arc and the cratonic region. An alternative hypothesis is to interpret an exhumation of basement rocks due to the renewed extensional activity during the deposition of the Tordillo Formation as is proposed in the northern Neuquén Basin (Mescua et al., 2008; 2014). Finally, in the Tarapacá Basin, the Lagunillas Formation has an important input of Precambrian and Paleozoic zircons (Figure 12a). This is probably because Precambrian and Early Paleozoic basement outcrops in the Arequipa-Antofalla and Pampia terranes were located in the eastern border of the basin. Oliveros et al. (2012) infer that these regions were progressively exhumed during the deposition of Lagunillas Formation and this allowed a voluminous contribution of old zircons. The causes of the exhumation of the basement rocks during the Late Jurassic are still unknown, but it could have been controlled by extensional faults located in the eastern border of the Tarapacá Basin as proposed by Oliveros et al. (2012).

6.5. Detrital zircon ages and the record of the magmatism in the southern Central Andes

The sedimentary record and specially the detrital zircon ages of the Andean retroarc basin should reflect the main peaks of magmatic activity along the southern Central Andes. The direct correlation between igneous activity and detrital zircon spectra is discussed but there are several examples around the world showing that crystallization ages of detrital and igneous zircons display remarkably similar patterns if the data set are large (Condie et al., 2009; 2011; Belousova et al., 2010; Hawkesworth et al., 2014; Paterson and Ducea, 2015). These contributions investigate the processes involved in the generation and the evolution of the continental crust but many authors have used the sedimentary record as a valid representation of the magmatic record (Hawkesworth et al., 2010; Cawood et al., 2012; Paterson and Ducea, 2015).

Early studies have defined the main magmatic pulses in the Andes according to different age databases (Ramos and Ramos, 1979; Perez and Ramos, 1990). The maximum frequency peaks obtained before do not coincide with those found in our work because the ages were mainly obtained by the K-Ar method, indicating minimum ages. Here we used the summary of the 330 Jurassic and Triassic zircon grains analyzed by U-Pb (LA-MC-ICP-MS) in the Tordillo and Lagunillas formations (Naipauer et al., 2012, 2015; Oliveros et al., 2012). The dataset showed peaks and troughs in the pattern of ages which are interpreted as corresponding to periods of maximum and minimum magmatic activity in the Andean and proto-Andean margin of Gondwana (Figure 12b). In the Triassic, a waning in activity is observed between ca. 243 and 204 Ma which is coherent with a decreasing magmatism related to the final break-up of Pangea (Mpodozis and Ramos, 2008). A major trough is observed at ca. 200 Ma in the boundary between the Triassic and the Jurassic, which suggests a decrease of the synrift magmatism along the Andean margin and the end of the Choiyoi magmatism (Sato et al., 2015). Since the Early Jurassic the magmatism has increased and two maximum age peaks of ca. 191 and 179 Ma are observed. A small trough at ca. 165 Ma is observed suggesting a decrease in the magmatic activity in the Middle Jurassic, but it quickly increases again during the Late Jurassic with two peaks at ca. 153 and 144 Ma (Figure 12b). The increase in magmatic activity during the Early Jurassic is attributed to the beginning of the new Andean magmatic cycle by the onset of the subduction (Mpodozis and Ramos, 1989; 2008; Oliveros et al., 2006). The trough at ca. 165 Ma and the later increase in the Late Jurassic can be explained by changes in the subduction regime, for example the relative convergence rate (Ramos, 2010), or by the shift to a more mafic composition of the magmatism with smaller zircon fertility. However, the mechanism and causes of changes in the magmatic activity and composition along the Andes are still poorly understood (Ramos and Folguera, 2005). In summary the age pattern obtained could be interpreted as a record of the magmatic activity during the Triassic and Jurassic of the southern Central Andes. Future U-Pb analyses on zircons from igneous and sedimentary rocks from the Central Andes are required for improving the results of this first approach.

Figure 12 around here

7. Summary and concluding remarks

The U-Pb age of 223.3 ± 1.9 Ma is interpreted as the best age for the timing of eruption of the Cerro Negro Andesite in the Río Grande depocenter and is the oldest absolute age obtained for the Precuyano Cycle in the Neuquén Basin. In contrast, this coeval synrift magmatism is not developed in the Atuel depocenter. The maximum depositional age at ca. 204 Ma obtained for the El Freno Formation indicates that the continental synrift sediments are at least 20 My younger than the synrift volcanism of the Cerro Negro Andesite. Thus, the correlation between the clastic continental synrift sequences from the Atuel Depocenter and the volcanic rocks from the Río Grande depocenter is not reasonable. Two different pulses of rifting according to the available absolute ages could be recognized, the oldest was developed during the Norian and the younger during the Rhaetian-Sinemurian.

The source regions for the clastic sediments of the El Freno Formation were locally and strongly influenced by the active volcanism coeval with an extensional tectonic regime. The U-Pb data show that the magmatic rocks from the Choiyoi magmatic province represents the main source rocks of sediment supply in the Atuel-La Valenciana depocenter. However, an important amount of detrital zircons with Middle to Late Triassic ages from the post-Choiyoi magmatic province is identified.

The maximum depositional age for the Tordillo Formation in the Atuel-La Valenciana depocenter is at ca. 149 Ma. As well as in other places of the Neuquén Basin, the U-Pb ages calculated in the Late Jurassic Tordillo Formation do not agree with the absolute age of the Kimmeridgian-Tithonian boundary (ca. 152 Ma).

The pattern of detrital ages of the Tordillo Formation is much broader than that defined for the same unit in the southern part of the basin. The main source region of sediments was the Andean magmatic arc developed to the west, but age peaks at the Carboniferous, Neoproterozoic, and Mesoproterozoic suggest participation of cratonic sources, which are well exposed to the east, in the San Rafael Block.

The pattern of zircon ages summarized for the Tordillo and Lagunillas formations should be interpreted as a record of the episodic nature of magmatic activity during the Triassic and Jurassic in the southern Central Andes. A waning of the magmatism is inferred to have happened during the Triassic. The evident age gap observed around ca. 200 Ma suggests cessation of the synrift magmatism. The later increase in magmatic activity during the Early Jurassic is attributed to the onset of Andean subduction. The trough at ca. 165 Ma and the later increase in the Late Jurassic could be explained by changes in the relative convergence rate in the Andean subduction regime, or by the shift to a more mafic composition of the magmatism with minor zircon fertility.

Acknowledgments

The authors acknowledge the financial support provided by CONICET and ANPCyT PICT-2010-2099 from Argentina; the FONDECYT grant 1120272 from Chile; and CNPq, CAPES and FINEP, for continuous financial support to the Geochronology Laboratory of the Universidade de Brasília. This is the contribution R-162 of the Instituto de Estudios Andinos "Don Pablo Groeber" (CONICET-UBA). We are grateful to the V. Oliveros (Universidad de Concepción, Chile) and another anonymous reviewer for their valuable comments and suggestions which greatly enhanced the manuscript.

References

Abre, P., Cingolani, C.A., Cairncross, B., Chemale Jr., F, 2012. Siliciclastic Ordovician to Silurian units of the Argentine Precordillera: Constraints on Provenance and tectonic setting in the Proto-Andean margin of Gondwana. Journal of South American Earth Sciences, 40, 1022.

Aguirre-Urreta, M.B., Pazos, P.J., Lazo, D.G., Fanning, C.M., Litvak, V.D., 2008. First U-Pb SHRIMP age of the Hauterivian stage, Neuquén Basin, Argentina. Journal of South American Earth Sciences, 26: 91-99.

Aguirre-Urreta, B., Lescano, M., Schmitz, M.D., Tunik, M., Concheyro, A., Rawson, P.F., Ramos, V.A., 2015. Filling the gap: new precise Early Cretaceous radioisotopic ages from the Andes. Geological Magazine 152(3): 557-564.

Aparicio, E.P., 1950. Hallazgo de sedimentos paleozoicos en las cabeceras del río Salado, Malargüe, Mendoza. Revista de la Asociación Geológica Argentina, 5(3), 127-135.

Avila, J.M., Chemale Jr., F., Mallmann, G., Kawashita, K., Armstrong, R., 2006. Combined stratigraphic and isotopic studies of Triassic strata, Cuyo Basin, Argentine Precordillera. Geological Society of America, Bulletin, 118, 1088-1098.

Azcuy, C.L., Carrizo, H.A., Caminos, R., 1999. Carbonífero y Pérmico de las Sierras Pampeanas, Famatina, Precordillera, Cordillera Frontal y Bloque de San Rafael. Geología Argentina, Anales del Instituto de Geología y Recursos Minerales 29, 261-318.

Balgord, E. A., Carrapa, B. 2015. Basin evolution of Upper Cretaceous–Lower Cenozoic strata in the Malargüe fold-and-thrust belt: northern Neuquén Basin, Argentina. Basin Research. doi: 10.1111/bre.12106

Barredo, S., Chemale, F., Ávila, J.N., Marsicano, C., Ottone, E.G., Ramos, V.A., 2012. Tectono-sequence stratigraphy and U-Pb zircon ages of the Rincon Blanco depocenter, northern Cuyo rift, Argentina. Gondwana Research, 21, 624-636.

Bechis, F., Giambiagi, L.B., Lanés, S., García, V.H., Tunik, M.A., 2009. Evidencias de extensión oblicua en los depósitos de sinrift del sector norte de la cuenca Neuquina. Revista de la Asociación Geológica Argentina, 65, 293-310.

Belousova, E.A., Kostitsyn, Y.A., Griffin, W.L., Begg, G.C., O'Reilly, S.Y., Pearson, N.J., 2010.
The growth of the continental crust: constraints from zircon Hf-isotope data. Lithos, 119, 457–466.

Bracaccini, O., 1970. Rasgos tectónicos de las acumulaciones Mesozoicas en las provincias de Mendoza y Neuquén. Revista de la Asociación Geológica Argentina, 35(2), 275-284.

Carbone, O., Franzese, J., Limeres, M., Delpino, D. and Martínez, R. 2011. El Ciclo Precuyano (Triásico Tardío - Jurásico Temprano) en la Cuenca Neuquina. In: Leanza, H.A, Arregui, C., Carbone, O., Danieli, J.C., Vallés, J.M. (Eds.), Geología y Recursos Naturales de la Provincia de Neuquén. Relatorio del VXIII Congreso Geológico Argentino, Buenos Aires, 63-75.

Cawood, P.A., Hawkesworth, C.J., Dhuime, B., 2012. Detrital zircon record and tectonic setting. Geology, 40, 875-878.

Charrier, R., Pinto, L. Rodríguez, M.P., 2007. Tectonostratigraphic evolution of the Andean Orogen in Chile. In: Moreno, T., Gibbons, W. (Eds.), The Geology of Chile. Geological Society, London, 21-114.

Charrier, R., Ramos, V.A., Tapia, F., Sagripanti, L., 2015. Tectono-stratigraphic evolution of the Andean Orogen between 31º and 37ºS (Chile and Western Argentina). In: Sepúlveda, S., Giambiagi, L., Pinto, L., Moreiras, S., Tunik, M., Hoke, G., Farías, M. (Eds.), Geodynamic Processes in the Andes of Central Chile and Argentina, Geological Society, Special Publications 399: 13-61, London.

Cohen, K.M., Finney, S.C., Gibbard, P.L., Fan, J.X., 2013. The ICS International Chronostratigraphic Chart. Episodes, 36, 199-204.

Condie, K.C., Belousova, E., Griffin, W.L., Sircombe, K.N., 2009. Granitoid events in space and time: Constraints from igneous and detrital zircon age spectra. Gondwana Research, 15, 228-242.

Condie, K.C., Bickford, M.E., Aster, R.C., Belousova, E., Scholl, D.W., 2011. Episodic zircon ages, Hf isotopic composition, and the preservation rate of continental crust. Geological Society of American, Bulletin, 123 (5/6), 951–957.

Cristallini, E.O., Tomezzoli, R.N., Pando, G., Gazzera, C., Martínez, J.M., Quiroga, J., Buhler, M., Bechis, F., Barredo, S., Zambrano, O., 2009. Controles precuyanos en la estructura de la cuenca Neuquina. Revista de la Asociación Geológica Argentina, 65, 248-264.

Damborenea, S.E., 1993. Formación El Freno. In Riccardi, A.C., Damborenea, S.E. (Eds.), Léxico Estratigráfico de la República Argentina, Volumen IX Jurásico. Asociación Geológica Argentina, Serie B, 21, 160-161.

Damborenea S.E., Maceñido, M.O., 1993. Formación Puesto Araya. In Riccardi, A.C., Damborenea, S.E. (Eds.), Léxico Estratigráfico de la República Argentina, Volumen IX Jurásico, Asociación Geológica Argentina, Serie B, 21, 345.

Davidson, J., Vicente, J. 1973. Características paleogeográficas y estructurales del área fronteriza de las nacientes del Teno (Chile) y Santa Elena (Argentina)(Cordillera Principal, 35° a 35°15’ latitud sur). V Congreso Geológico Argentino, v. 5, p. 11-55.

Dellapé, D.A., Pando, G.A., Uliana, M.A., Musacchio, E.A., 1978. Foraminíferos y ostrácodos del Jurásico en las inmediaciones del arroyo Picún Leufú y la ruta 40 (Provincia del Neuquén, Argentina) con algunas consideraciones sobre la estratigrafía de la Formación Lotena. VII Congreso Geológico Argentino, Actas II, 489-507, Buenos Aires.

Di Giulio, A., Ronchi, A., Sanfilippo, A., Tiepolo, M., Pimentel, M., Ramos, V.A., 2012. Detrital zircon provenance from the Neuquén Basin (South Central Andes): Cretaceous geodynamic evolution and sedimentary response in a retroarc-foreland basin. Geology, 40, 559-562.

Digregorio, R.E., Gulisano, C.A., Gutiérrez-Pleimling, A.R., Minitti, S.A., 1984. Esquema de la evolución geodinámica de la Cuenca Neuquina y sus implicancias paleogeográficas. IX Congreso Geológico Argentino, Actas II, 147-162, San Carlos de Bariloche.

Eppinger, K.J., Rosenfeld, U., 1996. Western margin and provenance of sediments of the Neuquén Basin (Argentina) in the Late Jurassic and Early Cretaceous. Tectonophysics, 259, 229-244.

Franzese, J.R., Spalletti, L.A. 2001. Late Triassic-early Jurassic continental extension in southwestern Gondwana: tectonic segmentation and pre-break-up rifting. Journal of South American Earth Sciences, 14, 257-270.

Franzese, J.R., Veiga, G.D., Schwarz, E., Gómez-Pérez, I., 2006. Tectono-stratigraphic evolution of a Mesozoic graben border system: the Chachil depocenter, southern Neuquén Basin, Argentina. Journal of the Geological Society of London, 163, 207-221.

Franzese, J.R., Veiga, G.D., Muravchik, M., Ancheta, M.D., D'Elía, L., 2007. Estratigrafía de 'sin-rift' (Triásico Superior-Jurásico Inferior) de la Cuenca Neuquina en la sierra de Chacaico, Neuquén, Argentina. Revista Geológica de Chile, 34(1), 49-62.

Gerth, E., 1931. La estructura geológica de la Cordillera argentina entre el río Grande y río Diamante en el sur de la provincia de Mendoza. Academia Nacional de Ciencias, Actas, v. 10, p. 125-172.

Giambiagi, L.B., Bechis, F., Lanés, S., Tunik, M.A., García, V.H., Suriano, J., Mescua, J.F., 2008. Formación y evolución triásico-jurásica del depocentro Atuel, cuenca Neuquina, provincia de Mendoza. Revista de la Asociación Geológica Argentina, 63, 520-533.

Giambiagi, L., Ghiglione, M., Cristallini, E., Bottesi, G., 2009, Kinematic models of basement/cover interactions: Insights from the Malargüe fold and thrust belt, Mendoza, Argentina. Journal of Structural Geology, 31, 1443–1457.

Giambiagi, L.B., Mescua, J.F., Bechis, F., Tassara, A., Hoke, G., 2012, Thrust belts of the southern Central Andes: Along-strike variations in shortening, topography, crustal geometry and denudation: Geological Society of America Bulletin, 124, 1339-1351.

González Díaz, E.F., 1972. Descripción geológica de la Hoja 27d San Rafael, Mendoza. Servicio Geológico Minero, Buenos Aires, Boletín 132.

Groeber, P. 1947. Observaciones geológicas a lo largo del meridiano 70°. 4, Hojas Bardas Blancas y Los Molles, Revista de la Asociación Geológica Argentina 2, p. 409-433. Reprint in Asociación Geológica Argentina, Serie C, Reimpresiones (1980).

Groeber, P., 1948. Las plataformas submarinas y su edad. Revista Ciencia e Investigación, 6, 224-231.

Gulisano, C.A., 1981. El ciclo cuyano en el norte de Neuquén y sur de Mendoza. XVIII Congreso Geológico Argentino, Actas III, 573-592, San Juan.

Gulisano, C.A., Gutiérrez Pleimling, A.R., 1994. Guía de campo El Jurásico de la Cuenca Neuquina, b) Provincia de Mendoza. Asociación Geológica Argentina, Serie E 3, 1-103, Buenos Aires.

Hallam, A., 1991. Relative importance of regional tectonics and eustasy for the Mesozoic of the Andes. In: Macdonald, D.I.M. (Ed.), Sedimentation, Tectonics and Eustasy: Sea-level Changes at Active Margins, vol. 12. Special publication of the International Association of Sedimentologists, pp. 189e200.

Hawkesworth, C., Dhuime, B., Pietranik, A., Cawood, P., Kemp, T., Storey, C., 2010. The Generation and Evolution of the Continental Crust: Journal of the Geological Society, 167, 229-248.

Hawkeswortha, C., Cawood, P., Dhuime, B., 2014. Continental growth and the crustal record. Tectonophysics 609, 651-660.

Hervé, F., Calderón, M., Fanning, C.M., Pankhurst, R.J., Godoy, E., 2013. Provenance variations in the Late Paleozoic accretionary complex of central Chile as indicated by detrital zircons. Gondwana Research, 23, 1122-1135.

Jordan, T. 1995. Retroarc foreland and related basins. In: Busby, C. and Ingersoll, R.V. Tectonics of sedimentary basins. Cambridge, Mass., USA, Blackwell Science, Chapter 9, 331-362.

Kamo, S.L., Riccardi, A.C., 2009. A new U-Pb zircon age for an ash layer at the Bathonian-Callovian boundary, Argentina. GFF, 131, 177-182.

Kay, S.M., Ramos, V.A., Mpodozis, C., and Sruoga, P., 1989. Late Paleozoic to Jurassic silicic magmatism at the Gondwana margin: Analogy to middle Proterozoic in North America? Geology, 17, 324-328.

Kleiman, L.E., Japas, M.S., 2009. The Choiyoi volcanic province at 34°S–36°S (San Rafael, Mendoza, Argentina): Implications for the late Palaeozoic evolution of the southwestern margin of Gondwana. Tectonophysics, 473, 283-299.

Kozlowski, E., Manceda, R., Ramos, V.A., 1993. Estructura. In Ramos, V.A. (Ed.), Geología y Recursos Naturales de Mendoza. XXII Congreso Geológico Argentino y II Congreso de Exploración de Hidrocarburos, Relatorio, 235-256.

Lanés, S., Palma, R.M., 1998. Environmental implications of oncoids and associated sediments from the Remoredo Formation (Lower Jurassic) Mendoza, Argetina. Palaeogeogr. Palaeoclimatol. Palaeoecol. 140, p. 357-366.

Lanés S., Salani, F.M., 1998. Petrografía, origen y paleoambiente sedimentario de las piroclastitas de la Formación Remoredo (Jurásico Temprano), Argentina (35°30'S-70°15'W). Rev. Geológica Chile 25, p. 141-152.

Lanés, S., 2005. Late Triassic to Early Jurassic sedimentation in northern Neuquén Basin, Argentina: Tectono-sedimentary evolution of the first transgression. Geologica Acta, 3(2), 81-106.

Lanés, S., Giambiagi, L., Bechis, F., Tunik, M., 2008. Late Triassic - Early Jurassic successions of the Atuel depocenter: sequence stratigraphy and tectonic controls. Revista de la Asociación Geológica Argentina, 63(4), 534-548.

Leanza, H.A., 1992. Estratigrafía del Paleozoico y Mesozoico anterior a los Movimientos Intermálmicos en la comarca del cerro Chachil, provincia del Neuquén. Revista de la Asociación Geológica Argentina, 45(3-4), 272-299.

Leanza, H.A., MAzzini, A., Corfu, F., Llambías, E.J., Svensen, H., Planke, S., Galland, O. 2013. The Chachil Limestone (Pliensbachian-earliest Toarcian) Neuquén Basin, Argentina: U-

Pb age calibration and its significance on the Early Jurassic evolution of southwestern Gondwana.

Legarreta, L., Kozlowski, E., 1984. Secciones condensadas del Jurásico-Cretácico de los Andes del sur de Mendoza: estratigrafía y significado tectonosedimentario. IX Congreso Geológico Argentino, v. 1, p. 286-297.

Legarreta, L., Gulisano, C.A., 1989. Análisis estratigráfico secuencial de la Cuenca Neuquina (Triásico superior-Terciario inferior, Argentina). In: Chebli, G., Spalletti, L. (Eds.), Cuencas Sedimentarias Argentinas. Serie Correlación Geológica (6) Universidad Nacional de Tucumán, 221-243.

Legarreta, L., Uliana, M.A., 1991. Jurassic–Cretaceous marine oscillations and geometry of backarc basin fill, central Argentine Andes. In: Macdonald, D.I.M. (Ed.), Sedimentation, Tectonics and Eustasy, Sea level Changes at Active Plate Margins, 12. International Association of Sedimentologists, Special Publication, 429-450, Oxford.

Legarreta, L., Gulisano, C.A., Uliana, M.A., 1993. Las secuencias sedimentarias Jurásico-Cretácico, in: Ramos, V.A. (Eds), Geología y Recursos Naturales de Mendoza, Relatorio 12° Congreso Argentino y 2° Congreso de exploración de hidrocarburos 1 (9), p. 87-114.

Legarreta, L., Uliana, M.A. 1999. El Jurásico y Cretácico de la Cordillera Principal y Cuenca Neuquina. In: Caminos, R. (Ed.), Geología Argentina. Instituto de Geología y Recursos Minerales, Buenos Aires, Anales, 29, 399-432.

Legarreta, L., Kokogian, D.A., Boggetti, D.A., 1989. Depositional sequences of the Malargüe Group (Upper Cretaceous-lower Tertiary), Neuquén Basin, Argentina. Cretaceous Research, 10, 337–356.

Llambías, E.J., Sato, A.M., 2011. Ciclo Gondwánico: la provincia magmática Choiyoi en Neuquén. In: Leanza, H.A, Arregui, C., Carbone, O., Danieli, J.C., Vallés, J.M. (Eds.), Geología y Recursos Naturales de la Provincia de Neuquén. Relatorio del VXIII Congreso Geológico Argentino, Buenos Aires, 53-62.

Llambías, E.J., Sato, A.M., Basei, M.A.S., 2005. El basamento prejurásico medio en el anticlinal Chihuido, Malargüe: evolución magmática y tectónica. Revista de la Asociación Geológica Argentina, 60(3), 567-578.

López de Azarevich, V.L., Escayola, M., Azarevich, M.B., Pimentel, M., Tassinari, C., 2009. The Guarguaraz complex and the Neoproterozoic- Cambrian evolution of southwestern Gondwana: geochemical signatures and geochronological constraints. Journal of South American Earth Sciences, 28(4), 333-344.

Manceda, R., Figueroa, D., 1995. Inversion of the Mesozoic Neuquén rift in the Malargüe fold-thrust belt, Mendoza, Argentina. In: Tankard, A.J. Suárez, R., Welsink, H.J. (Eds.), Petroleum Basins of South America. American Association of Petroleum Geologists, Memoir, 62, 369-382.

Mancuso, A.C., Chemale, F., Barredo, S.P., Ávila, J., Ottone, E.G., Marsicano, C., 2010. Age constraints for the northernmost outcrops of the Triassic Cuyana Basin, Argentina. Journal of South American Earth Sciences, 30, 97-103.

Mescua, J.F., Giambiagi, L.B., Bechis, F., 2008. Evidencias de tectónica extensional en el Jurásico Tardío (Kimmeridgiano) del suroeste de la provincia de Mendoza. Revista de la Asociación Geológica Argentina, 63(4), 512-519.

Mescua, J.F., Giambiagi, L.B., Tassara, A., Gimenez, M., Ramos, V.A., 2014. Influence of pre-Andean history over Cenozoic foreland deformation: Structural styles in the Malargüe fold-and-thrust belt at 35°S, Andes of Argentina. Geosphere, 10(3), 585-609.

Mosquera, A., Ramos, V.A., 2006. Intraplate deformation in the Neuquén Embayment. In: Kay, S.M., Ramos, V.A. (Eds.), Evolution of an Andean margin: A tectonic and magmatic view from the Andes to the Neuquén Basin (35º-39º lat). Geological Society of America Special Paper 407, 97-124.

Mpodozis, C., Ramos, V.A., 1989. The Andes of Chile and Argentina. In: Ericksen, G.E., Cañas, M.T., Reinemud, J.A. (Eds.), Geology of the Andes and Its Relation to Hydrocarbon and Mineral Resources Circumpacific Council for Energy and Mineral Resources, 11. Earth Science Series, 59-90.

Mpodozis, C., Ramos, V.A., 2008. Tectónica Jurásica en Argentina y Chile: extensión, subducción oblicua, rifting, deriva y colisiones? Revista de Asociación Geológica Argentina, 63 (4), 481-497.

Naipauer, M., García Morabito, E., Marques, J.C., Tunik, V., Rojas Vera, E., Vujovich, G.I., Pimentel, M.P., Ramos, V.A., 2012. Intraplate Late Jurassic deformation and exhumation in western central Argentina: Constraints from surface data and U-Pb detrital zircon ages. Tectonophysics, 524-525 (1), 59-75.

Naipauer, M., Tunik, M., Marques, J.C., Rojas Vera, E.A., Vujovich, G.I., Pimentel, M.M., Ramos, V.A., 2015. U-Pb detrital zircon ages of Upper Jurassic continental successions: implications for the provenance and absolute age of the Jurassic-Cretaceous boundary in the Neuquén Basin. In: Sepúlveda, S., Giambiagi, L., Pinto, L., Moreiras, S., Tunik, M., Hoke, G., Farías, M. (Eds.), Geodynamic Processes in the Andes of Central Chile and Argentina, 399. Geological Society of London, Special Publications, 399, p.131-154.

Naipauer, M., Ramos, VA., 2015. Changes in source areas at Neuquén Basin: Mesozoic evolution and tectonic setting based on U-Pb ages on zircons. In: Folguera, A. et al. (Eds.), Growth of the Southern Andes, Springer Brief Monography, accepted manuscript.

Nullo, F.E., Stephens, G., Combina, A., Dimieri, L., Baldauf, P., Bouza, P., 2005. Hoja Geológica 3569-III / 3572-IV Malargüe, Servicio Geológico y Minero Argentino, Boletín 346, 85 p., Buenos Aires.

Oliveros, V., Labbé, M., Rossel, P., Charrier, R., Encinas, A., 2012. Late Jurassic paleogeographic evolution of the Andean back-arc basin: New constrains from the Lagunillas Formation, northern Chile (27º 30´ - 38º 30´ S). Journal of South American Earth Sciences, 37, 25-40.

Ottone, E.G., Monti, M., Marsicano, C.A., de la Fuente, M.S., Naipauer, M., Armstrong, R. Mancuso, A.C., 2014. Age constraints for the Triassic Puesto Viejo Group (San Rafael depocenter, Argentina): SHRIMP U–Pb zircon dating and correlations across southern Gondwana. Journal of South American Earth Sciences, 56, 186-199.

Pángaro, F., Veiga, R., Vergani, G., 2002. Evolución tecto-sedimentaria del área de Cerro Bandera, Cuenca Neuquina, Argentina. V Congreso de Exploración y Desarrollo de Hidrocarburos, CD-ROM, 16 pp.

Pángaro, F., Pereira, D.M., Micucci, E., 2009. El sinrift de la Dorsal de Huincul, Cuenca Neuquina: evolución y control sobre la estratigrafía y estructura del área. Revista de la Asociación Geológica Argentina, 65(2), 265-277.

Pérez, D.J., Ramos, V.A., 1990. La actividad magmática Gondwánica. Late Paleozoic of South America, Annual Meeting of the Working Group, Abstracts, p. 89-92, Buenos Aires.

Ramos, E.D., Ramos, V.A., 1979. Los ciclos magmáticos de la República Argentina. VII Congreso Geológico Argentino, Actas I, 771-786, Buenos Aires.

Ramos, V.A., 1978. Estructura. VII Congreso Geológico Argentino, Relatorio, Neuquén, pp. 99-118.

Ramos, V.A., 1999. Las provincias geológicas del territorio argentino. In: Caminos, R.L. (Ed.), Geología Argentina. Segemar Anales, 29(3), 41-96.

Ramos, V.A., 2010. The tectonic regime along the Andes: Present-day and Mesozoic regimes. Geological Journal, 45, 2-25.

Ramos, V.A., Kay, S.M., 1991. Triassic rifting and associated basalts in the Cuyo basin, central Argentina. In: Harmon, R.S., Rapela, C.W. (Eds.), Andean Magmatism and its Tectonic Setting. Geological Society of America, Special Paper, 265, 79-91.

Ramos, V.A., Basei, M., 1997. The basement of Chilenia: an exotic continental terrane to Gondwana during the Early Paleozoic. In: Bradshaw, J.D., Weaver, S.D. (Eds.), Terrane Dynamics-97. International Conference on Terrane Geology, Conference Abstracts, 140-143, Christchurch.

Ramos, V.A., Folguera, A., 2005. Tectonic evolution of the Andes of Neuquén: Constraints derived from the magmatic arc and foreland deformation. In: Veiga, G.D., Spalletti, L.A., Howell, J.A., Schwarz, E., (Eds.), The Neuquén Basin: A case study in sequence stratigraphy and basin dynamics. Geological Society of London, Special Publications, 252, 15-35.

Ramos, V.A., Cegarra, M.I., Cristallini, E., 1996. Cenozoic tectonics of the High Andes of west-central Argentina (30–36°S latitude). Tectonophysics, 259, 185-200.

Rapela, C.W., Spalletti, L., Merodio, J., 1983. Evolución magmática y geotectónica de la "Serie Andesitica" andina (Paleoceno-Eoceno) en la Cordillera Norpatagónica. Revista de la Asociación Geológica Argentina 38, 469-484.

Riccardi, A.C., 1983. The Jurassic of Argentina and Chile. In: Moulade, M., Nairn, A.E.M., (Eds.), The Phanerozoic Geology of the World II, The Mesozoic B. Ed. Elsevier Scientific Publications, 201-263, Amsterdam.

Riccardi, A.C., Iglesia Llanos, M.P., 1999. Primer hallazgo de amonites en el Triásico de la Argentina. Revista de la Asociación Geológica Argentina, 54, 298-300.

Riccardi, A.C., Damborenea, S.E., Manceñido, M.O., Ballent, S.C., 1988. Hettangiano y Sinemuriano marinos en Argentina. V Congreso Geológico Chileno, Actas 2, C359-373, Santiago.

Riccardi, A., Damborenea, S.E., Manceñido, M.O, Scasso, S., Lanés, S., Iglesia Llanos, M.P., 1997. Primer registro de Triásico marino fosilífero de la Argentina. Revista de la Asociación Geológica Argentina 52, 228-234.

Rocha-Campos, A.C., Basei, M.A.S., Nutman, A.P., Kleiman, L.E., Varela, R., Llambías, E., Canile, F.M., da Rosa, O. de C.R., 2011. 30 million years of Permian volcanism recorded in the Choiyoi igneous province (W Argentina) and their source for younger ash fall deposits in the Paraná Basin: SHRIMP U-Pb zircon geochronology evidence. Gondwana Research, 19, 509-523.

Rossel, R., Oliveros, V., Mescua, J., Tapia, F., Ducea, M.N., Calderón, S., Charrier, R., Hoffman, D., 2014. The Upper Jurassic volcanism of the Río Damas-Tordillo Formation (33°-35.5°S): Insights on petrogenesis, chronology, provenance and tectonic implications. Andean Geology 41 (3), 529-557.

Sato, A.M., Llambías, E.J., Basei, M.A.S., Castro, C.E., 2015. Three stages in the Late Paleozoic to Triassic magmatism of southwestern Gondwana, and the relationships with the volcanogenic events in coeval basins. Journal of South American Earth Sciences, 63, 48-69.

Schiuma, M., Llambías, E.J., 2008. New ages and chemical analysis on Lower Jurassic volcanism close to the Huincul High, Neuquén. Revista de la Asociación Geológica Argentina, 63(4), 644-652.

Silvestro, J., Zubiri, M., 2008. Convergencia oblicua: modelo estructural alternativo para la Dorsal Neuquina (39ºS) – Neuquén. Revista de la Asociación Geológica Argentina, 63(1), 49-64.

Spalletti, L.A., Franzese, J.R., Morel, E. M., Artabe, A.E., 2005. Nuevo enfoque estratigráfico del Triásico-jurásico Temprano en la región del río Atuel, Provincia de Mendoza. XVI Congreso Geológico Argentino, Actas 3, 77-82, La Plata.

Spalletti, L.A., Morel, E.M., Franzese, J.R., Artabe, A.E., Ganuza, D.G., Zúñiga, A., 2007. Contribución al conocimiento sedimentológico y paleobotánico de la Formación El Freno (Jurásico Temprano) en el valle superior del río Atuel, Mendoza, Argentina. Ameghiniana, 44 (2), 367-386.

Spalletti, L.A., Fanning, C.M., Rapela, C.W., 2008. Dating the Triassic continental rift in the southern Andes: The Potrerillos Formation, Cuyo Basin, Argentina. Geologica Acta, 6, 267-283.

Spalletti, L.A., Franzese, J., Morel, E., D´Elia, L., Zúñiga, A., Fanning, M., 2010. Consideraciones acerca de la sedimentología, paleobotánica y geocronología de la Formación Piedra del Águila (Jurásico Inferior, Neuquén). Revista de la Asociación Geológica Argentina, 66(3), 305-313.

Spalletti, L.A., Arregui, C.D., Veiga, G.D., 2011. La Formación Tordillo y equivalentes (Jurásico Tardío) en la Cuenca Neuquina. In: Leanza, H.A, Arregui, C., Carbone, O., Danieli, J.C., Vallés, J.M. (Eds.), Geología y Recursos Naturales de la Provincia de Neuquén. Relatorio del VXIII Congreso Geológico Argentino, Buenos Aires, 99-111.

Stipanicic, P.N., Bonetti, M.I.R. 1970., Posiciones estratigráficas y edades de las principales floras jurásicas argentinas. Ameghiniana, 7(1), 57-78.

Stipanicic, P.N., Rodrigo, F., Baulies, O.L., Martínez, C.G., 1968. Las Formaciones presenonianas en el denominado Macizo Nordpatagónico y regiones adyacentes. Revista de la Asociación Geológica Argentina, 23(2), 367-388.

Tapia, F., Farías, M., Mescua, J., 2013. Structural architecture of the Jurassic western margin of the Neuquén Basin, Central Chile and Argentina (35°30’S). Bolletino di Geofisica, 54, 104-106.

Tickyj, H., Rodríguez Raising, M., Cingolani, C.A., Alfaro, M., Uriz, N., 2009, Graptolitos Ordovícicos en el sur de la Cordillera Frontal de Mendoza. Revista de la Asociación Geológica Argentina, 64, 295-302.

Thomas, W.A., Tucker, R.D., Astini, R.A., Denison, R.E., 2012. Ages of pre-rift basement and synrift rocks along the conjugate rift and transform margins of the Argentine Precordillera and Laurentia. Geosphere, 8(6), 1366-1383.

Tunik, M.A., Lanés, S., Bechis, F., Giambiagi, L., 2008. Análisis petrográfico de las areniscas jurásicas tempranas en el depocentro Atuel de la cuenca Neuquina. Revista de la Asociación Geológica Argentina, 63(4), 714-727.

Tunik, M., Folguera, A., Naipauer, M., Pimentel, M.M., Ramos, V.A. 2010. Early uplift and orogenic deformation in the Neuquén Basin: Constraints on the Andean uplift from U–Pb and Hf isotopic data of detrital zircons. Tectonophysics, 489 (1-4), 258-273.

Uliana, M.A., Biddle, K.T., 1988. Mesozoic-Cenozoic Paleogeographic and Geodynamic Evolution of Southern South America. Revista Brasileira de Geociencias, 18, 172-190.

Uliana, M.A., Biddle, K.T., Cerdán, J., 1989. Mesozoic extension and the formation of Argentina sedimentary basins. In: Tankard, A.J., Balkwill, H.R. (Eds.), Extensional Tectonics and Stratigraphy of the North Atlantic Margin. American Association of Petroleum Geologists, Memoir 46, 599-613.

Varela, R., Basei, M.A.S., González, P.D., Sato, A.M., Naipauer, M., Campos Neto, M., Cingolani, C.A., Meira, T.V., 2011. Accretion of Grenvillian terranes to the west of the Rio de la Plata craton, west of Argentina. International Journal of Earth Sciences, 100 (2), 243-272.

Veiga, G.D., Schwarz, E., Spalletti, L.A., Massaferro, J.L., 2013. Anatomy and sequence architecture of the early post-rift in the Neuquén Basin (Argentina): a response to physiography and relative sea-level changes. Journal of Sedimentary Research, 83, 746-765.

Vennari, V.V., Lescano, M., Naipauer, M., Aguirre-Urreta, B., Concheyro, A., Schaltegger, U., Armstrong, R., Pimentel, M., Ramos, V.A., 2014. New constraints in the Jurassic-Cretaceous boundary in the High Andes using high-precision U-Pb data. Gondwana Research, 26, 374-385.

Vergani, G.D., Tankard, A.J. Belotti, H.J., Welsink, H.J., 1995. Tectonic evolution and paleogeography of the Neuquén Basin, Argentina. In: Tankard, A.J., Suárez Soruco, R., Welsink, H.J. (Eds.), Petroleum Basins of South America. American Association of Petroleum Geologists, Memoirs, 62, 383-402.

Vicente, J.C., 2005. Dynamic paleogeography of the Jurassic Andean Basin: pattern of transgression and localization of main straits through the magmatic arc. Revista de la Asociación Geológica Argentina, 60, 221-250.

Vicente, J.C., 2006. Dynamic Paleogeography of the Jurassic Andean Basin: pattern of regression and general considerations on main features. Revista de la Asociación Geológica Argentina, 61, 408-437.

Willner, A.P., Gerdes, A., Massonne, H.J., 2008. History of crustal growth and recycling at the Pacific convergent margin of South America at latitudes 29º–36ºS revealed by U-Pb and Lu-Hf isotope study of detrital zircon from late Paleozoic accretionary systems. Chemical Geology, 253(3-4), 114-129.

Zamora Valcarce, G., Zapata, T., Del Pino, D., Ansa, A., 2006. Structural evolution and magmatic characteristics of the Agrio Fold-and-thrust belt. In: Kay, S.M., Ramos, V.A. (Eds.), Evolution of an Andean margin: A tectonic and magmatic view from the Andes to the Neuquén Basin (35º-39º lat). Geological Society of America, Special Paper 407, 125-145.

Figure captions

Figure 1. a) Triassic and b) Jurassic paleogeography of the Central and Southern Andes (adapted from Riccardi 1983; Mpodozis and Ramos, 1989; Vicente, 2005; Charrier et al., 2007, 2015).

Figure 2. Location of the main morphotectonic features in the southern Central Andes between 34º and 41º SL and the study region (modified from Naipauer and Ramos, 2015).

Figure 3. Geological map of the studied region showing analyzed U-Pb samples (modified from Groeber, 1947; Nullo et al., 2005; Giambiagi et al., 2008; Giambiagi et al., 2009). Note that the Tordillo Formation was mapped separately from the Mendoza Group.

Figure 4. Tectonostratigraphic chart of the study region showing lithostratigraphic and tectonic settings of the Neuquén Basin (modified from Gulisano and Gutiérrez Pleimling, 1994; Giambiagi et al., 2008). The U-Pb (ID-TIMS) zircon ages of previous studies are from a) Vennari et al. (2014); b) Leanza et al. (2013); and c) Llambías et al. (2005). U-Pb (LA-ICP-MS) samples investigated in this work are also shown.

Figure 5. a) Regional view of the Cerro Negro Andesite and the Remoredo Formation in the Río Grande section; b) fine red sandstones from the Río Salado section; c) and d) red sandstone from the Cerro Chivato, southern margin of the Atuel River, sample locality (JtCC-420).

Figure 6. LA-ICP-MS U-Pb ages of zircons from sample AR-15 of the Cerro Negro Andesite (Precuyano cycle); a) U-Pb concordia plot (concordant ages in black and discordant ages in red); b) weighted mean $^{206}Pb/^{238}U$ age, light blue age was rejected from the mean age calculation.

Figure 7. Frequency histogram and relative probability plots of U–Pb (LA-MC-ICP-MS) ages of detrital zircons from El Freno Formation: a) sample AR-07 and b) sample AR-08. On the right, SEM images with spots and ages of selected dated zircons are shown.

Figure 8. U-Pb Concordia plots the samples analyzed: a, and b) El Freno Formation (only concordant ages younger than 300 Ma are represented); c, d, e, and f) Tordillo Formation (only concordant ages younger than 380 Ma are represented for samples AR-09, JTCC-420, and JTRS-407; and concordant ages younger than 200 Ma are represented for sample AR-11).

Figure 9. Frequency histogram and relative probability plots of U-Pb (LA-MC-ICP-MS) ages of detrital zircons from the Tordillo Formation: a) sample AR-09; b) sample JTCC-420; c) AR-11; and d) sample JTRS-407. On the right, SEM images with spots and ages of selected dated zircons are shown.

Figure 10. Summary of the U–Pb (LA-MC-ICP-MS) zircon ages for the two analyzed samples from El Freno Formation (AR-07 and AR-08). The possible source areas of the main age peaks are interpreted. Time intervals of the magmatism of Choiyoi and post-Choiyoi are from Sato et al. (2015).

Figure 11. Summary of the U–Pb (LA-MC-ICP-MS) zircon ages for the three analyzed samples of the Tordillo Formation (AR-09, JTCC-420, and AR-11). The main peaks of ages are interpreted as the most important source areas. Time intervals of the magmatism of Choiyoi and post-Choiyoi are from Sato et al. (2015).

Figure 12. a) Summary of the U–Pb (LA-MC-ICP-MS) zircon ages of the Tordillo Formation (data from this work and from Naipauer et al., 2012, 2014) and from Lagunillas Formation (data from Oliveros et al., 2012); b) Summary of Jurassic and Triassic zircon grains analyzed in the Tordillo and Lagunillas formations.

Table caption

Table 1. Major detrital zircon age population defined for the El Freno Formation (AR-07 and AR-08 samples) and the Tordillo Formation (AR-09, JTCC-420, AR-11, and JTRS-407 samples), Atuel depocenter, Neuquén Basin.

Samples	**Andean Cycle (pars.)**		**Gondwanic cycle**		**Famatinian cycle**	**Brazilian cycle**	**Mesoproterozoic cycle**
number	Jurassic	Triassic	Permian	Carboniferous	Dv, Sil, and Od	Cm. and Neopz.	Mesopz.
AR-07		64%	34%				
AR-08		28%	68%		2%	2%	
AR-09	55%	12%	5%	17%	1%	5%	5%
JTCC-420	31%	23%	21%	15%	6%		4%
AR-11	39%	10%	17%	12%	12%		12%
JTRS-407	51%	10%	12%	6%	11%	8%	

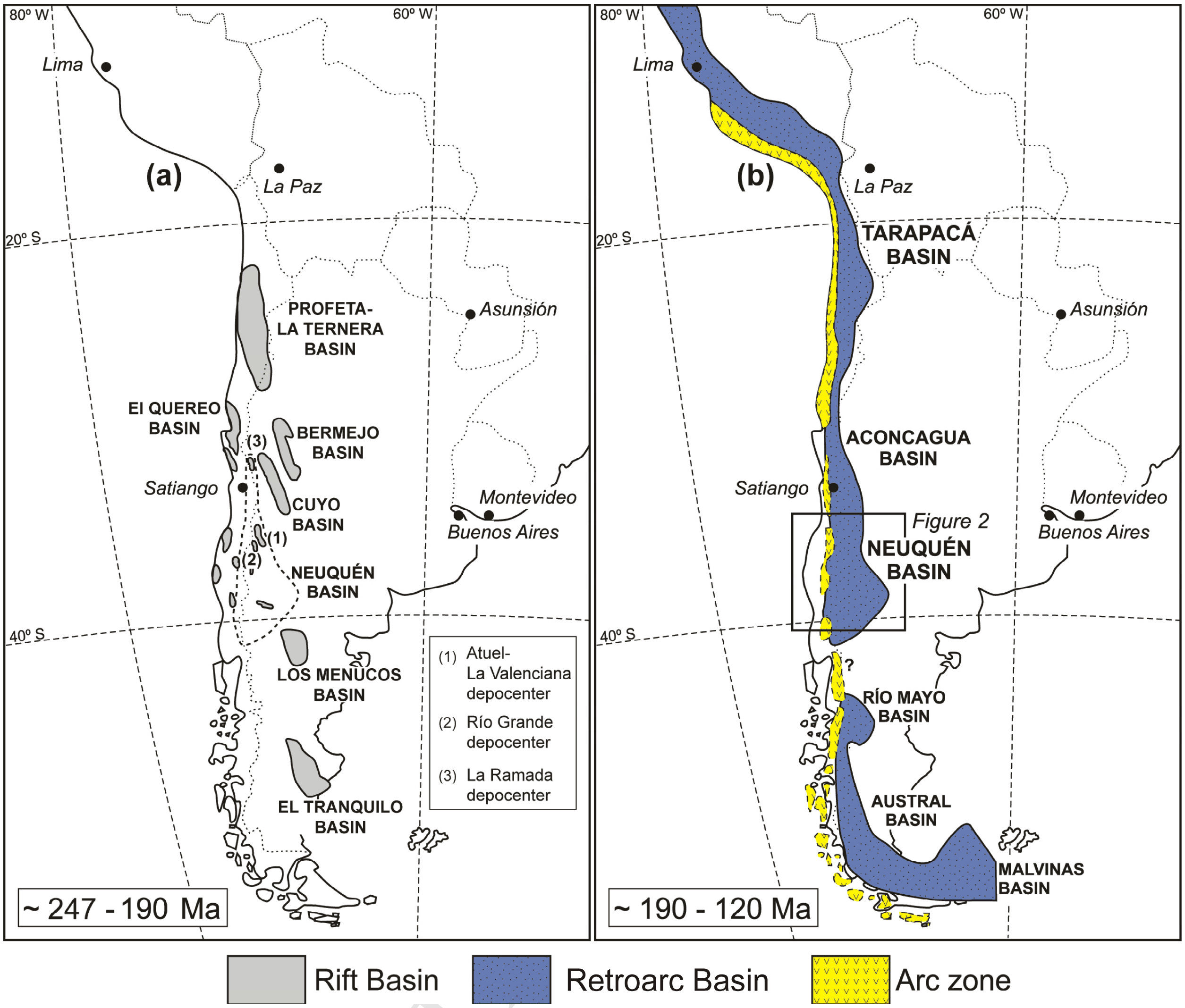
80º W
60º W
Lima
La Paz
(a)
20º S
PROFETA-
LA TERNERA
BASIN
Asunsión
EI QUEREO
BASIN
BERMEJO
BASIN
(3)
Satiango
CUYO
BASIN
Montevideo
Buenos Aires
(1)
(2)
NEUQUÉN
BASIN
40º S
LOS MENUCOS
BASIN
EL TRANQUILO
BASIN
(1) Atuel-
La Valenciana
depocenter
(2) Río Grande
depocenter
(3) La Ramada
depocenter
~ 247 - 190 Ma
(b)
TARAPACÁ
BASIN
ACONCAGUA
BASIN
Figure 2
NEUQUÉN
BASIN
?
RÍO MAYO
BASIN
AUSTRAL
BASIN
MALVINAS
BASIN
~ 190 - 120 Ma
Rift Basin
Retroarc Basin
Arc zone

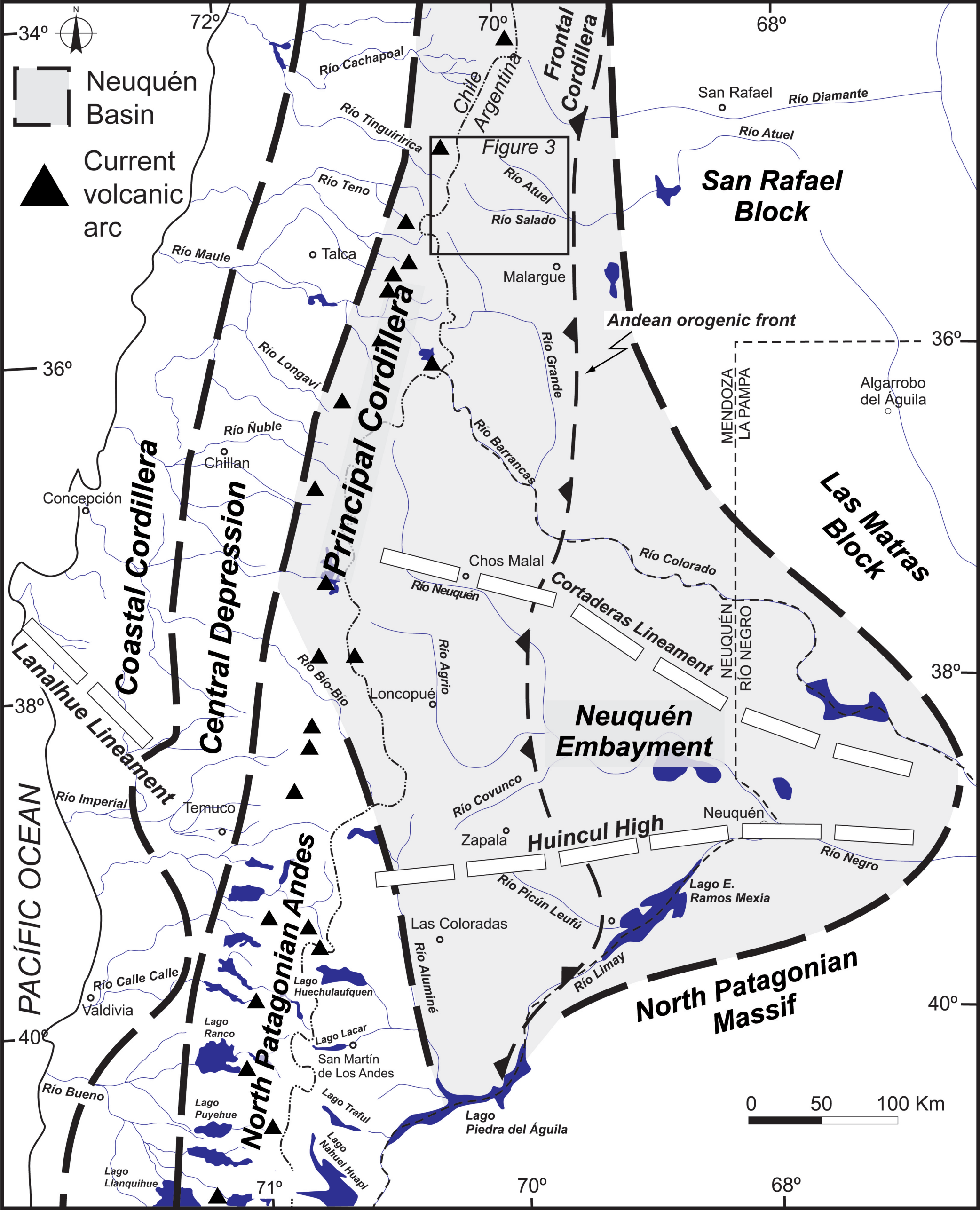
Neuquén Basin
Current volcanic arc
Río Cachapoal
Río Tinguiririca
Río Teno
Río Maule
Talca
Chile
Argentina
Frontal Cordillera
San Rafael
Río Diamante
Río Atuel
Figure 3
Río Salado
San Rafael Block
Malargue
Andean orogenic front
Río Longaví
Principal Cordillera
Río Grande
Río Barrancas
Río Ñuble
Chillan
Concepción
Coastal Cordillera
Central Depression
MENDOZA
LA PAMPA
Algarrobo del Águila
Las Matras Block
Chos Malal
Río Neuquén
Cortaderas Lineament
Río Colorado
NEUQUÉN
RÍO NEGRO
Río Agrio
Río Bío-Bío
Loncopué
Lanalhue Lineament
Neuquén Embayment
Río Imperial
Temuco
Río Covunco
Neuquén
Zapala
Huincul High
Río Negro
Río Picún Leufú
Lago E. Ramos Mexia
Las Coloradas
North Patagonian Andes
PACÍFIC OCEAN
Río Aluminé
Río Limay
North Patagonian Massif
Río Calle Calle
Valdivia
Lago Huechulaufquen
Lago Ranco
Lago Lacar
San Martín de Los Andes
Lago Traful
Lago Piedra del Águila
Río Bueno
Lago Puyehue
Lago Nahuel Huapi
Lago Llanquihue
0
50
100 Km
34º
36º
38º
40º
72º
70º
68º
71º
N

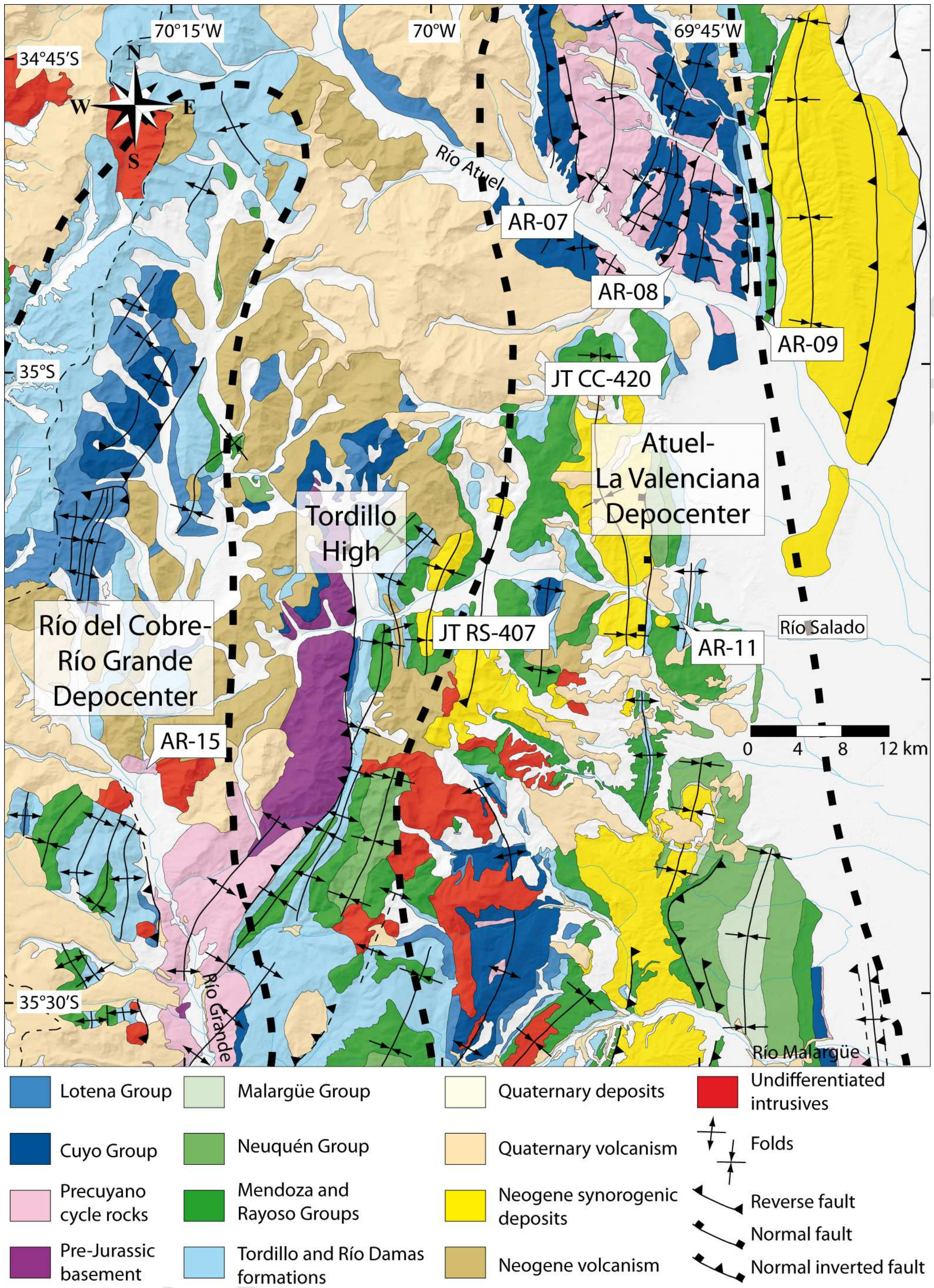
70°15'W
70°W
69°45'W
34°45'S
35°S
35°30'S
N
S
W
E
Río Atuel
AR-07
AR-08
AR-09
JT CC-420
Atuel-
La Valenciana
Depocenter
Tordillo
High
Río del Cobre-
Río Grande
Depocenter
JT RS-407
AR-11
Río Salado
AR-15
0 4 8 12 km
Río Grande
Río Malargüe
Lotena Group
Cuyo Group
Precuyano cycle rocks
Pre-Jurassic basement
Malargüe Group
Neuquén Group
Mendoza and Rayoso Groups
Tordillo and Río Damas formations
Quaternary deposits
Quaternary volcanism
Neogene synorogenic deposits
Neogene volcanism
Undifferentiated intrusives
Folds
Reverse fault
Normal fault
Normal inverted fault

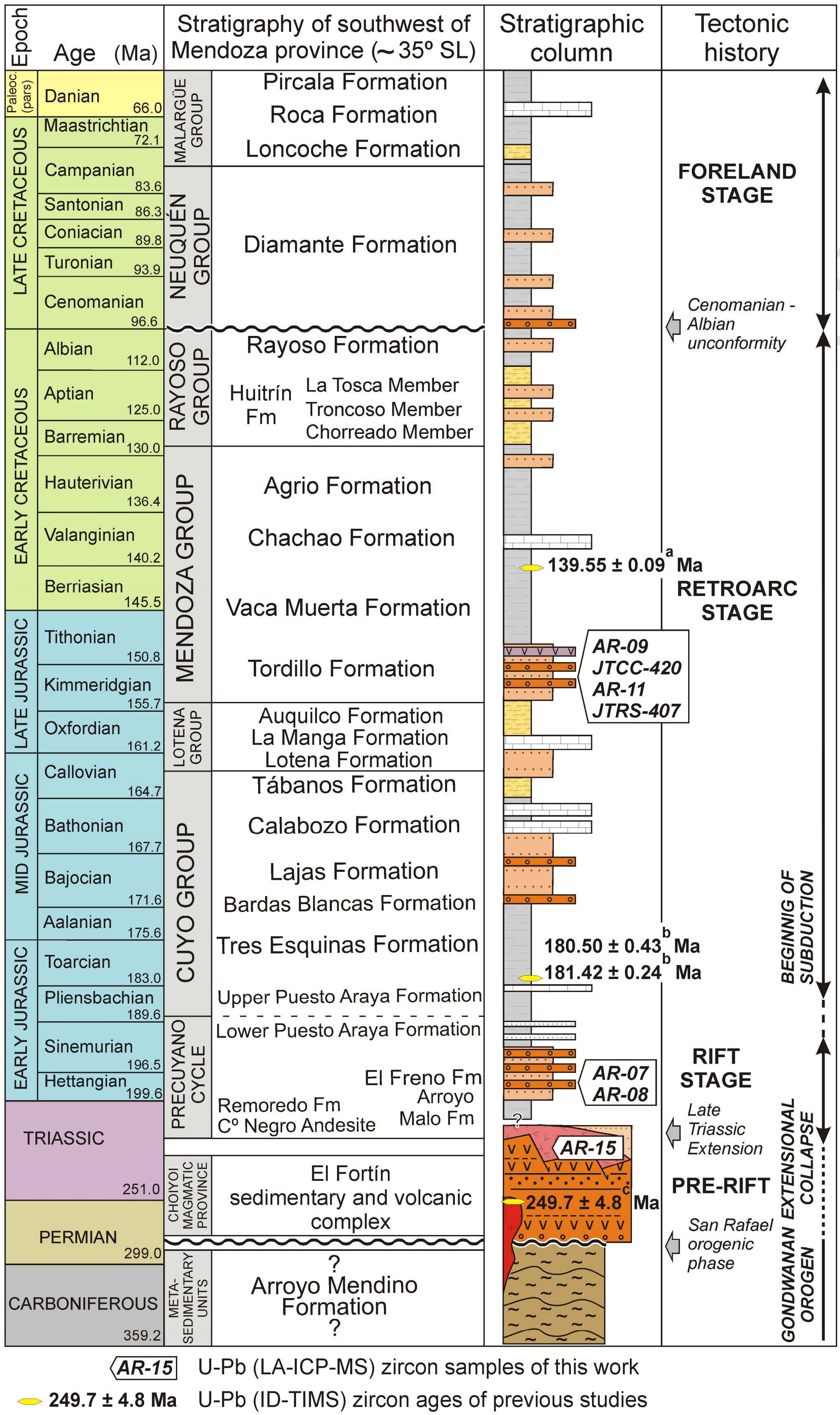
Epoch
Age (Ma)
Stratigraphy of southwest of Mendoza province (~35º SL)
Stratigraphic column
Tectonic history
Paleoc. (pars)
Danian 66.0
LATE CRETACEOUS
Maastrichtian 72.1
Campanian 83.6
Santonian 86.3
Coniacian 89.8
Turonian 93.9
Cenomanian 96.6
EARLY CRETACEOUS
Albian 112.0
Aptian 125.0
Barremian 130.0
Hauterivian 136.4
Valanginian 140.2
Berriasian 145.5
LATE JURASSIC
Tithonian 150.8
Kimmeridgian 155.7
Oxfordian 161.2
MID JURASSIC
Callovian 164.7
Bathonian 167.7
Bajocian 171.6
Aalanian 175.6
EARLY JURASSIC
Toarcian 183.0
Pliensbachian 189.6
Sinemurian 196.5
Hettangian 199.6
TRIASSIC 251.0
PERMIAN 299.0
CARBONIFEROUS 359.2
MALARGÜE GROUP
Pircala Formation
Roca Formation
Loncoche Formation
NEUQUÉN GROUP
Diamante Formation
RAYOSO GROUP
Rayoso Formation
Huitrín Fm
La Tosca Member
Troncoso Member
Chorreado Member
MENDOZA GROUP
Agrio Formation
Chachao Formation
Vaca Muerta Formation
Tordillo Formation
LOTENA GROUP
Auquilco Formation
La Manga Formation
Lotena Formation
CUYO GROUP
Tábanos Formation
Calabozo Formation
Lajas Formation
Bardas Blancas Formation
Tres Esquinas Formation
Upper Puesto Araya Formation
PRECUYANO CYCLE
Lower Puesto Araya Formation
El Freno Fm
Arroyo Malo Fm
Remoredo Fm
Cº Negro Andesite
CHOIYOI MAGMATIC PROVINCE
El Fortín sedimentary and volcanic complex
META-SEDIMENTARY UNITS
?
Arroyo Mendino Formation
?
139.55 ± 0.09 a Ma
AR-09
JTCC-420
AR-11
JTRS-407
180.50 ± 0.43 b Ma
181.42 ± 0.24 b Ma
AR-07
AR-08
?
AR-15
249.7 ± 4.8 c Ma
FORELAND STAGE
Cenomanian - Albian unconformity
RETROARC STAGE
BEGINNIG OF SUBDUCTION
RIFT STAGE
Late Triassic Extension
PRE-RIFT
San Rafael orogenic phase
GONDWANAN OROGEN
EXTENSIONAL COLLAPSE
AR-15 U-Pb (LA-ICP-MS) zircon samples of this work
249.7 ± 4.8 Ma U-Pb (ID-TIMS) zircon ages of previous studies


a)
Cerro Negro Andesite
Remoredo Formation
b)
c)
d)

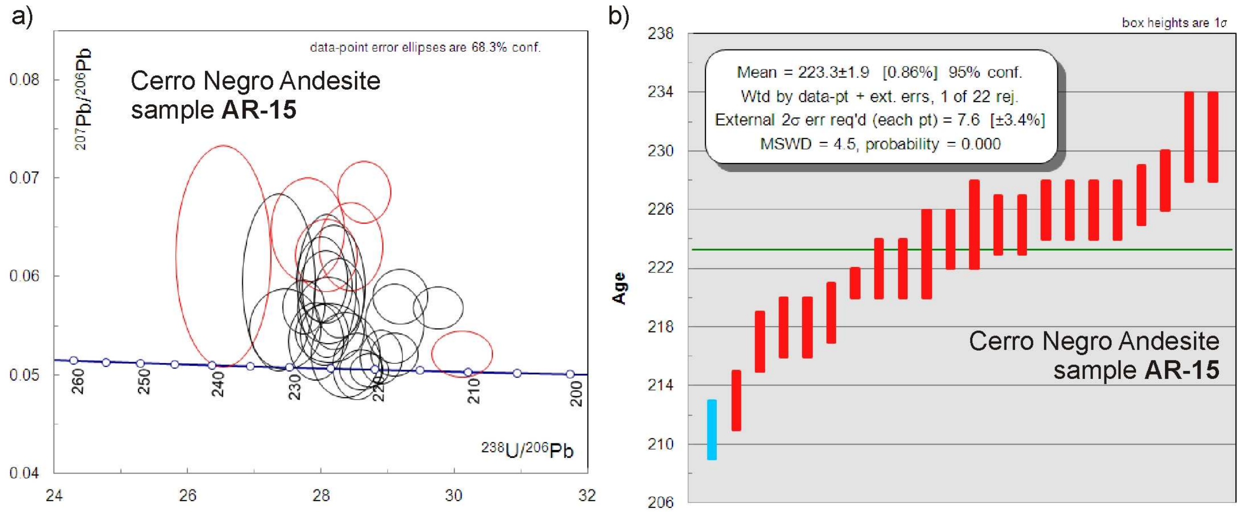

a)
data-point error ellipses are 68.3% conf.
Cerro Negro Andesite
sample AR-15
207Pb/206Pb
238U/206Pb
b)
box heights are 1σ
Mean = 223.3±1.9 [0.86%] 95% conf.
Wtd by data-pt + ext. errs, 1 of 22 rej.
External 2σ err req'd (each pt) = 7.6 [±3.4%]
MSWD = 4.5, probability = 0.000
Age
Cerro Negro Andesite
sample AR-15

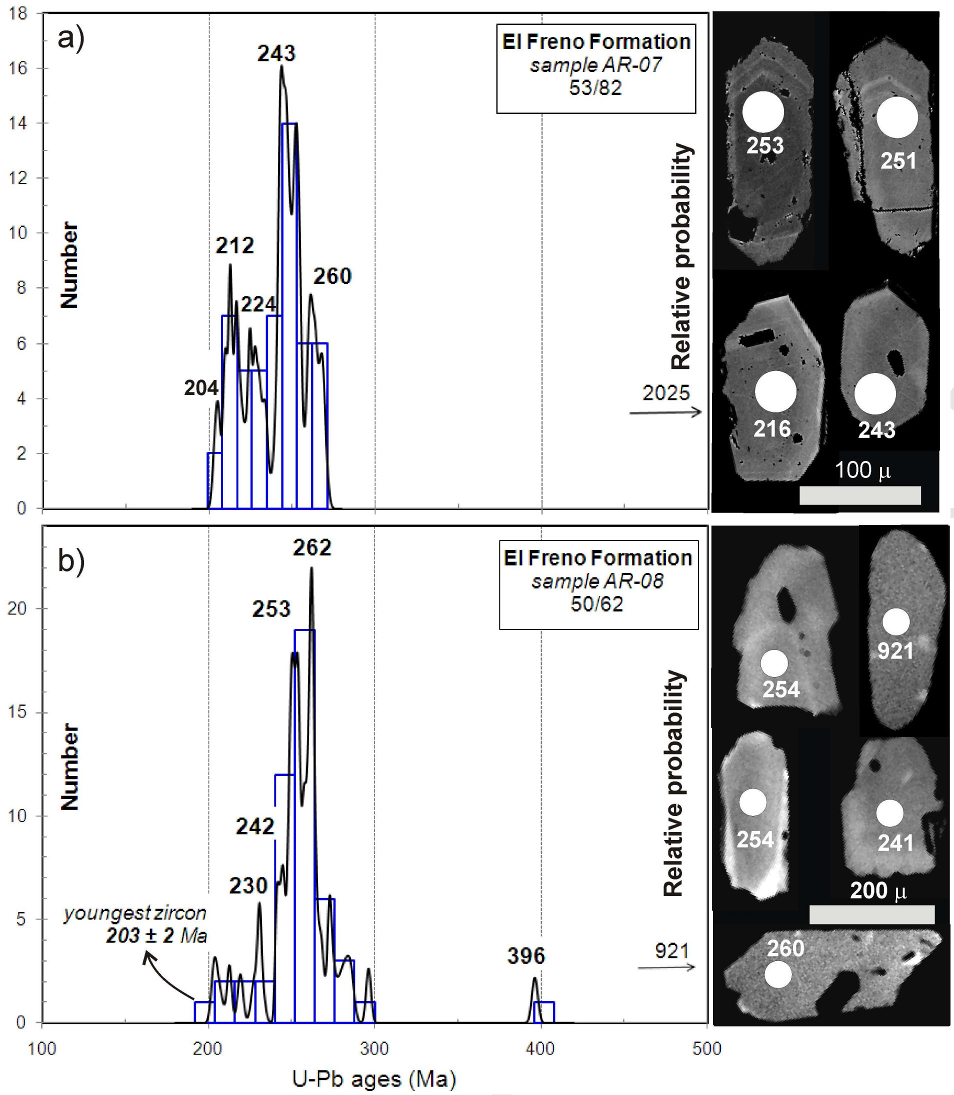

a)
El Freno Formation
sample AR-07
53/82
243
212
224
260
204
Number
Relative probability
2025
253
251
216
243
100 µ
b)
El Freno Formation
sample AR-08
50/62
262
253
242
230
youngest zircon
203 ± 2 Ma
396
921
Number
Relative probability
254
921
254
241
200 µ
260
U-Pb ages (Ma)

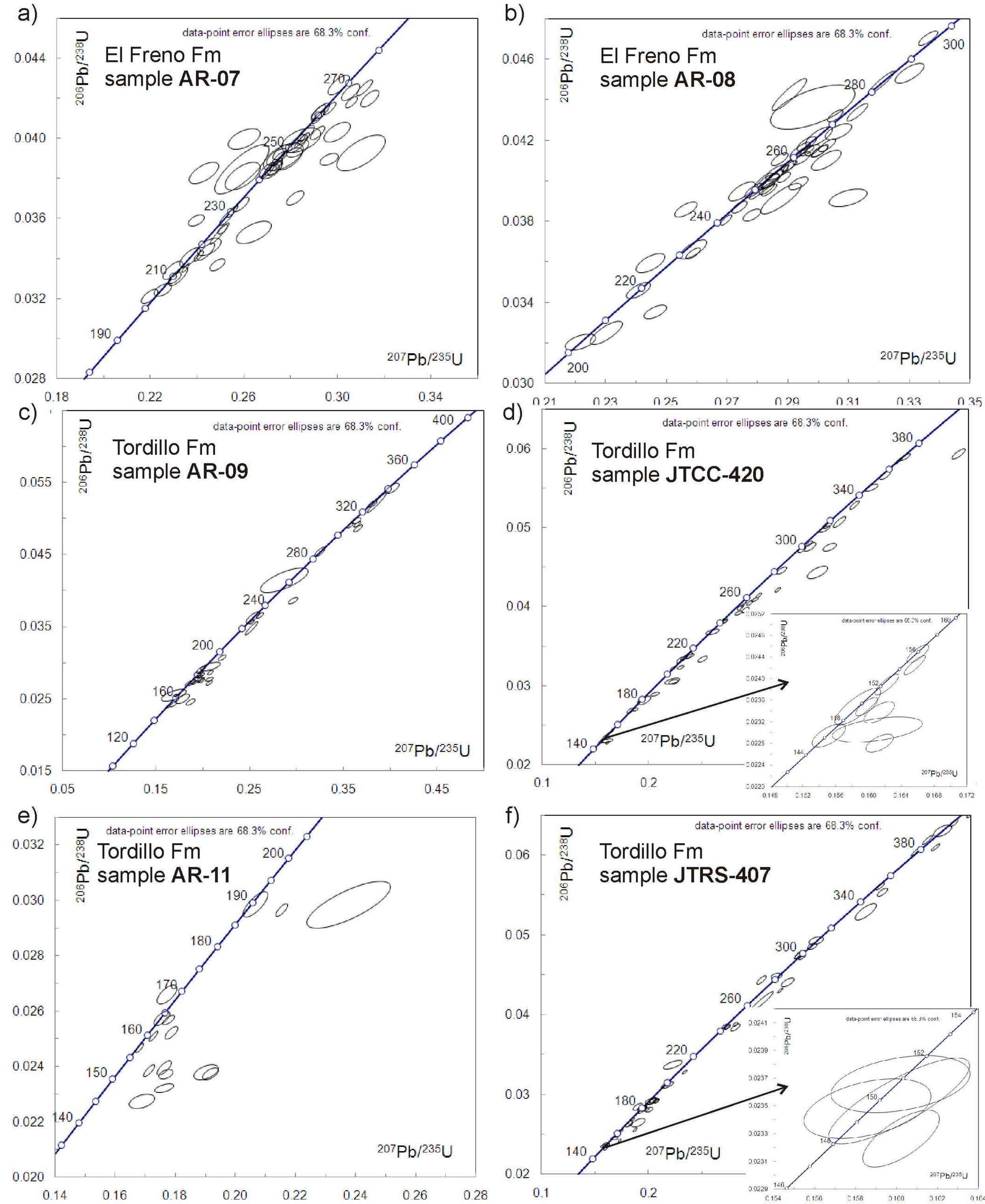
a)
El Freno Fm
sample AR-07
b)
El Freno Fm
sample AR-08
c)
Tordillo Fm
sample AR-09
d)
Tordillo Fm
sample JTCC-420
e)
Tordillo Fm
sample AR-11
f)
Tordillo Fm
sample JTRS-407
data-point error ellipses are 68.3% conf.
$^{206}Pb/^{238}U$
$^{207}Pb/^{235}U$

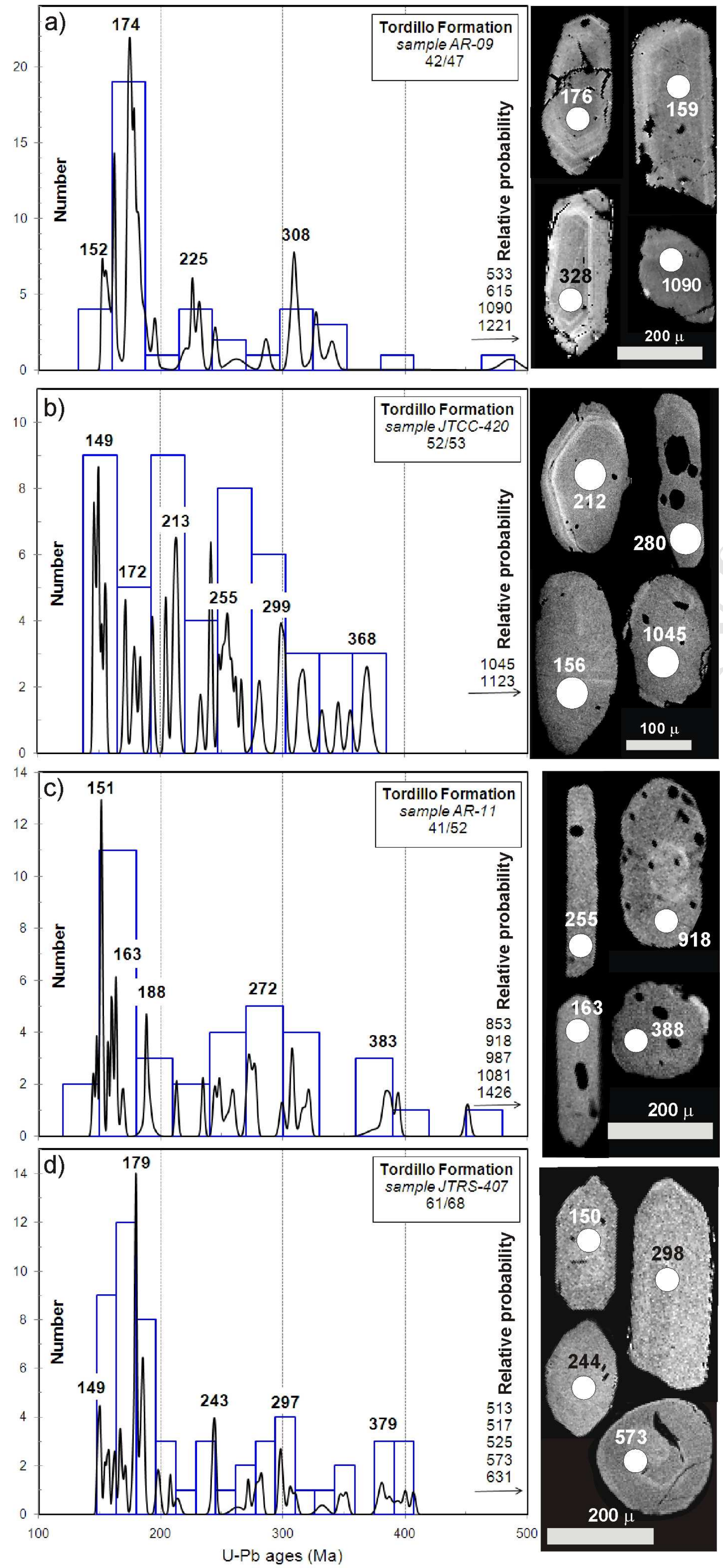

a)
Tordillo Formation
sample AR-09
42/47
174
152
225
308
533
615
1090
1221
176
159
328
1090
200 µ
b)
Tordillo Formation
sample JTCC-420
52/53
149
172
213
255
299
368
1045
1123
212
280
156
1045
100 µ
c)
Tordillo Formation
sample AR-11
41/52
151
163
188
272
383
853
918
987
1081
1426
255
918
163
388
200 µ
d)
Tordillo Formation
sample JTRS-407
61/68
179
149
243
297
379
513
517
525
573
631
150
298
244
573
200 µ
Number
Relative probability
U-Pb ages (Ma)

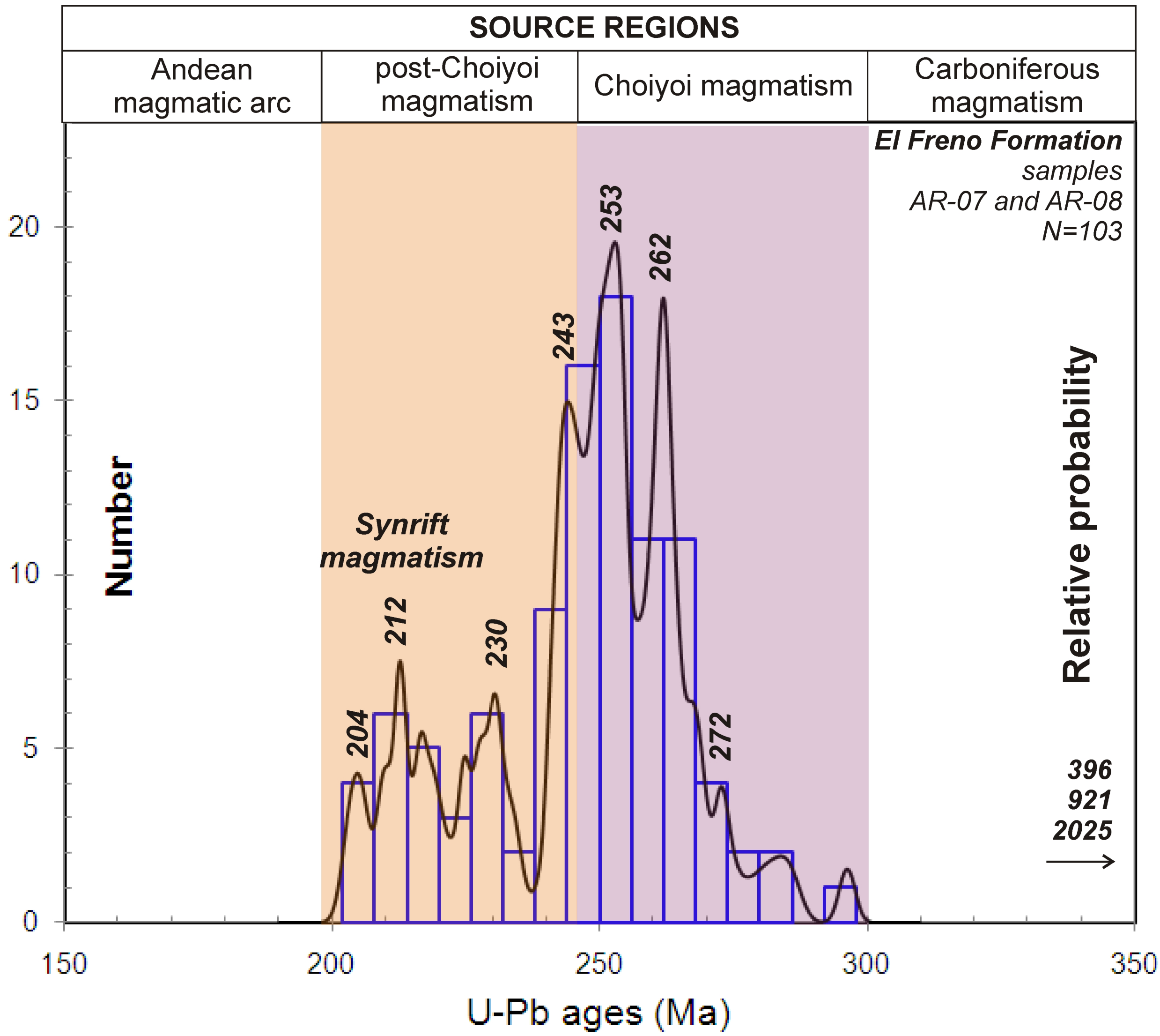

SOURCE REGIONS
Andean magmatic arc
post-Choiyoi magmatism
Choiyoi magmatism
Carboniferous magmatism
El Freno Formation
samples
AR-07 and AR-08
N=103
Synrift magmatism
Number
Relative probability
204
212
230
243
253
262
272
396
921
2025
0
5
10
15
20
150
200
250
300
350
U-Pb ages (Ma)

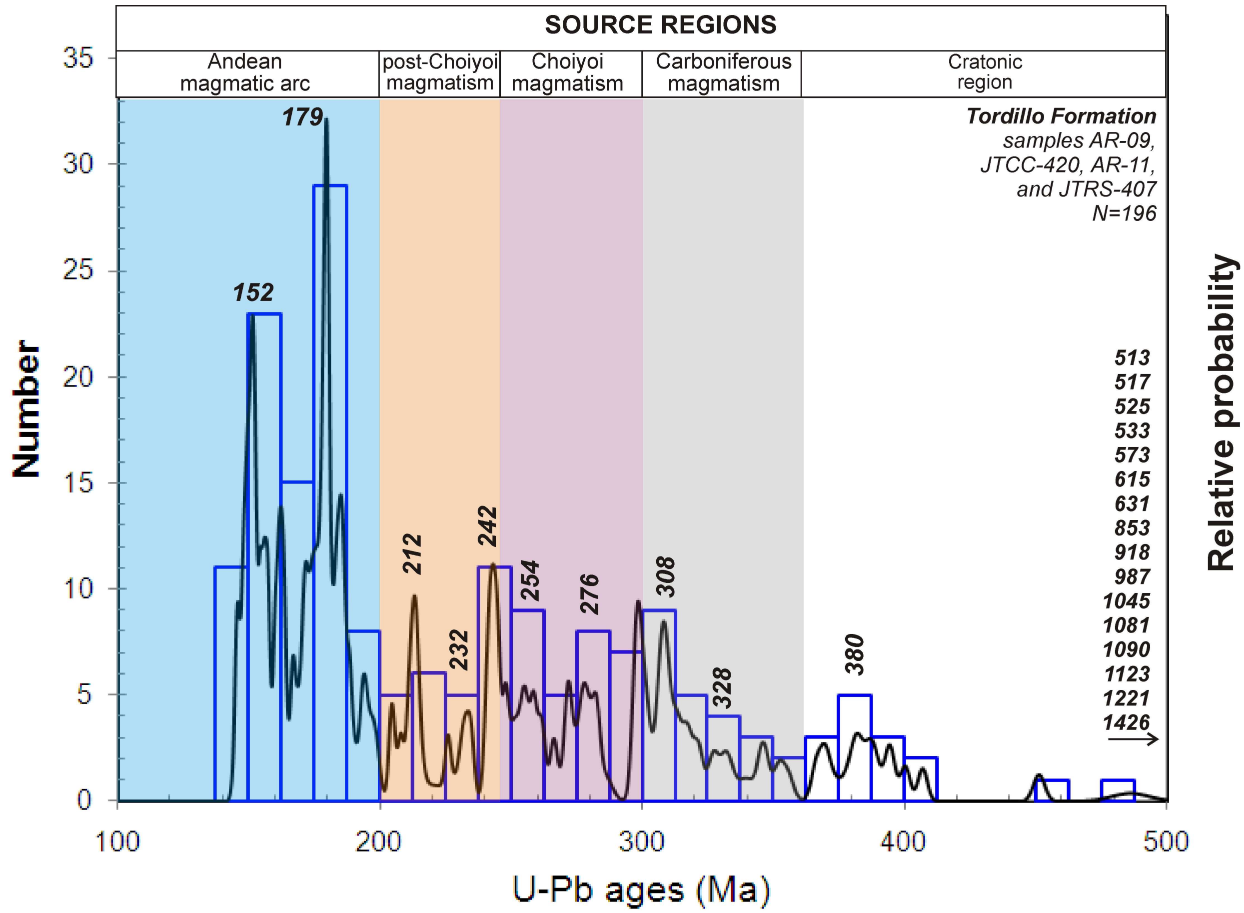
SOURCE REGIONS
Andean magmatic arc
post-Choiyoi magmatism
Choiyoi magmatism
Carboniferous magmatism
Cratonic region
Tordillo Formation
samples AR-09, JTCC-420, AR-11, and JTRS-407
N=196
Number
Relative probability
U-Pb ages (Ma)
179
152
212
232
242
254
276
308
328
380
513
517
525
533
573
615
631
853
918
987
1045
1081
1090
1123
1221
1426

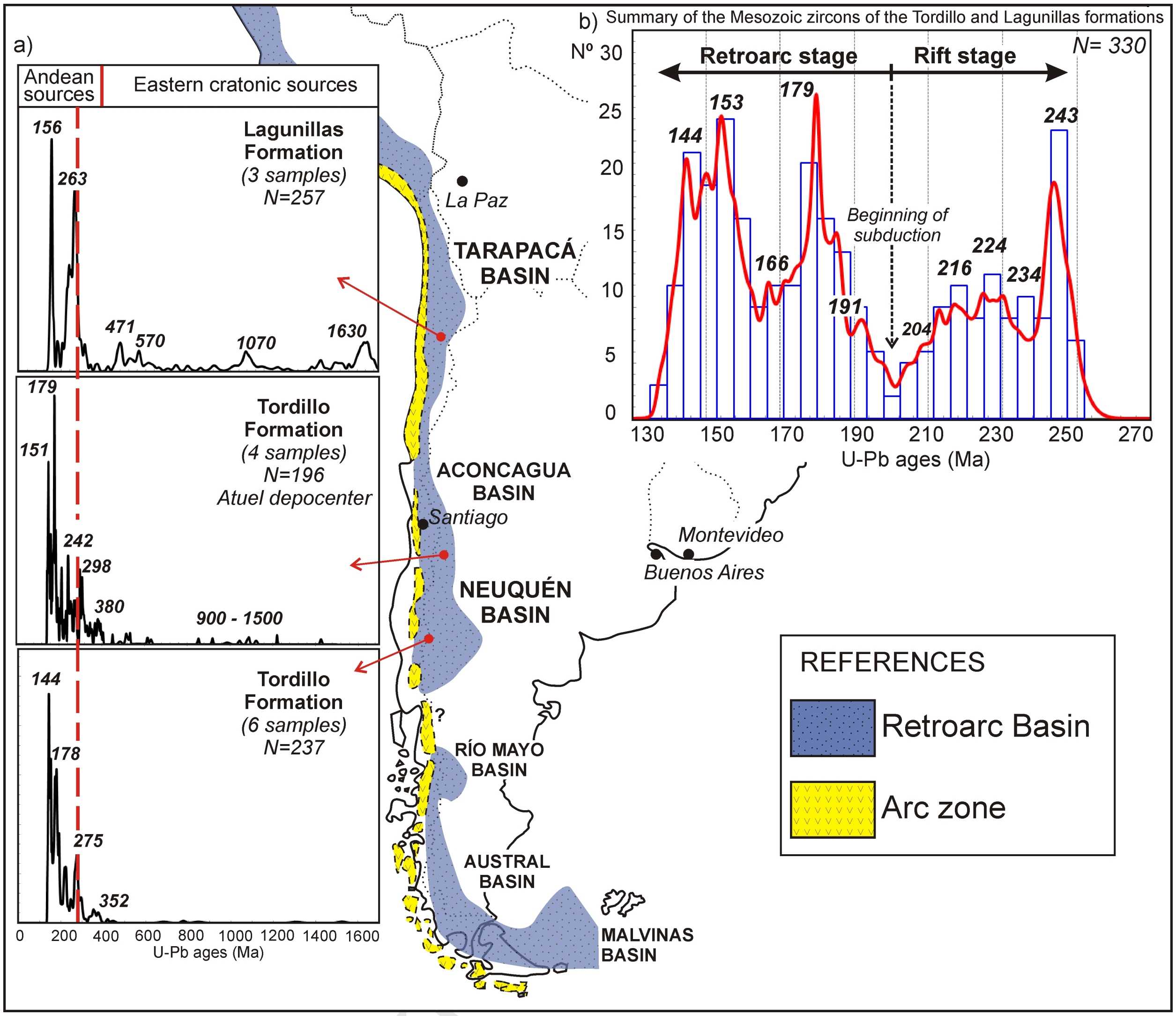
a)
Andean sources
Eastern cratonic sources
Lagunillas Formation
(3 samples)
N=257
156
263
471
570
1070
1630
Tordillo Formation
(4 samples)
N=196
Atuel depocenter
179
151
242
298
380
900 - 1500
Tordillo Formation
(6 samples)
N=237
144
178
275
352
0 200 400 600 800 1000 1200 1400 1600
U-Pb ages (Ma)
La Paz
TARAPACÁ BASIN
ACONCAGUA BASIN
Santiago
NEUQUÉN BASIN
RÍO MAYO BASIN
AUSTRAL BASIN
MALVINAS BASIN
Montevideo
Buenos Aires
b) Summary of the Mesozoic zircons of the Tordillo and Lagunillas formations
Nº
N= 330
Retroarc stage
Rift stage
144
153
179
166
191
204
216
224
234
243
Beginning of subduction
0 5 10 15 20 25 30
130 150 170 190 210 230 250 270
U-Pb ages (Ma)
REFERENCES
Retroarc Basin
Arc zone

Highlights

- Two different pulses of rifting could be recognized, the oldest developed during the Norian and the younger during the Rhaetian-Sinemurian.
- The maximum depositional age for the Tordillo Formation in the Atuel-La Valenciana depocenter is at ca. 149 Ma.
- The main source region of sediment in the Tordillo Formation was the Andean magmatic arc, but basement regions were also present probably located to the east.
- The zircon detrital ages summarized for the Late Jurassic sediments were interpreted as a record of the episodic magmatic activity in the southern Central Andes.

Supplementary data A

Analytical methods

*Samples **AR-07; AR-08; AR-09; AR-11; JTCC-420**; and **JTRS-407** (Laboratório de Geocronologia, Instituto de Geociências da Universidade de Brasília, Brasil):*

The zircon grains were radon selected and set in epoxy resin mounts. The mount surface was polished to expose the grain interiors. Backscattered electron images of zircons were obtained using an SEM JEOL JSM 5800 at Universidade de Brasilia (UnB), Brazil. The samples were loaded into a New Wave UP213 Nd:YAG laser (λ=213 nm), linked to a Thermo Finnigan Neptune Multi-collector ICPMS. Helium was used as the carrier gas and mixed with argon before entering the ICP. The laser was run at a frequency of 10 Hz and energy of 34% and the diameter with a spot size of 30 µm. Laser induced fractionation of the 206Pb/238U ratio was corrected using the linear regression method (Kosler et al., 2002). Two international zircon standards were analyzed throughout the U-Pb analyses. The zircon standard GJ-1 (Jackson et al, 2004) was used as the primary standard in a standard-sample bracketing method, accounting for mass bias and drift correction. The resulting correction factor for each sample analysis considers the relative position of each analysis within the sequence of 4 samples bracketed by two standard and two blank analyses each (Albarède et al, 2004). Analyses were performed using spot size of 30 µm. The Temora 2 standard (Black et al, 2004) was run at the start and the end of each analytical session, yielding accuracy around 2% and precision in the range of 1 %. The errors of sample analyses were propagated by quadratic addition of the external uncertainty observed for the standards to the reproducibility and within-run precision of each unknown analysis. The instrumental set-up and further details of the analytical method applied are given by Buhn et al (2009). Masses 204, 206 and 207 were measured with ion counters, and 238U was analyzed on a Faraday cup. 202Hg signal was monitored by an ion counter for correction of the isobaric interference between 204Hg and 204Pb. The signals during ablation were taken in 40 cycles of 1 sec each. For data evaluation, only coherent intervals of signal response were considered. Data reduction was performed with an in-house Excel spreadsheet, which considers blank values, zircon standards composition and errors, and error propagation. The 204Pb signal intensity was calculated and corrected using a natural 202Hg/204Hg ratio of 4.346. Common Pb correction was applied for zircons with 206Pb/204Pb lower than 1000, applying the common lead composition following the Stacey and Kramers (1975) model. Plotting of U-Pb data was performed using ISOPLOT v.3 (Ludwig, 2003) and errors for isotopic ratios are presented at the 2σ level. Because of the statistical treatment applied in calculating Concordia Ages, those are more precise than any individual U-Pb or Pb-Pb ages (Ludwig, 2003) and, in the present study, always correspond to less than the 2% accuracy obtained from the intercalibration of the standards. Consequently, the Isoplot calculated errors were modified in order to incorporate this uncertainty level and, hence, represent a more realistic age in terms of the analytical limitations of the method. The age probability plots (Ludwig, 2003) used in this study were constructed using the 206Pb/238U age for young (<1.0 Ga) zircons and the 206Pb/207Pb age for older (>1.0 Ga) grains

Sample ***AR-15*** *(Laboratorio de Estudios Isotópicos, Geoscience Center, Universidad Nacional Autónoma de México, México):*

The selected zircons were mounted on double-sided adhesive tape along ordered rows of about 1.5 cm length. The mount was then cast in epoxy resin, allowed to dry for about 8 hours, ground with sandpaper (#1500 grit) until the crystals were exposed, and then finally polished with a 6 μm and 1 μm sized diamond compound. The polished crystals were then imaged with a binocular microscope, and under cathodoluminescence, using an ELM-3R luminoscope. The mounts were then rinsed with 18.2 MΩ water in an ultrasonic bath for 15 minutes, followed by superficial cleaning with 1 mol l-1 ultra pure HNO3 just before the sample was introduced into the ablation cell, in order to avoid impurities and extraneous common Pb. The standard analytical parameters used for U-Pb zircon geochronology were a constant laser output energy of ~ 160 mJ, a demagnification of 25x and a spot diameter of 34 μm, although smaller spots sizes were also successfully employed. These parameters corresponded to a fluence of 8 J cm-2 on the target, and produced a flat-bottom ablation crater of about 25 μm depth after a total of 150 pulses with a repetition rate of 5 Hz.

The ICP-MS was optimized prior to each analytical session using a NIST SRM 612 glass reference sample, on a raster scan of 0.5 mm min-1 at 5 Hz, and a spot diameter of 34 μm. Typical signal intensities of ~ 110000 cps 238U and about 50000 cps 208Pb were usually achieved, with a 238U/232Th ratio of ~ 1.05 and a ThO+/Th+

ratio ≤ 0.4%. A helium flow rate of 600 ml min-1 was used to carry ablated material to the ICP, with an additional 2.7 ml min-1 N2 gas added after the ablation cell that was in turn mixed with ~ 700 ml of Ar make-up gas. As previously reported (e.g., Durrant 1994, Hu et al. 2008), the injection of a small amount of N2 (< 3 ml) has the effect of increasing signal intensity for the whole mass range, thus providing improved statistics on isotope ratios.

BIBLIOGRAFÍA

Albarede, F., Telouk, P., Blichert-Toft, J., Boyet, M., Agranier, A. and Nelson, B. 2004. Precise and accurate isotopic measurements using multiple-collector ICPMS. Geochimica et Cosmochimica Acta, 68 (12), 2725-2744.

Black, L.P., Kamo, S.L., Allen, C.M., Davis, D.W., Aleinikoff, J.N., Valley, J.W., Mundil, R., Campbell, I.H., Korsch, R.J., Williams, I.S., and Foudoulis, C., 2004. Improved 206Pb/238U microprobe geochronology by the monitoring of a trace-element-related matrix effect; SHRIMP, ID-TIMS, ELA-ICP-MS and oxygen isotope documentation for a series of zircon standards: Chemical Geology, 205, 115-140.

Buhn, B., Pimentel, M.M., Matteini, M. and Dantas, E. 2009. High spatial resolution analysis of Pb and U isotopes for geochronology by laser ablation multi-collector inductively coupled plasma mass spectrometry (LA-MC-ICP-MS). Anais da Academia Brasileira de Ciências, 81, 99-114.

Durrant S.F., 1994. Feasibility of improvement in analytical performance in laser ablation inductively coupled plasma-mass spectrometry (LA-ICP-MS) by addition of nitrogen to the argon plasma. Fresenius Journal of Analytical Chemistry, 349, 768-771.

Hu Z.C., Gao S., Liu Y.S., Hu S.H., Chen H.H. and Yuan H.L., 2008. Signal enhancement in laser ablation ICP-MS by addition of nitrogen in the central channel gas. Journal of Analytical Atomic Spectrometry, 23, 1093-1101.

Jackson, S.E., Pearson, N.J., Griffin, W.L., Belousova, E.A. 2004. The application of laser ablation-inductively coupled plasma-mass spectrometry to in situ U–Pb zircon geochronology. Chemical Geology, 211, 47-69.

Košler, J., Fonneland, H., Sylvester, P., Tubrett, M., Pedersen, R.B. 2002. U–Pb dating of detrital zircons for sediment provenance studies–a comparison of laser ablation ICP-MS and SIMS techniques. Chemical Geology, 182, 605-618.

Ludwig, K.R. 2003. Isoplot 3.00: A geochronological toolkit for Microsoft Excel. Berkeley Geochronological Center, Special Publication, 4, 70p.

Stacey, J.S. and Kramers, J.D. 1975. Approximation of terrestrial lead isotope evolution by a two-stage model. Earth and Planetary Science Letters, 26, 207-221.

Supplementary data B. Summary of analytical results by U-Pb LAM-MC-ICP-MS zircons data.

Data analyzed in the Universidade de Brasilia (UnB), Brazil
SAMPLE AR-07 - El Freno Formation (34°52'5.24" S - 69°51'38.31" W)

Spot number	f(206)%	Th/U	6/4 ratio	7/6 ratio	1s(%)	7/5 ratio	1s(%)	6/8 ratio	1s(%)	Rho	7/6 age	1s(abs)	7/5 age	1s(abs)	6/8 age	1s(abs)	Conc (%)[1]	Conc (%)[2]
030-Z23	0,11	0,54	16486,38264	0,04963	0,7	0,2197	1,1	0,0321143	0,8	0,69	110,6	17,8	201,7	1,9	203,8	1,5	184	101
037-Z28	0,05	0,56	34844,82622	0,05041	0,9	0,2254	1,1	0,0324275	0,7	0,55	147,2	21,7	206,4	2,1	205,7	1,4	140	100
096-Z74	0,04	1,25	48593,33917	0,04986	0,8	0,2296	1,2	0,0333973	0,9	0,72	121,6	19,8	209,9	2,3	211,8	1,9	174	101
107-Z83	0,08	0,88	24212,96667	0,05058	0,5	0,2304	0,7	0,0330391	0,6	0,69	155,4	11,9	210,5	1,4	209,5	1,2	135	100
014-Z9	0,06	0,83	29666,7199	0,05075	0,7	0,2317	1,2	0,0331175	0,9	0,77	163,2	17,7	211,6	2,3	210,0	1,9	129	99
005-Z2	0,01	0,57	154905,3977	0,05085	0,2	0,2351	0,5	0,0335333	0,4	0,88	167,8	3,8	214,4	0,9	212,6	0,9	127	99
068-Z52	0,06	0,73	32204,20556	0,05045	0,8	0,2370	1,2	0,0340774	0,9	0,72	149,1	20,1	216,0	2,4	216,0	2,0	145	100
075-Z57	0,51	0,00	3574,969431	0,04843	0,8	0,2398	0,9	0,0359065	0,5	0,52	52,6	18,1	218,2	1,8	227,4	1,2	432	104
015-Z10	0,01	0,56	126488,0648	0,05115	0,3	0,2408	0,6	0,0341381	0,5	0,81	181,4	6,5	219,0	1,1	216,4	1,0	119	99
019-Z14	2,10	0,52	872,7474927	0,04602	1,4	0,2428	1,7	0,0382709	0,9	0,64	-70,6	34,9	220,7	3,4	242,1	2,2	-343	110
090-Z70	0,36	0,84	5053,83236	0,05148	0,6	0,2437	1,0	0,0343383	0,8	0,78	196,3	14,5	221,5	2,0	217,6	1,7	111	98
045-Z34	0,04	0,68	51848,62159	0,05139	1,1	0,2451	1,4	0,0345871	0,8	0,57	192,4	26,2	222,6	2,7	219,2	1,8	114	98
016-Z11	0,35	1,09	5269,379463	0,05355	0,6	0,2487	0,9	0,0336908	0,6	0,62	287,2	14,7	225,6	1,7	213,6	1,2	74	95
006-Z3	0,02	0,39	92692,54727	0,05134	0,3	0,2495	1,1	0,0352414	1,0	0,95	190,2	7,7	226,1	2,2	223,3	2,2	117	99
074-Z56	0,02	0,67	98171,65682	0,05131	0,3	0,2509	0,5	0,0354729	0,4	0,69	188,7	7,7	227,3	1,1	224,7	1,0	119	99
059-Z45	0,05	0,92	34295,37191	0,05084	0,4	0,2527	0,8	0,0360453	0,7	0,85	167,1	9,1	228,7	1,6	228,3	1,5	137	100
054-Z40	0,01	0,30	230130,8865	0,05091	0,3	0,2551	0,6	0,0363475	0,5	0,85	170,6	6,7	230,7	1,3	230,2	1,2	135	100
097-Z75	0,15	0,56	11858,13479	0,05114	0,5	0,2588	0,8	0,0367017	0,7	0,78	181,2	11,5	233,7	1,7	232,4	1,5	128	99
069-Z53	1,82	0,37	1008,819214	0,04891	2,1	0,2592	3,0	0,0384345	2,1	0,80	76,2	48,1	234,0	6,1	243,1	5,1	319	104
008-Z5	0,24	4,33	7790,614505	0,04938	1,5	0,2595	1,9	0,0381174	1,2	0,63	99,0	35,7	234,3	4,0	241,2	2,9	244	103
058-Z44	1,06	0,50	1729,870943	0,04720	1,5	0,2602	1,7	0,0399771	0,9	0,53	-8,9	35,6	234,8	3,6	252,7	2,1	-2829	108
048-Z37	1,29	0,60	1422,90232	0,05427	1,6	0,2642	1,9	0,0353094	1,0	0,60	317,7	35,8	238,1	4,0	223,7	2,3	70	94
017-Z12	0,01	0,85	164135,5258	0,05112	0,3	0,2704	0,6	0,0383598	0,6	0,89	180,0	6,1	243,0	1,4	242,7	1,4	135	100
050-Z39	0,15	0,54	12224,10371	0,05120	0,9	0,2713	1,2	0,0384259	0,8	0,61	183,9	21,6	243,7	2,6	243,1	1,8	132	100
088-Z68	0,02	0,71	95917,68966	0,05144	0,4	0,2725	0,6	0,0384247	0,5	0,59	194,6	10,5	244,7	1,4	243,1	1,1	125	99
109-Z85	0,06	0,39	28299,44004	0,05133	0,6	0,2727	0,9	0,0385249	0,6	0,67	189,7	14,8	244,8	1,9	243,7	1,5	128	100
105-Z81	0,01	0,50	167073,2994	0,05136	0,3	0,2740	0,6	0,0386925	0,5	0,77	191,0	8,2	245,9	1,4	244,7	1,2	128	100
013-Z8	0,03	0,68	71182,29393	0,05088	0,8	0,2741	1,0	0,0390736	0,7	0,64	169,0	18,3	246,0	2,3	247,1	1,7	146	100
060-Z46	0,01	0,47	134329,8936	0,05113	0,3	0,2747	0,7	0,038962	0,6	0,83	180,7	8,2	246,4	1,5	246,4	1,5	136	100
063-Z47	0,03	0,33	66346,1707	0,05088	0,5	0,2757	0,8	0,0393081	0,6	0,72	169,0	12,9	247,3	1,8	248,5	1,6	147	101
043-Z32	0,71	0,56	2566,366929	0,05138	1,7	0,2768	2,0	0,0390711	1,1	0,59	192,1	38,1	248,1	4,4	247,1	2,8	129	100
064-Z48	0,02	0,52	103430,6366	0,05200	1,0	0,2793	1,4	0,038958	0,9	0,68	219,7	23,1	250,1	3,0	246,4	2,3	112	99

010-Z7	0,73	0,54	2528,218348	0,05523	0,7	0,2819	0,9	0,0370202	0,6	0,67	357,5	14,9	252,2	2,0	234,3	1,4	66	93
009-Z6	0,04	0,44	44475,92895	0,05164	0,6	0,2829	1,0	0,0397367	0,7	0,73	203,6	15,2	253,0	2,2	251,2	1,8	123	99
049-Z38	0,05	0,55	33515,14599	0,05197	0,9	0,2829	1,1	0,0394877	0,7	0,60	218,2	20,9	253,0	2,6	249,7	1,8	114	99
108-Z84	0,09	0,30	19756,30034	0,05169	0,2	0,2841	0,5	0,0398576	0,5	0,93	205,8	4,1	253,9	1,2	252,0	1,3	122	99
065-Z49	0,07	0,65	27550,85476	0,05170	1,6	0,2845	1,9	0,0399049	1,0	0,51	206,5	38,7	254,2	4,3	252,2	2,5	122	99
099-Z77	0,19	0,79	9761,367709	0,05181	0,3	0,2855	0,6	0,0399704	0,5	0,83	211,3	7,2	255,0	1,4	252,6	1,3	120	99
104-Z80	0,04	0,77	44207,79571	0,05164	0,5	0,2865	0,9	0,0402386	0,7	0,75	203,7	12,6	255,8	1,9	254,3	1,7	125	99
018-Z13	0,02	0,54	106472,0273	0,05250	0,4	0,2914	0,7	0,040249	0,6	0,75	242,0	9,7	259,6	1,6	254,4	1,4	105	98
100-Z78	0,02	0,68	108605,1854	0,05151	0,3	0,2917	0,6	0,0410713	0,6	0,85	197,8	6,9	259,9	1,4	259,5	1,4	131	100
080-Z62	0,03	0,30	65495,13118	0,05122	0,3	0,2918	0,7	0,0413167	0,6	0,82	184,6	8,0	260,0	1,5	261,0	1,5	141	100
029-Z22	0,08	0,60	22235,57812	0,05138	0,5	0,2925	0,9	0,0412943	0,7	0,79	191,9	11,9	260,6	2,0	260,9	1,8	136	100
083-Z63	0,08	0,59	23033,06225	0,05516	0,7	0,2963	0,9	0,0389615	0,5	0,51	354,7	15,8	263,5	2,0	246,4	1,2	69	93
087-Z67	0,10	0,39	18164,69308	0,05182	0,3	0,2964	0,6	0,0414873	0,5	0,82	211,9	6,9	263,6	1,4	262,0	1,3	124	99
046-Z35	0,02	0,45	103381,3131	0,05394	1,0	0,2998	1,3	0,0403169	0,8	0,61	303,8	22,5	266,3	2,9	254,8	2,0	84	96
093-Z71	0,03	0,65	53822,64555	0,05110	0,7	0,3006	1,0	0,042669	0,8	0,73	179,1	15,8	266,9	2,4	269,4	2,0	150	101
086-Z66	0,21	0,34	8816,141198	0,05237	0,6	0,3055	0,9	0,0423029	0,6	0,71	236,3	13,3	270,7	2,0	267,1	1,7	113	99
103-Z79	0,04	0,41	42761,47095	0,05311	0,3	0,3061	0,5	0,041798	0,5	0,74	268,2	7,2	271,1	1,3	264,0	1,2	98	97
084-Z64	0,18	0,35	10046,6058	0,05724	1,6	0,3100	2,2	0,0392778	1,5	0,67	437,6	37,7	274,2	5,4	248,4	3,7	57	91
076-Z58	0,08	0,39	22260,31072	0,05312	0,3	0,3115	0,7	0,0425316	0,6	0,85	268,9	7,8	275,4	1,7	268,5	1,6	100	98
027-Z20	0,30	0,57	6139,371768	0,05420	0,6	0,3137	0,9	0,0419807	0,6	0,686	314,9	13,5	277,1	2,1	265,1	1,6	84	96
040-Z31	0,10	0,44	15160,9799	0,12832	1,1	6,1814	1,6	0,3493641	1,2	0,737	2024,7	19,8	2001,8	14,3	1931,6	20,4	95	96
Rejected analyses																		
034-Z25	0,46	0,42	3969,470805	0,03435	11,0	0,1771	11,3	0,0373814	2,8	0,263	-842,0	289,3	165,5	17,2	236,6	6,5	-28	143
039-Z30	0,95	1,14	1931,590159	0,04199	7,4	0,1794	7,6	0,0309844	1,5	0,228	-299,7	179,3	167,5	11,6	196,7	3,0	-66	117
047-Z36	3,66	1,14	503,756509	0,05154	2,3	0,1917	2,5	0,0269746	1,1	0,6	199,3	51,9	178,1	4,1	171,6	1,9	86	96
024-Z17	5,43	1,38	338,5529996	0,04603	10,8	0,2014	11,2	0,0317395	2,9	0,466	-70,1	245,3	186,3	18,9	201,4	5,7	-287	108
077-Z59	0,65	1,13	2802,986308	0,03860	9,8	0,2148	9,9	0,0403478	0,7	0,076	-519,3	244,3	197,5	17,5	255,0	1,9	-49	129
025-Z18	0,52	1,01	3535,782184	0,05013	6,5	0,2215	6,5	0,0320416	0,7	0,109	134,5	145,3	203,1	11,9	203,3	1,4	151	100
057-Z43	3,37	0,61	543,8048576	0,04580	4,4	0,2328	4,5	0,0368654	1,1	0,338	-82,3	103,7	212,5	8,6	233,4	2,4	-283	110
026-Z19	0,08	0,63	22259,6182	0,04257	6,4	0,2357	6,4	0,0401504	0,8	0,113	-264,3	166,2	214,9	12,4	253,8	2,0	-96	118
004-Z1	0,73	0,35	2499,330534	0,04467	6,5	0,2379	6,5	0,0386226	0,7	0,114	-143,8	153,1	216,7	12,6	244,3	1,8	-170	113
020-Z15	0,70	0,51	2606,388269	0,04776	1,0	0,2450	1,1	0,0372014	0,5	0,443	19,1	23,3	222,5	2,2	235,5	1,2	1233	106
007-Z4	0,27	0,46	6675,649099	0,05066	2,8	0,2547	2,9	0,0364564	0,6	0,196	159,1	68,2	230,3	6,0	230,8	1,5	145	100
066-Z50	0,12	0,67	14875,30378	0,05067	2,5	0,2551	2,7	0,0365057	1,0	0,371	159,6	59,2	230,7	5,5	231,1	2,3	145	100
106-Z82	0,47	0,93	3859,562014	0,05038	1,8	0,2669	1,9	0,0384205	0,7	0,341	146,2	40,8	240,2	4,0	243,0	1,6	166	101
055-Z41	0,01	0,82	206262,4292	0,04946	0,7	0,2675	0,8	0,0392203	0,4	0,372	102,8	17,8	240,7	1,8	248,0	1,0	241	103
085-Z65	0,35	1,18	5183,747667	0,05081	3,1	0,2691	3,4	0,0384057	1,4	0,409	166,0	75,1	241,9	7,4	242,9	3,4	146	100

079-Z61	0,39	0,58	4681,449584	0,04643	6,8	0,2767	6,9	0,0432223	1,2	0,177	-48,8	158,6	248,0	15,2	272,8	3,2	-559	110
094-Z72	1,19	0,71	1535,818086	0,04961	6,0	0,2777	6,0	0,0405969	1,0	0,186	109,9	134,8	248,8	13,2	256,5	2,5	233	103
089-Z69	0,38	0,68	4823,897833	0,04973	3,5	0,2780	3,6	0,0405465	0,8	0,212	115,6	81,4	249,1	8,0	256,2	2,0	222	103
044-Z33	0,09	0,49	20065,58359	0,05280	1,1	0,2789	1,2	0,0383031	0,4	0,278	255,2	26,0	249,8	2,6	242,3	1,1	95	97
078-Z60	0,54	0,63	3364,636157	0,04885	2,3	0,2799	2,4	0,0415521	0,8	0,341	73,1	52,7	250,5	5,3	262,4	2,1	359	105
036-Z27	0,63	0,36	2905,739992	0,05245	7,4	0,2958	7,4	0,0408998	0,6	0,076	239,8	162,3	263,1	17,1	258,4	1,5	108	98
067-Z51	0,15	0,57	12042,94864	0,05282	1,3	0,2959	1,5	0,0406226	0,7	0,397	255,9	31,5	263,2	3,4	256,7	1,7	100	98
038-Z29	0,06	0,40	32311,44462	0,05229	0,9	0,2975	1,0	0,0412685	0,5	0,393	232,5	21,4	264,5	2,4	260,7	1,3	112	99
035-Z26	2,75	0,69	663,8951637	0,05075	13,3	0,3068	13,4	0,0438469	1,6	0,166	163,2	284,3	271,7	31,4	276,6	4,3	170	102
023-Z16	0,25	0,48	7325,672176	0,05559	1,5	0,3121	1,6	0,0407181	0,5	0,232	372,2	34,5	275,8	3,8	257,3	1,2	69	93
056-Z42	0,14	0,52	13193,60663	0,05509	2,4	0,3122	2,5	0,0411043	0,7	0,23	351,8	56,5	275,9	6,1	259,7	1,7	74	94
033-Z24	2,66	0,73	685,9084204	0,05417	13,7	0,3188	13,8	0,0426822	1,7	0,175	313,5	285,3	281,0	33,4	269,4	4,6	86	96
073-Z55	0,03	0,41	65739,98491	0,05849	0,8	0,3239	1,0	0,0401634	0,4	0,355	485,3	19,3	284,9	2,4	253,8	1,1	52	89
028-Z21	0,11	0,59	16996,53586	0,06631	1,5	0,3882	1,6	0,0424584	0,7	0,368	756,4	32,1	333,1	4,6	268,1	1,7	35	80

SAMPLE AR-08 - El Freno Formation (34°55'44.37"S - 69°46'8.16"W)

Spot number	f(206)%	Th/U	6/4 ratio	7/6 ratio	1s(%)	7/5 ratio	1s(%)	6/8 ratio	1s(%)	Rho	7/6 age	1s(abs)	7/5 age	1s(abs)	6/8 age	1s(abs)	Conc (%)[1]	Conc (%)[2]
039-Z30	0,14	0,91	12891	0,05018	1,3	0,2217	1,5	0,03204	0,9	0,53	136,5	30,5	203,3	2,8	203,3	1,7	149	100
028-Z21	0,29	0,76	6323	0,05136	0,9	0,2302	1,5	0,03250	1,2	0,78	191,0	22,2	210,3	2,9	206,2	2,4	108	98
023-Z16	0,09	0,53	20211	0,05329	0,7	0,2463	1,0	0,03352	0,7	0,63	276,2	17,4	223,6	2,0	212,6	1,4	77	95
103-Z79	0,08	0,82	24042	0,05050	0,8	0,2408	1,1	0,03458	0,8	0,68	151,8	18,2	219,1	2,1	219,2	1,7	144	100
080-Z62	0,21	0,58	8925	0,04938	1,0	0,2447	1,3	0,03594	0,9	0,65	98,9	23,6	222,3	2,6	227,6	2,0	230	102
108-Z84	0,11	0,16	16107	0,05151	0,3	0,2587	0,6	0,03643	0,5	0,75	198,0	8,0	233,6	1,2	230,6	1,1	116	99
006-Z3	0,08	0,00	24391	0,05127	0,7	0,2588	1,1	0,03660	0,9	0,73	186,9	17,9	233,7	2,4	231,8	2,0	124	99
007-Z4	0,05	0,48	36916	0,05137	0,2	0,2697	0,5	0,03807	0,4	0,81	191,6	5,0	242,4	1,0	240,9	1,0	126	99
037-Z28	0,09	0,40	21212	0,05266	0,5	0,2781	0,7	0,03830	0,5	0,61	249,0	11,7	249,2	1,5	242,3	1,2	97	97
033-Z24	0,41	0,41	4435	0,04819	0,7	0,2564	1,0	0,03859	0,7	0,68	40,5	16,2	231,7	2,0	244,1	1,6	602	105
034-Z25	0,05	0,56	36816	0,05137	0,4	0,2741	0,6	0,03870	0,5	0,71	191,5	8,9	246,0	1,3	244,8	1,2	128	100
029-Z22	0,31	0,38	5903	0,05335	0,8	0,2877	1,5	0,03911	1,3	0,84	278,8	19,2	256,8	3,4	247,3	3,1	89	96
013-Z8	0,11	0,48	16438	0,05738	1,1	0,3098	1,3	0,03916	0,7	0,52	443,1	25,6	274,0	3,2	247,6	1,8	56	90
024-Z17	0,02	0,16	113322	0,05150	0,2	0,2796	0,6	0,03938	0,5	0,86	197,3	5,8	250,4	1,3	249,0	1,3	126	99
027-Z20	0,10	0,55	19218	0,05050	0,7	0,2749	1,1	0,03948	0,8	0,72	151,5	16,9	246,6	2,3	249,6	1,9	165	101
044-Z33	0,05	0,50	38492	0,05118	0,4	0,2789	0,7	0,03952	0,6	0,77	182,8	10,0	249,8	1,6	249,8	1,4	137	100
008-Z5	0,15	0,37	12224	0,05204	0,3	0,2837	0,6	0,03954	0,5	0,85	221,4	6,3	253,6	1,3	250,0	1,3	113	99
109-Z85	0,06	0,31	32784	0,05180	0,3	0,2831	0,6	0,03963	0,5	0,79	211,0	7,1	253,1	1,3	250,5	1,2	119	99
048-Z37	0,37	0,53	5006	0,05339	0,5	0,2935	0,7	0,03986	0,5	0,65	280,6	11,6	261,3	1,7	252,0	1,3	90	96
089-Z69	0,13	0,53	13925	0,05145	0,6	0,2835	0,9	0,03996	0,7	0,71	194,9	14,0	253,4	2,0	252,6	1,6	130	100

038-Z29	0,04	0,51	43747	0,05153	0,4	0,2842	0,7	0,04000	0,6	0,79	198,6	8,9	254,0	1,5	252,8	1,4	127	100
019-Z14	0,09	0,43	20854	0,05106	0,3	0,2818	0,7	0,04003	0,6	0,87	177,5	7,3	252,1	1,5	253,0	1,5	143	100
009-Z6	0,03	0,25	65565	0,05158	0,3	0,2858	1,0	0,04018	1,0	0,96	201,2	6,4	255,3	2,3	254,0	2,5	126	99
096-Z74	0,09	0,30	20869	0,05209	0,3	0,2887	0,5	0,04019	0,4	0,75	223,8	6,2	257,5	1,1	254,0	1,1	113	99
025-Z18	0,02	0,41	95206	0,05151	0,3	0,2858	0,6	0,04024	0,5	0,75	198,0	7,8	255,3	1,3	254,3	1,2	128	100
004-Z1	0,06	0,35	31637	0,05137	0,6	0,2863	0,9	0,04041	0,6	0,70	191,6	13,6	255,6	1,9	255,4	1,6	133	100
056-Z42	0,06	0,31	32826	0,05174	0,2	0,2903	0,5	0,04070	0,5	0,84	208,2	5,2	258,8	1,2	257,2	1,2	124	99
074-Z56	0,21	0,51	8721	0,05168	0,4	0,2904	0,6	0,04075	0,5	0,70	205,5	8,7	258,9	1,4	257,5	1,2	125	99
040-Z31	0,05	0,63	36366	0,05352	0,7	0,3026	1,1	0,04101	0,8	0,72	285,9	16,5	268,4	2,5	259,1	2,0	91	97
083-Z63	0,07	0,41	25904	0,05073	0,4	0,2873	0,6	0,04107	0,5	0,71	162,5	9,6	256,4	1,5	259,5	1,3	160	101
059-Z45	0,04	0,46	44495	0,05197	0,4	0,2946	0,6	0,04110	0,5	0,76	218,6	8,5	262,1	1,4	259,7	1,3	119	99
079-Z61	0,01	0,43	152545	0,05153	0,2	0,2938	0,6	0,04135	0,5	0,89	198,9	5,1	261,6	1,3	261,2	1,3	131	100
099-Z77	0,02	0,43	79217	0,05255	0,3	0,3005	0,6	0,04147	0,5	0,83	244,2	7,0	266,8	1,4	261,9	1,4	107	98
094-Z72	0,02	0,32	95964	0,05253	0,3	0,3003	0,6	0,04147	0,5	0,74	243,2	7,5	266,7	1,3	261,9	1,2	108	98
100-Z78	0,03	0,42	61282	0,05180	0,3	0,2963	0,5	0,04149	0,4	0,75	210,7	6,5	263,5	1,2	262,1	1,1	124	99
057-Z43	0,15	0,31	12052	0,05205	0,3	0,2979	0,5	0,04151	0,4	0,68	222,1	7,8	264,8	1,3	262,2	1,1	118	99
064-Z48	0,06	0,00	32139	0,05135	0,4	0,2940	0,8	0,04152	0,6	0,81	190,5	9,8	261,7	1,8	262,3	1,6	138	100
010-Z7	0,15	0,19	12453	0,05265	0,3	0,3030	0,6	0,04175	0,5	0,78	248,2	7,6	268,8	1,4	263,7	1,3	106	98
067-Z51	0,17	0,50	10814	0,05135	0,4	0,2961	0,7	0,04182	0,5	0,71	190,4	10,5	263,3	1,6	264,1	1,4	139	100
045-Z34	0,07	0,44	24972	0,05164	0,6	0,3003	1,0	0,04218	0,7	0,72	203,8	15,3	266,7	2,3	266,3	1,9	131	100
073-Z55	0,07	0,69	25027	0,05242	0,7	0,3067	0,9	0,04244	0,6	0,62	238,2	16,4	271,6	2,2	267,9	1,6	112	99
066-Z50	0,19	0,92	9804	0,05128	0,3	0,3056	0,5	0,04322	0,4	0,74	187,5	7,1	270,7	1,3	272,7	1,2	145	101
084-Z64	0,16	0,42	11764	0,05232	0,3	0,3129	0,8	0,04337	0,7	0,86	233,7	8,2	276,4	1,8	273,7	1,8	117	99
088-Z68	1,26	0,61	1453	0,04955	2,6	0,2982	3,1	0,04364	1,6	0,60	107,1	60,8	265,0	7,2	275,4	4,4	257	104
106-Z82	0,37	0,64	4885	0,04762	0,6	0,2905	1,3	0,04425	1,2	0,91	12,1	13,3	259,0	3,0	279,1	3,2	2306	108
058-Z44	0,18	0,34	10065	0,05188	0,3	0,3206	0,9	0,04482	0,9	0,94	214,3	6,9	282,4	2,2	282,7	2,4	132	100
050-Z39	0,21	0,38	8648	0,05282	0,6	0,3301	1,0	0,04532	0,7	0,72	256,0	14,7	289,6	2,4	285,7	2,0	112	99
060-Z46	0,23	0,31	7865	0,05183	0,3	0,3362	0,6	0,04704	0,5	0,80	212,2	7,4	294,3	1,5	296,3	1,5	140	101
068-Z52	0,01	0,36	163411	0,05414	0,2	0,4734	0,5	0,06342	0,5	0,88	312,3	4,4	393,6	1,6	396,4	1,8	127	101
086-Z66	0,03	0,44	63068	0,07177	0,2	1,6336	0,6	0,16509	0,5	0,87	921,0	5,2	983,2	3,7	985,0	4,9	107	100
Rejected analysis																		
076-Z58	0,89	0,65	2071	0,04665	2,2	0,2147	2,3	0,03338	0,8	0,37	-37,4	51,5	197,5	4,1	211,7	1,7	-566	107
105-Z81	0,09	0,57	19361	0,04895	1,9	0,2421	2,1	0,03587	0,7	0,29	78,1	47,5	220,1	4,1	227,2	1,5	291	103
055-Z41	1,03	0,56	1781	0,04763	3,3	0,2395	3,4	0,03647	0,7	0,20	12,7	77,3	218,0	6,6	230,9	1,5	1823	106
015-Z10	0,25	0,55	7199	0,05047	0,9	0,2620	1,1	0,03765	0,6	0,47	150,0	21,4	236,3	2,2	238,2	1,3	159	101
035-Z26	0,78	0,48	2335	0,04913	2,1	0,2629	2,4	0,03881	1,1	0,50	86,7	49,6	237,0	5,1	245,5	2,7	283	104
093-Z71	0,44	0,63	4158	0,05327	1,6	0,3027	1,7	0,04122	0,6	0,31	275,3	35,8	268,5	4,0	260,4	1,5	95	97

046-Z35	0,08	0,39	22872	0,05326	1,3	0,3038	1,4	0,04137	0,5	0,27	274,7	31,3	269,3	3,3	261,3	1,3	95	97
065-Z49	0,80	0,31	2298	0,05139	3,0	0,3012	3,0	0,04250	0,7	0,22	192,5	67,4	267,3	7,1	268,3	1,7	139	100
097-Z75	0,36	0,37	5073	0,05307	1,0	0,3112	1,2	0,04253	0,6	0,48	266,7	23,9	275,1	2,9	268,5	1,7	101	98
107-Z83	0,15	0,31	12155	0,04892	2,2	0,2870	2,2	0,04254	0,4	0,12	76,7	53,8	256,2	5,1	268,6	1,1	350	105
026-Z19	0,42	0,47	4354	0,04680	3,0	0,2760	3,3	0,04277	1,3	0,42	-29,8	71,2	247,4	7,2	270,0	3,5	-906	109
016-Z11	1,62	0,29	1126	0,05074	1,8	0,3205	2,0	0,04581	0,69	0,39	162,5	42,2	282,3	4,8	288,7	1,9	178	102

SAMPLE AR-09 - Tordillo Formation (34°57'33.22"S - 69°41'11.48"W)

Spot number	f(206)%	Th/U	6/4 ratio	7/6 ratio	1s(%)	7/5 ratio	1s(%)	6/8 ratio	1s(%)	Rho	7/6 age	1s(abs)	7/5 age	1s(abs)	6/8 age	1s(abs)	Conc (%)[1]	Conc (%)[2]
090-Z58	0,01	0,47	150708	0,04940	0,7517	0,1624	0,9737	0,02385	0,62	0,812	166,7	17,6	152,8	1,4	151,9	0,9	91	99
124-Z80	0,36	0,33	5068	0,05053	0,8164	0,1686	1,229	0,02419	0,92	0,727	219,3	18,9	158,2	1,8	154,1	1,4	70	97
057-Z36	0,39	0,46	4695	0,05526	1,1555	0,1867	1,6207	0,02451	1,13	0,686	422,6	25,6	173,8	2,6	156,1	1,8	37	90
076-Z48	0,04	0,28	47120	0,05179	1,9716	0,1783	2,6829	0,02497	1,82	0,673	276,0	45,2	166,6	4,1	159,0	2,9	58	95
070-Z44	0,06	0,56	29295	0,04948	0,4364	0,1731	0,7152	0,02538	0,57	0,735	170,6	10,2	162,1	1,1	161,5	0,9	95	100
060-Z39	0,10	0,41	17817	0,04812	4,6261	0,1688	5,1251	0,02544	2,21	0,656	105,0	109,3	158,4	7,5	162,0	3,5	154	102
095-Z61	0,04	0,42	51630	0,04867	0,5458	0,1710	0,743	0,02548	0,50	0,586	131,8	12,8	160,3	1,1	162,2	0,8	123	101
106-Z68	0,05	0,90	37681	0,05522	0,617	0,2070	1,0491	0,02720	0,85	0,788	421,0	13,8	191,1	1,8	173,0	1,4	41	91
036-Z23	0,09	0,52	21422	0,04978	1,7106	0,1869	2,0337	0,02723	1,10	0,775	185,0	39,8	174,0	3,3	173,2	1,9	94	100
022-Z13	0,03	0,84	69000	0,05078	0,5683	0,1909	0,9336	0,02727	0,74	0,764	231,0	13,1	177,4	1,5	173,4	1,3	75	98
009-Z4	0,05	1,40	39989	0,05014	0,6482	0,1893	0,9546	0,02738	0,70	0,696	201,6	15,0	176,0	1,5	174,1	1,2	86	99
118-Z76	0,14	1,76	12828	0,05242	0,7527	0,1986	1,0838	0,02748	0,78	0,688	303,6	17,2	184,0	1,8	174,8	1,3	58	95
024-Z15	0,09	0,36	19866	0,05205	0,6213	0,1979	1,1617	0,02757	0,98	0,947	287,4	14,2	183,3	1,9	175,3	1,7	61	96
012-Z7	0,18	0,75	10406	0,05422	1,1062	0,2070	1,3121	0,02769	0,71	0,684	380,3	24,9	191,1	2,3	176,1	1,2	46	92
078-Z50	0,05	1,25	34007	0,05131	0,6635	0,1960	0,9282	0,02770	0,65	0,858	254,6	15,3	181,7	1,5	176,1	1,1	69	97
027-Z16	0,01	0,13	247698	0,04982	0,2147	0,1925	0,5086	0,02803	0,46	0,848	186,4	5,0	178,8	0,8	178,2	0,8	96	100
072-Z46	0,01	1,25	162011	0,05072	0,8711	0,1963	1,0731	0,02807	0,63	0,774	228,2	20,1	182,0	1,8	178,5	1,1	78	98
016-Z9	0,15	1,85	12375	0,05072	0,9	0,1979	1,3	0,02829	0,84	0,64	227,9	21,7	183,3	2,1	179,9	1,5	79	98
011-Z6	0,03	0,38	71764	0,05018	0,6	0,1971	1,1	0,02848	0,92	0,83	203,2	13,6	182,6	1,8	181,0	1,6	89	99
112-Z72	0,11	1,78	16257	0,05268	0,7	0,2080	1,0	0,02864	0,76	0,70	314,9	16,1	191,9	1,8	182,0	1,4	58	95
005-Z2	0,07	1,23	25977	0,04941	1,0	0,1977	1,6	0,02902	1,20	0,76	167,3	23,1	183,2	2,6	184,4	2,2	110	101
102-Z66	0,53	1,46	3498	0,05120	3,1	0,2083	3,4	0,02950	1,34	0,65	249,9	69,2	192,1	5,9	187,4	2,5	75	98
071-Z45	0,20	1,88	9224	0,05207	0,9	0,2205	1,2	0,03072	0,88	0,68	288,4	19,9	202,4	2,3	195,0	1,7	68	96
023-Z14	0,03	0,42	71113	0,05252	0,6	0,2520	1,8	0,03480	1,73	0,94	307,9	14,1	228,2	3,7	220,5	3,7	72	97
123-Z79	0,33	0,70	5485	0,05115	0,7	0,2515	0,8	0,03566	0,51	0,51	247,4	15,3	227,8	1,7	225,9	1,1	91	99
004-Z1	0,10	0,98	19063	0,05066	1,1	0,2532	1,8	0,03625	1,44	0,79	225,6	25,3	229,2	3,7	229,5	3,2	102	100
029-Z18	0,06	0,86	30707	0,05178	0,6	0,2612	1,0	0,03659	0,74	0,74	275,6	13,9	235,7	2,0	231,7	1,7	84	98
077-Z49	0,12	0,89	15341	0,05560	0,7	0,2962	1,1	0,03864	0,79	0,70	436,4	16,4	263,4	2,5	244,4	1,9	56	93

006-Z3	0,11	0,33	16148	0,05016	5,2	0,2867	5,9	0,04145	2,76	0,72	202,5	121,0	255,9	13,3	261,8	7,1	129	102
119-Z77	0,06	0,56	30645	0,05190	0,7	0,3247	1,2	0,04537	0,92	0,78	281,1	16,0	285,5	2,9	286,1	2,6	102	100
113-Z73	0,03	0,47	63962	0,05454	0,4	0,3655	0,8	0,04861	0,68	0,81	393,3	9,9	316,3	2,2	306,0	2,0	78	97
046-Z29	0,02	0,48	77829	0,05286	0,3	0,3575	0,6	0,04906	0,51	0,80	322,6	6,9	310,4	1,6	308,7	1,5	96	99
081-Z51	0,09	0,60	19956	0,05380	0,3	0,3649	0,7	0,04919	0,57	0,84	362,8	7,0	315,8	1,8	309,5	1,7	85	98
015-Z8	0,02	0,38	92882	0,05310	0,7	0,3634	0,9	0,04963	0,59	0,57	333,2	16,0	314,7	2,5	312,3	1,8	94	99
125-Z81	0,10	0,55	18964	0,05309	0,5	0,3809	0,8	0,05203	0,59	0,72	332,8	10,9	327,7	2,1	327,0	1,9	98	100
100-Z64	0,05	0,52	38334	0,05362	0,5	0,3858	1,8	0,05218	1,73	0,97	355,3	10,3	331,3	5,1	327,9	5,5	92	99
033-Z20	0,07	0,64	26557	0,05385	0,8	0,4023	1,2	0,05419	0,90	0,72	364,8	18,5	343,4	3,5	340,2	3,0	93	99
010-Z5	0,01	0,28	207950	0,06689	0,5	0,7224	1,6	0,07833	1,56	0,95	834,3	10,3	552,1	7,0	486,1	7,3	58	88
054-Z35	0,01	0,12	285330	0,05860	0,3	0,6965	0,5	0,08620	0,43	0,73	552,4	7,4	536,7	2,3	533,0	2,2	96	99
040-Z25	0,00	0,29	511561	0,06203	0,2	0,8560	0,6	0,10008	0,57	0,96	675,2	3,2	628,0	2,8	614,9	3,3	91	98
034-Z21	0,01	0,27	299804	0,07579	0,2	1,7766	0,5	0,17002	0,42	0,84	1089,5	3,7	1037,0	3,0	1012,2	3,9	93	98
111-Z71	0,01	0,35	269544	0,08096	0,1	2,3376	0,5	0,20941	0,48	0,96	1220,5	2,3	1223,8	3,5	1225,7	5,3	100	100
Rejected analysis																		
089-Z57	0,24	0,65	7593	0,06198	2,0	0,2153	2,6	0,02519	1,6	0,61	673,4	43,8	198,0	4,7	160,4	2,6	24	81
028-Z17	0,52	0,48	3526	0,04472	1,0	0,1674	1,4	0,02716	1,0	0,70	-71,0	23,5	157,2	2,0	172,7	1,7	-243	110
035-Z22	0,85	0,33	2177	0,05776	0,8	0,2172	0,9	0,02727	0,6	0,53	520,6	16,6	199,6	1,7	173,4	1,0	33	87
039-Z24	0,12	0,60	15238	0,06386	7,8	0,2542	10,4	0,02887	6,9	0,66	736,9	164,9	230,0	21,5	183,5	12,5	25	80
084-Z54	0,05	0,57	38842	0,08869	41,1	0,7474	45,0	0,06112	18,4	0,67	1397,6	787,3	566,7	195,5	382,4	68,4	27	67

SAMPLE AR-11 - Tordillo Formation (35°11'54.75"S - 69°45'54.20"W)

Spot number	f(206)%	Th/U	6/4 ratio	7/6 ratio	1s(%)	7/5 ratio	1s(%)	6/8 ratio	1s(%)	Rho	7/6 age	1s(abs)	7/5 age	1s(abs)	6/8 age	1s(abs)	Conc (%)[1]	Conc (%)[2]
067-Z43	0,15	0,30	12403	0,05385	1,5	0,1689	1,7	0,02275	0,8	0,42	364,7	33,6	158,5	2,5	145,0	1,1	40	92
066-Z42	0,08	0,25	24031	0,05507	1,1	0,1763	1,2	0,02321	0,5	0,55	415,1	24,6	164,8	1,8	147,9	0,7	36	90
089-Z57	0,45	0,36	4097	0,05409	0,8	0,1768	0,9	0,02371	0,5	0,43	374,8	17,5	165,3	1,4	151,1	0,7	40	91
094-Z60	0,10	0,35	18601	0,05853	0,7	0,1916	0,9	0,02374	0,6	0,59	549,7	15,0	178,0	1,5	151,2	0,9	28	85
033-Z20	0,58	0,35	3180	0,05799	1,2	0,1902	1,4	0,02379	0,7	0,49	529,4	26,2	176,8	2,3	151,5	1,1	29	86
126-Z81	0,04	0,35	46439	0,05212	0,4	0,1713	0,7	0,02384	0,6	0,81	290,5	8,1	160,6	1,0	151,9	0,9	52	95
065-Z41	0,29	0,76	6389	0,05339	0,6	0,1762	0,9	0,02394	0,7	0,73	345,3	13,1	164,8	1,4	152,5	1,0	44	93
114-Z74	0,05	0,28	35165	0,04945	0,2	0,1681	0,5	0,02466	0,4	0,81	169,2	5,3	157,8	0,7	157,0	0,7	93	100
120-Z78	0,20	0,45	9036	0,04991	0,2	0,1727	0,5	0,02509	0,5	0,88	190,7	4,9	161,7	0,8	159,8	0,8	84	99
046-Z29	0,22	0,60	8288	0,05135	0,5	0,1786	0,8	0,02523	0,6	0,73	256,5	11,4	166,8	1,2	160,6	1,0	63	96
024-Z15	0,13	0,23	13984	0,05020	0,6	0,1777	0,8	0,02568	0,5	0,71	204,1	14,1	166,1	1,2	163,4	0,7	80	98
029-Z18	0,05	0,60	36530	0,04947	0,7	0,1755	1,0	0,02573	0,7	0,66	170,1	16,6	164,2	1,5	163,8	1,1	96	100
045-Z28	0,74	0,45	2495	0,04834	0,9	0,1772	1,3	0,02659	0,9	0,66	116,0	21,4	165,7	1,9	169,2	1,4	146	102
101-Z65	0,03	1,12	63957	0,05270	0,3	0,2154	0,6	0,02965	0,5	0,78	315,8	7,0	198,1	1,0	188,4	0,9	60	95

085-Z55	21,15	1,44	87	0,05777	3,1	0,2377	3,9	0,02984	1,8	0,76	521,2	66,9	216,5	7,6	189,5	4,4	36	88
011-Z06	0,28	0,61	6596	0,05022	0,8	0,2067	1,3	0,02985	1,0	0,76	205,1	19,3	190,8	2,3	189,6	1,9	92	99
078-Z50	0,05	0,66	38984	0,05482	0,8	0,2540	1,0	0,03361	0,6	0,56	404,8	17,1	229,8	2,0	213,1	1,3	53	93
091-Z59	0,00	0,42	669156	0,05303	0,8	0,2712	1,0	0,03709	0,5	0,70	330,1	19,0	243,6	2,1	234,8	1,2	71	96
057-Z36	0,31	0,52	5982	0,05532	0,4	0,2946	0,7	0,03863	0,6	0,77	425,3	9,2	262,2	1,7	244,3	1,4	57	93
073-Z47	0,27	0,77	6741	0,05892	1,1	0,3188	1,3	0,03924	0,5	0,60	564,2	24,9	281,0	3,1	248,1	1,3	44	88
125-Z80	1,33	0,55	1372	0,04744	0,4	0,2636	1,4	0,04030	1,3	0,96	71,4	9,4	237,6	2,9	254,7	3,3	357	107
059-Z38	0,17	0,57	10930	0,05859	1,0	0,3316	1,2	0,04105	0,7	0,55	551,8	21,2	290,8	3,0	259,3	1,8	47	89
040-25	0,05	0,44	33838	0,05374	0,6	0,3183	0,9	0,04296	0,7	0,70	360,1	13,3	280,6	2,2	271,2	1,8	75	97
042-Z27	0,12	0,35	14858	0,05324	0,4	0,3172	0,7	0,04321	0,6	0,92	338,9	9,3	279,7	1,8	272,7	1,6	80	97
021-Z12	0,03	0,52	65090	0,05347	0,7	0,3221	1,0	0,04368	0,6	0,61	348,9	16,3	283,5	2,4	275,6	1,7	79	97
121-Z79	0,09	0,35	20063	0,05223	0,4	0,3171	0,7	0,04402	0,5	0,90	295,7	9,3	279,6	1,7	277,7	1,5	94	99
054-Z35	0,06	0,41	31227	0,05493	1,1	0,3602	1,3	0,04756	0,7	0,75	409,5	24,7	312,4	3,5	299,5	2,1	73	96
022-Z13	0,00	0,35	370988	0,05297	0,2	0,3566	0,6	0,04882	0,5	0,90	327,5	4,6	309,7	1,5	307,3	1,5	94	99
088-Z56	0,02	0,26	87321	0,05271	0,4	0,3559	0,7	0,04897	0,5	0,67	316,5	10,0	309,2	1,8	308,2	1,5	97	100
041-Z26	0,03	0,60	67488	0,05306	0,7	0,3683	1,1	0,05034	0,8	0,72	331,5	16,5	318,4	3,0	316,6	2,5	96	99
100-Z64	0,02	0,39	112854	0,05492	0,5	0,3871	0,7	0,05113	0,5	0,68	408,9	10,4	332,3	2,0	321,4	1,7	79	97
107-Z69	0,00	0,33	899504	0,05939	3,0	0,4955	3,8	0,06052	2,4	0,62	581,3	64,1	408,7	12,7	378,8	8,7	65	93
106-Z68	0,00	0,32	370077	0,05896	0,6	0,4987	0,8	0,06135	0,6	0,64	565,6	13,1	410,9	2,8	383,8	2,2	68	93
102-Z66	0,01	0,66	273790	0,05429	0,4	0,4646	0,7	0,06206	0,6	0,81	383,2	8,1	387,4	2,2	388,1	2,2	101	100
015-Z08	0,01	0,14	186378	0,05455	0,2	0,4745	0,5	0,06309	0,4	0,88	393,8	3,9	394,3	1,5	394,4	1,7	100	100
109-Z71	0,00	0,05	1502626	0,05559	0,5	0,5558	0,7	0,07251	0,5	0,83	436,0	11,3	448,8	2,6	451,3	2,2	103	101
079-Z51	0,10	0,34	18437	0,07204	0,6	1,1402	1,0	0,11479	0,9	0,94	987,1	11,3	772,6	5,6	700,5	5,8	71	91
113-Z73	0,05	0,20	36516	0,06966	0,2	1,2311	0,5	0,12817	0,5	0,92	918,5	3,5	814,9	2,9	777,4	3,6	85	95
027-Z16	0,00	0,21	395874	0,06749	0,2	1,3312	0,6	0,14307	0,5	0,93	852,8	3,6	859,4	3,3	862,0	4,4	101	100
112-Z72	0,09	0,28	19661	0,07548	0,3	1,8954	0,5	0,18212	0,5	0,80	1081,4	5,1	1079,5	3,5	1078,5	4,5	100	100
108-Z70	0,00	0,31	740237	0,09003	0,2	3,0566	0,5	0,24624	0,5	0,83	1426,2	4,3	1421,9	3,9	1419,1	5,8	100	100
Rejected analysis																		
084-Z54	0,39	0,94	4740	0,03827	11,6	0,1401	11,7	0,02655	1,5	0,12	-466,8	282,3	133,1	14,5	168,9	2,5	-36	127
039-Z24	0,05	0,45	35866	0,06321	7,1	0,2413	9,5	0,02768	6,3	0,66	715,5	150,7	219,5	18,7	176,0	10,9	25	80
036-Z23	0,05	0,28	39641	0,06313	15,0	0,2511	16,4	0,02885	6,6	0,66	712,5	318,6	227,5	33,4	183,4	11,9	26	81
010-Z05	0,06	0,33	29464	0,07286	14,1	0,3449	20,2	0,03434	14,4	0,71	1009,9	286,9	300,9	52,6	217,6	30,9	22	72
127-Z82	8,97	0,39	204	0,03852	60,2	0,2115	61,0	0,03981	8,6	0,27	-449,0	1113,7	194,8	102,7	251,7	23,3	-56	129
058-Z37	3,68	0,27	497	0,09109	22,1	0,5008	32,7	0,03988	23,2	0,72	1448,4	371,1	412,3	105,2	252,1	59,4	17	61
090-Z58	0,10	0,61	17775	0,09234	13,9	0,5759	18,1	0,04523	11,6	0,64	1474,4	264,1	461,8	67,3	285,2	32,4	19	62
082-Z52	0,29	0,28	6272	0,06625	5,9	0,4903	7,7	0,05368	5,0	0,65	814,2	122,4	405,1	25,6	337,1	16,3	41	83
048-Z31	0,37	0,55	4949	0,08237	29,9	0,6319	32,6	0,05564	12,9	0,65	1254,2	495,1	497,3	120,7	349,1	43,7	28	70

023-Z14	0,26	0,33	6806	0,16167	24,5	1,5658	34,1	0,07024	23,8	0,70	2473,2	413,7	956,8	211,5	437,6	100,5	18	46
083-Z53	1,80	1,26	972	0,19069	37,6	3,3005	59,0	0,12553	44,7	0,76	2748,1	513,4	1481,2	379,4	762,3	319,0	28	51

SAMPLE JTCC-420 - Tordillo Formation (34°59'40.63"S - 69°45'31.97"W)

Spot number	f(206)%	Th/U	6/4 ratio	7/6 ratio	1s(%)	7/5 ratio	1s(%)	6/8 ratio	1s(%)	Rho	7/6 age	1s(abs)	7/5 age	1s(abs)	6/8 age	1s(abs)	Conc (%)[1]	Conc (%)[2]
117-Z75	0,03	0,76	65833	0,05132	0,5	0,1614	0,7	0,02280	0,5	0,60	255,1	11,1	151,9	1,0	145,4	0,7	57	96
125-Z81	0,05	0,97	38437	0,04904	0,6	0,1552	0,9	0,02295	0,6	0,66	149,9	14,3	146,5	1,2	146,2	0,9	98	100
102-Z66	0,06	1,09	32019	0,05067	2,2	0,1611	2,3	0,02306	0,7	0,48	225,6	50,0	151,6	3,2	146,9	1,0	65	97
093-Z59	0,02	0,75	87585	0,05005	0,5	0,1613	0,8	0,02338	0,6	0,66	197,1	12,2	151,8	1,1	149,0	0,8	76	98
047-Z30	0,04	1,07	44782	0,04935	0,3	0,1598	0,6	0,02348	0,5	0,77	164,6	6,8	150,5	0,8	149,6	0,7	91	99
123-Z79	0,04	0,90	49852	0,04901	0,7	0,1587	1,2	0,02348	1,0	0,80	148,2	15,7	149,5	1,6	149,6	1,4	101	100
101-Z65	0,01	0,49	136041	0,04925	0,3	0,1622	0,6	0,02389	0,5	0,84	159,6	6,4	152,7	0,8	152,2	0,8	95	100
099-Z63	0,01	0,65	207838	0,04954	0,2	0,1656	0,5	0,02425	0,5	0,88	173,3	4,6	155,6	0,8	154,5	0,7	89	99
033-Z20	0,03	0,49	72543	0,04922	0,3	0,1660	0,5	0,02446	0,5	0,78	158,4	6,5	155,9	0,8	155,8	0,7	98	100
028-Z17	0,05	0,47	39391	0,04934	0,8	0,1826	1,1	0,02685	0,8	0,67	164,1	18,3	170,3	1,7	170,8	1,3	104	100
039-Z24	0,03	1,08	66753	0,05032	0,8	0,1873	1,0	0,02700	0,6	0,52	210,0	18,4	174,4	1,6	171,7	1,0	82	99
058-Z37	0,08	0,35	23655	0,04947	0,6	0,1919	1,0	0,02813	0,8	0,79	170,1	13,3	178,2	1,6	178,9	1,4	105	100
077-Z49	0,08	0,81	22857	0,05044	1,4	0,1958	1,9	0,02816	1,3	0,66	215,3	32,8	181,6	3,2	179,0	2,3	83	99
060-Z39	0,15	0,98	12600	0,05163	1,2	0,2058	1,3	0,02892	0,6	0,62	268,9	26,9	190,0	2,3	183,8	1,0	68	97
075-Z47	0,36	0,62	5079	0,05316	1,2	0,2234	1,4	0,03048	0,6	0,39	335,6	27,9	204,7	2,5	193,5	1,2	58	95
024-Z15	0,04	0,82	41188	0,05272	2,0	0,2220	2,2	0,03055	0,8	0,61	316,7	45,1	203,6	4,0	194,0	1,6	61	95
096-Z62	0,02	1,50	100718	0,05030	0,6	0,2232	0,8	0,03218	0,5	0,81	209,0	13,1	204,6	1,4	204,2	1,0	98	100
083-Z53	0,23	1,76	7872	0,05163	0,6	0,2301	0,8	0,03233	0,6	0,65	268,8	13,1	210,3	1,5	205,1	1,2	76	98
017-Z10	0,03	0,84	56812	0,05012	0,7	0,2300	1,0	0,03328	0,7	0,70	200,6	15,8	210,2	1,9	211,0	1,5	105	100
036-Z23	0,13	0,40	13994	0,05449	1,0	0,2507	1,2	0,03337	0,7	0,70	391,3	22,0	227,1	2,5	211,6	1,5	54	93
021-Z12	0,03	0,79	58611	0,05044	0,6	0,2331	0,9	0,03351	0,7	0,73	215,2	13,4	212,7	1,7	212,5	1,5	99	100
012-Z7	0,02	0,66	118701	0,05131	0,8	0,2389	1,0	0,03376	0,5	0,74	254,7	18,0	217,5	1,9	214,1	1,1	84	98
087-Z55	0,04	0,94	47553	0,05086	0,7	0,2373	1,1	0,03384	0,8	0,75	234,5	15,9	216,2	2,1	214,6	1,8	92	99
114-Z74	0,03	0,89	55812	0,05123	1,5	0,2599	1,7	0,03679	0,7	0,62	251,4	35,0	234,6	3,5	232,9	1,6	93	99
120-Z78	0,02	0,99	95645	0,05123	0,9	0,2690	1,0	0,03808	0,6	0,72	251,0	19,9	241,9	2,2	240,9	1,3	96	100
119-Z77	0,01	0,72	346444	0,05112	0,2	0,2686	0,6	0,03811	0,6	0,93	246,0	4,8	241,6	1,3	241,1	1,4	98	100
065-Z41	0,01	1,03	133202	0,05164	0,3	0,2722	0,5	0,03823	0,4	0,77	269,7	6,2	244,5	1,1	241,9	1,1	90	99
030-Z19	0,04	1,01	45445	0,05264	0,6	0,2844	0,8	0,03918	0,4	0,65	313,2	14,1	254,1	1,7	247,7	1,0	79	97
015-Z8	0,02	1,23	102876	0,05325	0,4	0,2909	0,7	0,03962	0,5	0,71	339,7	9,8	259,3	1,6	250,5	1,3	74	97
100-Z64	0,04	0,27	43511	0,05196	0,5	0,2861	0,7	0,03994	0,6	0,72	283,5	10,8	255,5	1,7	252,5	1,4	89	99
112-Z72	0,00	0,06	461038	0,05207	0,1	0,2893	0,6	0,04029	0,5	0,95	288,7	3,3	258,0	1,3	254,6	1,3	88	99
106-Z68	0,04	0,43	50878	0,05285	0,3	0,2949	0,6	0,04047	0,5	0,80	322,2	7,4	262,4	1,5	255,7	1,3	79	97

054-Z35	0,02	0,67	105515	0,05308	0,6	0,2994	0,7	0,04091	0,5	0,74	332,3	12,9	265,9	1,7	258,4	1,1	78	97
118-Z76	0,02	0,61	108597	0,05317	0,3	0,3037	0,6	0,04143	0,5	0,79	335,9	6,4	269,3	1,3	261,7	1,2	78	97
045-Z28	0,23	0,63	7790	0,05518	0,3	0,3209	0,5	0,04218	0,5	0,81	419,7	5,9	282,6	1,3	266,3	1,3	63	94
051-Z32	2,44	0,71	750	0,05863	1,3	0,3584	1,8	0,04434	1,2	0,67	553,3	28,1	311,0	4,8	279,7	3,4	51	90
107-Z69	0,04	0,54	51866	0,05283	0,6	0,3249	0,9	0,04460	0,7	0,72	321,6	14,0	285,7	2,3	281,3	1,9	87	98
105-Z67	0,02	0,54	105734	0,05272	0,5	0,3435	0,7	0,04725	0,5	0,70	317,0	10,3	299,8	1,8	297,6	1,6	94	99
027-Z16	0,07	0,64	25114	0,05650	0,8	0,3701	1,1	0,04751	0,7	0,62	472,1	18,5	319,7	3,1	299,2	2,1	63	94
089-Z57	0,06	0,61	28309	0,05355	0,7	0,3516	1,0	0,04761	0,7	0,71	352,3	15,3	305,9	2,7	299,8	2,2	85	98
088-Z56	0,03	0,62	65823	0,05303	0,3	0,3509	0,6	0,04798	0,5	0,78	330,2	7,5	305,4	1,6	302,1	1,5	91	99
084-Z54	0,04	0,42	49958	0,05312	0,7	0,3649	0,9	0,04982	0,5	0,76	333,8	16,9	315,9	2,5	313,4	1,7	94	99
005-Z2	0,03	0,66	57674	0,05296	0,5	0,3679	0,8	0,05038	0,6	0,70	327,1	11,7	318,1	2,1	316,8	1,8	97	100
041-Z26	0,03	0,22	72397	0,05425	0,5	0,3792	1,0	0,05069	0,9	0,85	381,5	11,4	326,5	2,8	318,8	2,7	84	98
113-Z73	0,02	0,34	85079	0,05398	0,3	0,3935	0,7	0,05287	0,7	0,86	370,1	7,7	336,9	2,1	332,1	2,1	90	99
006-Z3	0,03	0,45	70254	0,05388	0,9	0,4090	1,0	0,05505	0,5	0,71	366,1	19,3	348,1	3,0	345,5	1,8	94	99
124-Z80	0,01	0,48	126081	0,05402	0,5	0,4221	0,8	0,05668	0,6	0,74	371,9	11,0	357,6	2,4	355,4	2,1	96	99
082-Z52	0,00	0,34	463445	0,05393	0,2	0,4346	0,5	0,05845	0,5	0,93	368,1	3,8	366,5	1,7	366,2	1,8	99	100
048-Z31	0,01	0,39	161600	0,05420	0,6	0,4407	0,8	0,05898	0,5	0,80	379,3	12,5	370,8	2,3	369,4	1,8	97	100
035-Z22	0,01	0,11	149930	0,06000	0,5	0,4911	0,9	0,05935	0,7	0,82	603,7	10,4	405,6	3,0	371,7	2,7	62	92
011-Z6	0,03	0,19	49803	0,07413	0,3	1,5194	0,7	0,14865	0,6	0,89	1045,1	5,5	938,2	4,2	893,4	5,2	85	95
023-Z14	0,00	0,43	362688	0,07705	0,3	1,8926	0,6	0,17814	0,5	0,82	1122,5	5,7	1078,5	3,9	1056,8	5,1	94	98

Rejected analysis

040-Z25	0,26	1,15	6982	0,06704	7,1	0,3356	9,6	0,03630	6,4	0,67	839,0	148,6	293,8	24,5	229,9	14,5	27	78

SAMPLE JTRS-407 - Tordillo Formation (35°10'40.62"S - 69°52'31.95"W)

Spot number	f(206)%	Th/U	6/4 ratio	7/6 ratio	1s(%)	7/5 ratio	1s(%)	6/8 ratio	1s(%)	Rho	7/6 age	1s(abs)	7/5 age	1s(abs)	6/8 age	1s(abs)	Conc (%)[1]	Conc (%)[2]
097-Z75	0,03	0,37	56154	0,04995	0,5	0,1602	0,8	0,02326	0,6	0,70	192,8	11,8	150,9	1,1	148,2	0,9	77	98
043-Z32	0,05	0,52	36715	0,04898	1,1	0,1586	1,3	0,02348	0,6	0,41	147,0	26,7	149,5	1,8	149,6	0,9	102	100
010-Z7	0,05	0,51	37376	0,04934	1,1	0,1601	1,4	0,02354	0,9	0,82	164,2	26,2	150,8	2,0	150,0	1,3	91	99
105-Z81	0,03	0,45	61174	0,04911	1,3	0,1602	1,4	0,02366	0,6	0,35	153,1	29,8	150,9	2,0	150,7	0,9	98	100
048-Z37	0,05	0,39	34781	0,05188	0,4	0,1731	0,7	0,02420	0,5	0,75	280,1	8,7	162,1	1,0	154,1	0,8	55	95
106-Z82	0,05	0,61	36187	0,04976	1,3	0,1681	1,4	0,02450	0,5	0,31	183,6	30,0	157,8	2,0	156,1	0,8	85	99
096-Z74	0,06	0,67	28681	0,04993	0,5	0,1704	0,7	0,02475	0,5	0,79	191,6	12,2	159,7	1,0	157,6	0,7	82	99
070-Z54	0,03	0,60	54317	0,04956	0,8	0,1731	1,0	0,02533	0,7	0,82	174,6	18,5	162,1	1,6	161,3	1,1	92	99
038-Z29	0,38	0,38	4871	0,05323	0,4	0,1875	0,7	0,02556	0,6	0,78	338,4	8,6	174,5	1,1	162,7	0,9	48	93
077-Z59	0,04	0,47	43082	0,05065	0,3	0,1829	0,6	0,02620	0,5	0,83	224,9	6,5	170,6	0,9	166,7	0,9	74	98
089-Z69	0,06	0,45	32090	0,05009	0,9	0,1816	1,3	0,02629	0,9	0,67	199,3	21,7	169,4	2,0	167,3	1,5	84	99
009-Z6	0,16	1,39	11278	0,05221	1,8	0,1903	2,2	0,02643	1,3	0,59	294,5	40,0	176,9	3,6	168,2	2,2	57	95

025-Z18	0,02	0,63	105296	0,04983	0,6	0,1848	0,9	0,02689	0,6	0,61	187,1	14,9	172,2	1,4	171,1	1,0	91	99
019-Z14	0,04	0,93	48503	0,05026	0,5	0,1930	0,9	0,02785	0,7	0,78	207,0	12,2	179,2	1,5	177,1	1,3	86	99
014-Z9	0,25	0,91	7389	0,05170	1,0	0,2003	1,2	0,02809	0,7	0,50	272,2	23,1	185,3	2,0	178,6	1,2	66	96
017-Z12	0,22	1,12	8247	0,05060	1,3	0,1963	1,4	0,02814	0,6	0,38	222,7	29,0	182,0	2,3	178,9	1,1	80	98
103-Z79	0,04	1,09	46702	0,04975	1,2	0,1935	1,4	0,02821	0,6	0,41	183,5	29,1	179,6	2,3	179,3	1,1	98	100
015-Z10	0,01	0,37	172089	0,04980	0,2	0,1940	0,5	0,02826	0,4	0,81	185,7	4,8	180,1	0,8	179,6	0,7	97	100
107-Z83	0,04	0,30	46107	0,04954	0,5	0,1931	0,7	0,02827	0,4	0,49	173,5	12,8	179,3	1,2	179,7	0,8	104	100
059-Z45	0,11	1,44	16749	0,04974	0,4	0,1940	0,6	0,02829	0,5	0,67	183,1	9,4	180,0	1,0	179,8	0,8	98	100
026-Z19	0,02	0,34	82575	0,05024	0,7	0,1959	0,9	0,02829	0,4	0,48	206,0	17,1	181,7	1,4	179,8	0,8	87	99
008-Z5	0,02	0,38	89470	0,05020	0,2	0,1962	0,6	0,02834	0,6	0,93	204,3	4,5	181,9	1,0	180,2	1,0	88	99
108-Z84	0,11	1,13	16384	0,04845	1,1	0,1900	1,5	0,02845	1,0	0,64	121,5	26,0	176,7	2,4	180,8	1,7	149	102
076-Z58	0,03	0,75	63308	0,05014	0,6	0,1995	0,9	0,02886	0,6	0,83	201,7	14,8	184,7	1,4	183,4	1,0	91	99
033-Z24	0,06	1,11	30951	0,05064	0,9	0,2030	1,3	0,02907	0,9	0,70	224,3	21,2	187,7	2,3	184,8	1,7	82	98
057-Z43	0,34	0,23	5384	0,05136	0,7	0,2066	0,9	0,02917	0,6	0,58	257,0	15,3	190,7	1,5	185,4	1,0	72	97
037-Z28	0,02	0,21	122317	0,05158	0,6	0,2076	0,8	0,02918	0,6	0,65	266,9	13,5	191,5	1,5	185,4	1,1	69	97
030-Z23	0,03	0,35	67782	0,05034	1,8	0,2027	2,0	0,02920	0,9	0,57	210,7	41,2	187,4	3,4	185,5	1,6	88	99
088-Z68	0,04	1,17	44378	0,05045	0,9	0,2035	1,1	0,02926	0,6	0,55	215,7	19,8	188,1	1,8	185,9	1,2	86	99
100-Z78	0,06	1,23	33266	0,05079	1,4	0,2182	1,6	0,03116	0,9	0,75	231,3	31,8	200,4	2,9	197,8	1,7	86	99
084-Z64	0,06	1,21	31995	0,05002	0,4	0,2151	1,0	0,03119	1,0	0,93	196,1	8,2	197,8	1,8	198,0	1,9	101	100
040-Z31	0,06	0,48	33393	0,05175	0,4	0,2338	0,7	0,03276	0,5	0,85	274,4	10,3	213,3	1,3	207,8	1,0	76	97
080-Z62	0,11	0,68	16283	0,04795	2,4	0,2228	2,6	0,03370	1,2	0,69	97,0	55,6	204,2	4,8	213,6	2,4	220	105
027-Z20	0,02	0,04	74248	0,05307	0,7	0,2808	1,1	0,03838	0,8	0,76	331,8	15,1	251,3	2,4	242,8	2,0	73	97
016-Z11	0,02	0,56	87722	0,05161	0,5	0,2736	0,7	0,03845	0,5	0,79	268,4	12,4	245,6	1,6	243,2	1,1	91	99
109-Z85	0,01	0,86	178295	0,05120	0,7	0,2719	0,9	0,03851	0,6	0,54	250,1	16,7	244,2	2,0	243,6	1,3	97	100
007-Z4	0,02	0,59	78227	0,05261	0,4	0,2810	0,6	0,03874	0,4	0,60	312,1	8,5	251,5	1,3	245,0	1,0	79	97
020-Z15	0,05	0,29	34721	0,05315	1,2	0,3051	2,4	0,04164	2,0	0,96	335,0	27,3	270,4	5,6	263,0	5,2	78	97
006-Z3	0,12	0,13	14948	0,05437	0,3	0,3226	0,5	0,04303	0,5	0,90	386,5	6,5	283,9	1,3	271,6	1,2	70	96
029-Z22	0,03	0,10	57780	0,05430	0,8	0,3298	1,2	0,04406	0,8	0,68	383,4	19,0	289,5	3,0	277,9	2,3	72	96
039-Z30	0,87	0,39	2101	0,04992	0,6	0,3054	1,0	0,04437	0,8	0,80	191,3	13,2	270,6	2,4	279,9	2,3	146	103
058-Z44	0,47	0,54	3879	0,05168	0,9	0,3194	1,0	0,04482	0,5	0,36	271,3	21,3	281,4	2,6	282,7	1,3	104	100
060-Z46	0,07	0,17	25791	0,05270	0,5	0,3435	0,7	0,04726	0,5	0,83	316,0	10,5	299,8	1,7	297,7	1,4	94	99
035-Z26	0,02	0,44	115212	0,05192	0,3	0,3391	0,7	0,04737	0,6	0,90	281,9	5,9	296,5	1,7	298,3	1,8	106	101
023-Z16	0,04	0,53	51022	0,05201	0,6	0,3408	0,9	0,04753	0,7	0,72	285,9	14,1	297,8	2,4	299,3	2,1	105	101
087-Z67	0,06	0,28	32433	0,05259	0,6	0,3524	0,8	0,04860	0,5	0,53	311,2	14,5	306,5	2,2	305,9	1,5	98	100
104-Z80	0,01	0,40	160050	0,05243	1,1	0,3562	1,2	0,04928	0,6	0,44	304,1	24,7	309,4	3,3	310,1	1,9	102	100
028-Z21	0,05	0,19	39101	0,05517	1,0	0,4022	1,7	0,05287	1,3	0,77	419,2	22,9	343,3	4,8	332,1	4,2	79	97
024-Z17	0,04	0,30	40689	0,05482	0,5	0,4181	0,7	0,05531	0,6	0,74	405,0	10,1	354,7	2,2	347,1	2,0	86	98

063-Z47	0,04	0,45	45218	0,05374	0,3	0,4157	0,6	0,05611	0,5	0,82	360,1	7,2	353,0	1,9	351,9	1,9	98	100
095-Z73	0,09	0,35	19202	0,05387	0,2	0,4496	0,7	0,06053	0,7	0,95	365,8	4,7	377,0	2,3	378,8	2,5	104	100
055-Z41	0,04	0,57	43633	0,05560	0,2	0,4674	0,5	0,06096	0,5	0,90	436,6	4,3	389,4	1,7	381,5	1,9	87	98
034-Z25	0,01	0,14	164485	0,05391	0,2	0,4599	0,7	0,06188	0,6	0,92	367,1	5,4	384,2	2,1	387,1	2,4	105	101
090-Z70	0,03	0,42	59708	0,05457	0,9	0,4743	1,2	0,06304	0,8	0,62	394,5	21,0	394,1	3,9	394,1	2,9	100	100
085-Z65	0,03	0,24	53163	0,05485	0,2	0,4846	0,5	0,06407	0,5	0,81	406,2	5,4	401,2	1,7	400,3	1,8	99	100
064-Z48	0,01	0,39	145867	0,05572	0,2	0,5005	0,5	0,06515	0,4	0,86	441,2	4,4	412,1	1,7	406,9	1,8	92	99
018-Z13	0,02	0,15	111850	0,05947	0,3	0,6794	0,8	0,08286	0,7	0,89	584,2	7,4	526,4	3,3	513,2	3,6	88	97
005-Z2	0,02	0,48	86341	0,06083	0,9	0,7004	1,2	0,08350	0,8	0,64	633,3	18,7	539,0	4,9	517,0	3,9	82	96
093-Z71	0,09	0,13	19797	0,05728	0,2	0,6706	1,0	0,08490	1,0	0,98	502,3	4,3	521,1	4,3	525,3	5,2	105	101
083-Z63	0,04	0,09	42164	0,06434	0,7	0,8244	6,8	0,09293	6,7	0,99	752,8	15,6	610,5	31,1	572,9	36,9	76	94
099-Z77	0,01	0,18	189806	0,06312	0,2	0,8948	0,8	0,10281	0,8	0,95	712,4	5,1	648,9	3,9	630,8	4,6	89	97
Rejected analysis																		
044-Z33	0,09	0,77	20380	0,08456	15,1	0,2827	16,8	0,02425	7,4	0,44	1305,4	293,6	252,8	37,7	154,4	11,3	12	61
073-Z55	1,46	0,58	1267	0,03827	1,9	0,1352	2,7	0,02562	1,9	0,69	-466,4	50,8	128,8	3,3	163,1	3,1	-35	127
049-Z38	0,13	0,36	13824	0,05943	1,1	0,2436	1,5	0,02973	1,0	0,67	582,7	23,7	221,4	3,0	188,9	1,9	32	85
004-Z1	0,10	0,39	19050	0,04407	4,9	0,2998	5,0	0,04934	0,9	0,16	-106,7	121,3	266,2	11,7	310,4	2,6	-291	117
047-Z36	0,41	0,23	4466	0,07691	11,4	0,6087	15,7	0,05740	10,7	0,69	1118,9	212,2	482,7	58,6	359,8	37,7	32	75
046-Z35	3,85	0,27	453	0,17599	42,2	2,9844	46,1	0,12299	18,0	0,65	2615,5	570,6	1403,7	301,4	747,7	130,8	29	53
050-Z39	0,34	0,61	5150	0,20129	48,7	3,8521	53,8	0,13879	22,9	0,69	2836,7	793,6	1603,7	433,8	837,8	180,3	30	52

Conc (%)[1]**:** Concordance (%) 6/8 - 7/6

Conc (%)[2]**:** Concordance (%) 6/8 - 7/5

Data analyzed in the Universidad Nacional Autónoma de México (UNAM), Mexico

SAMPLE AR-15 - Cerro Negro Andesite (35°19'55.11"S - 70°17'23.09"W)

Spot number	U (ppm)	Th (ppm)	Th/U	7/6 ratio	1s	7/5 ratio	1s	6/8 ratio	1s(%)	Rho	7/6 age	1s(abs)	7/5 age	1s(abs)	6/8 age	1s(abs)	Disc (%)
Zircon_31_044	317,641	228,39	0,61	0,05341	0,003	0,2646	0,0132	0,03581	0,0004	0,19	346,0	99,0	238,0	11,0	227,0	2,0	4,6
Zircon_34_047	142,133	137,97	0,82	0,05467	0,003	0,2722	0,0138	0,03642	0,0005	0,26	399,0	98,0	244,0	11,0	231,0	3,0	5,3
Zircon_36_050	726,099	1016,7	1,19	0,05051	0,001	0,2439	0,0068	0,03496	0,0003	0,28	219,0	55,0	222,0	6,0	222,0	2,0	0,0
Zircon_37_051	340,257	229,54	0,57	0,05212	0,002	0,2369	0,0075	0,03320	0,0003	0,32	291,0	61,0	216,0	6,0	211,0	2,0	2,3
Zircon_38_052	767,216	650,17	0,72	0,05044	0,001	0,2421	0,0056	0,03481	0,0002	0,29	215,0	45,0	220,0	5,0	221,0	1,0	-0,5
Zircon_39_053	326,099	425,35	1,11	0,05904	0,005	0,2899	0,0255	0,03561	0,0004	0,17	569,0	160,0	258,0	20,0	226,0	2,0	12,4
Zircon_42_057	170,401	431,77	2,15	0,05202	0,003	0,2515	0,0142	0,03525	0,0004	0,22	286,0	111,0	228,0	11,0	223,0	3,0	2,2
Zircon_43_058	463,291	1002,4	1,84	0,05185	0,002	0,2469	0,0088	0,03460	0,0003	0,21	279,0	71,0	224,0	7,0	219,0	2,0	2,2
Zircon_45_060	700,234	381,1	0,46	0,05428	0,002	0,2656	0,0101	0,03554	0,0004	0,32	383,0	72,0	239,0	8,0	225,0	3,0	5,9

Zircon_46_062	185,259	442,32	2,03	0,05519	0,003	0,2614	0,0128	0,03436	0,0003	0,20	420,0	96,0	236,0	10,0	218,0	2,0	7,6
Zircon_47_063	303,943	118,22	0,33	0,05780	0,003	0,2798	0,0131	0,03537	0,0003	0,18	522,0	97,0	250,0	10,0	224,0	2,0	10,4
Zircon_48_064	313,299	254,83	0,69	0,05410	0,002	0,2668	0,0104	0,03565	0,0003	0,21	375,0	82,0	240,0	8,0	226,0	2,0	5,8
Zircon_49_065	482,03	1187,4	2,09	0,05693	0,002	0,2825	0,0093	0,03604	0,0003	0,23	489,0	67,0	253,0	7,0	228,0	2,0	9,9
Zircon_50_066	155,121	152,98	0,84	0,05891	0,004	0,2842	0,0204	0,03547	0,0004	0,16	564,0	150,0	254,0	16,0	225,0	2,0	11,4
Zircon_53_070	246,522	771,67	2,66	0,05656	0,002	0,2763	0,0115	0,03557	0,0004	0,27	474,0	84,0	248,0	9,0	225,0	2,0	9,3
Zircon_54_071	810,597	666,68	0,70	0,05684	0,001	0,2619	0,0069	0,03361	0,0003	0,31	485,0	52,0	236,0	6,0	213,0	2,0	9,7
Zircon_55_072	121,313	60,737	0,42	0,05938	0,006	0,2971	0,0300	0,03654	0,0005	0,13	581,0	213,0	264,0	23,0	231,0	3,0	12,5
Zircon_56_074	527,711	487,18	0,78	0,05795	0,002	0,2758	0,0092	0,03426	0,0003	0,29	528,0	67,0	247,0	7,0	217,0	2,0	12,1
Zircon_57_075	328,559	362,49	0,94	0,05087	0,002	0,2430	0,0109	0,03503	0,0003	0,19	235,0	97,0	221,0	9,0	222,0	2,0	-0,5
Zircon_58_076	282,966	499,41	1,50	0,05894	0,002	0,2891	0,0122	0,03562	0,0003	0,21	565,0	85,0	258,0	10,0	226,0	2,0	12,4
Zircon_59_077	330,276	647,11	1,66	0,05208	0,001	0,2476	0,0072	0,03436	0,0003	0,27	289,0	61,0	225,0	6,0	218,0	2,0	3,1
Zircon_60_078	189,209	206,7	0,93	0,05971	0,003	0,2947	0,0144	0,03569	0,0003	0,18	593,0	100,0	262,0	11,0	226,0	2,0	13,7
Rejected analysis																	
Zircon_33_046	206,955	274,27	1,12	0,06218	0,002	0,3015	0,0122	0,03561	0,0004	0,27	680,0	74,0	268,0	10,0	226,0	2,0	15,7
Zircon_41_056	124,004	175,19	1,20	0,06470	0,003	0,3208	0,0178	0,03597	0,0005	0,24	765,0	102,0	283,0	14,0	228,0	3,0	19,4
Zircon_44_059	136,456	164,45	1,02	0,06307	0,003	0,3017	0,0146	0,03515	0,0004	0,23	711,0	89,0	268,0	11,0	223,0	2,0	16,8
Zircon_51_068	113,992	75,114	0,56	0,06208	0,007	0,3226	0,0403	0,03768	0,0007	0,14	677,0	253,0	284,0	31,0	238,0	4,0	16,2
Zircon_52_069	406,073	1000,5	2,09	0,06858	0,002	0,3276	0,0103	0,03490	0,0003	0,29	886,0	59,0	288,0	8,0	221,0	2,0	23,3